



INSTITUT FÜR
MECHANIK UND
MECHATRONIK
Mechanics & Mechatronics



DISSERTATION

Holistic energy optimization of rail vehicles

ausgeführt zum Zwecke der Erlangung des akademischen Grades
eines Doktors der technischen Wissenschaften
unter der Leitung von

Ao.Univ.Prof. Dipl.-Ing. Dr.techn. Martin Kozek

am Institut für Mechanik und Mechatronik
Abteilung für Regelungstechnik und Prozessautomatisierung

eingereicht an der Technischen Universität Wien,
Fakultät für Maschinenwesen und Betriebswissenschaften

von

Dipl.-Ing. Christian Dullinger
Hörnesgasse 17/11
1030 Wien

Geboren am 14.01.1985
Matr.Nr.: 00426533

Wien, am 8. Juni 2018

Acknowledgements

First of all I would like to thank my mentor and supervisor Prof. Martin Kozek, who gave me the opportunity to write this PhD Thesis at the TU Wien, Institute of Mechanics and Mechatronics, Workgroup of Control and Process Automation. I am thankful for his support and professional advice.

Furthermore I want to thank Dr. Walter Struckl for initiating the research project between the TU Wien as research partner and the Siemens AG Österreich as industrial partner.

Above all I am very grateful for the support of my parents, Brigitta and Erhard, as well as of my sister Silvia; in many different ways during my doctoral study as well as all through my whole life.

Eidesstattliche Erklärung

Ich erkläre eidesstattlich, dass ich die Arbeit selbständig angefertigt, keine anderen als die angegebenen Hilfsmittel benutzt und alle aus ungedruckten Quellen, gedruckter Literatur oder aus dem Internet im Wortlaut oder im wesentlichen Inhalt übernommenen Formulierungen und Konzepte gemäß den Richtlinien wissenschaftlicher Arbeiten zitiert, durch Fußnoten gekennzeichnet bzw. mit genauer Quellenangabe kenntlich gemacht habe.

Wien, am 8. Juni 2018

Christian Dullinger

Kurzfassung

Die vorliegende Dissertation entstand im Rahmen eines seit 2014 laufenden Kooperationsprojektes an der Technischen Universität Wien. Die enthaltenen Veröffentlichungen sind im Laufe dieses Projekts zwischen dem Institut für Mechanik und Mechatronik (Abteilung für Regelungstechnik und Prozessautomatisierung) als Forschungspartner und der Siemens AG Österreich als Industriepartner entstanden. Das Projekt wurde von der Österreichischen Forschungsförderungsgesellschaft (FFG Nr. 846041) gefördert.

Gesamtheitliche Energiesimulation und -optimierung von städtischen Schienenfahrzeugen ist ein wichtiges Thema um Schienenfahrzeuge im Städtischen Verkehr konkurrenzfähig zu erhalten. Der Schwerpunkt liegt auf der Entwicklung neuer Methoden für die Modellierung von Fahrzeug-Subsystemen, deren Interaktion und Design- und Betriebsoptimierung des gesamten Fahrzeuges. In diesem Zusammenhang wurden eine Methodik zur multikriteriellen gemischt-ganzzahligen Optimierung sowie eine Sensitivitätsanalyse für Zielkriterien (z.B.: Gesamtenergieverbrauch) von städtischen Schienenfahrzeugen bezüglich Auslegungsparametern und Betriebsbedingungen entwickelt. Des Weiteren wurden im Anschluss an das Forschungsprojekt die entwickelten Methoden in ein umfangreiches Softwaretool mit graphischer Benutzeroberfläche implementiert.

In der vorliegenden Dissertation wird ein einzigartiges Konzept zur gesamtheitlichen Energiesimulation und -optimierung von städtischen Schienenfahrzeugen präsentiert. Das Gesamtmodell des Fahrzeugs ist modular strukturiert und besteht aus einfach zu parametrierenden validierten Subsystemen. Alle wesentlichen energieverbrauchenden Subsysteme können mittels Modellen von adäquatem Detailierungsgrad berücksichtigt werden. Die Interaktion zwischen den Subsystemen wird simuliert und durch die Betriebsbedingungen und Komponenten-Regler getrieben. Abgesehen von Energiesignalen bietet das Konzept viele andere Zeitsignale, welche wertvolle Informationen für das Konstruieren, Dimensionieren, Testen und Betreiben des Fahrzeugs enthalten. Verschiedene Ablauf-Varianten des Konzepts ermöglichen eine fallspezifische Simulation oder Optimierung. Des Weiteren kann eine übergeordnete multikriterielle gemischt-ganzzahlige Optimierung angewendet werden um das System hinsichtlich einer Vielzahl von Auslegungsparametern und Betriebsbedingungen zu optimieren. Zusätzlich können mittels einer sogenannten Brute-Force-Methode alle möglichen Kombinationen simuliert werden um die Sensitivität von Zielsetzungen (z.B.: Gesamtenergieverbrauch) bezüglich dieser Parameter zu analysieren.

Abstract

The presented PhD Thesis was performed in the course of a cooperative project at TU Wien starting in 2014. The publications originated in this project between the Institute of Mechanics and Mechatronics (Division of Control and Process Automation) as research partner, and Siemens AG Österreich as industrial partner. The project has been funded by the Austrian Research Promotion Agency (FFG No. 846041).

The pressing issue of holistic energy simulation and optimization of urban rail vehicles is discussed in this work. The research was focused on the development of new methodologies for modeling the rail vehicle's subsystems, their interaction, the overall vehicle, and design and operation optimization of the vehicle. In this context a new framework for multi-objective mixed-integer optimization of the urban rail vehicle and sensitivity analysis of objectives (e.g. total energy) with respect to design parameters and operational conditions has been developed. Moreover, in a follow-up of the research project the developed methodologies were implemented in an extensive software tool with user-friendly graphical user interface (GUI).

In this PhD Thesis a unique framework for holistic energy simulation and optimization of urban rail vehicles is presented. The overall modular structured model consists of easy to parameterize validated subsystems. All essential energy consuming subsystems can be considered via models of adequate detail level. Interaction between subsystems is simulated and driven by the operational conditions and component-level controllers. Apart from energy signals the framework provides many other time signals, which contain valuable information for design, sizing, testing, and operation of the vehicle. Different work flow variants of the framework enable a case specific simulation or optimization. Furthermore a superordinated multi-objective mixed-integer optimization (MOMIO) can be applied to optimize the system with respect to a multitude of design parameters and operational conditions. Additionally a Brute-Force-Method (BFM) simulating all possible combinations enables to analyze the sensitivity of objectives (e.g. total energy) with respect to those parameters.

Contents

1 Overview	1
1.1 Motivation and problem statement	1
1.1.1 State-of-the-art review	2
1.1.2 Problem definition	4
1.2 Goals	4
1.3 Methodology	4
1.3.1 System component models	4
1.3.2 Optimization methods and controllers	9
1.4 Implementation of the methodologies in a software tool	14
1.5 Summary of scientific approaches	15
1.6 Scientific contributions of this work	16
Bibliography	18
2 Publications	21
2.1 Publication A	22
2.2 Publication B	37
2.3 Publication C	52
List of scientific publications	67
Curriculum Vitae	69

List of Figures

1.1	Overview of the urban rail vehicle and the individual subsystems (blue) and environmental influences (red).	4
1.2	Sketch: mechanical and electrical powers and power losses at sampling instance k ; adopted from [1] (Publication B)	5
1.3	Thermal model brake resistor	5
1.4	Traction battery (TB) submodels	6
1.5	Simulation model for the power consumption of air compressor	7
1.6	Schematic illustration of the thermal rail vehicle model; adopted from [2] (Publication A)	8
1.7	Conceptual HVAC system; adopted from [3] (Publication C)	9
1.8	Workflow of the train trajectory optimizer (TTO); adopted from [1] (Publication B)	10
1.9	Excerpt of the FSM HVAC controller of the Viennese Ultra Low Floor tram (with global states electrical heating and cooling); adopted from [2] (Publication A)	11
1.10	Basic control architecture of the AHC; taken from [3] (Publication C)	12
1.11	Multi-objective mixed-integer optimization (MOMIO) of system configuration; adopted from [1] (Publication B)	13
1.12	Work flow variants of the simulation/optimization software tool.	14

Acronyms

AHC advanced HVAC controller

ASHRAE American Society of Heating Refrigerating, and Air-Conditioning Engineers

BFM Brute-Force-Method

DC direct current

DOFs degrees of freedom

DVs decision variables

EHA exhaust air

EMS energy management system

ESS energy storage system

FSM finite state machine

GA genetic algorithm

GUI graphical user interface

HVAC heating ventilation and air conditioning

IDA indoor air

KPIs key performance indicators

MCP main container pipe

MILP mixed-integer linear programming

MIMO multi-input multi-output

MOMIO multi-objective mixed-integer optimization

MPC model predictive control

NSGA Non-dominated Sorting Genetic Algorithm

ODA outdoor air

PEM Prediction Error Method

PID proportional-integral-derivative

RCA recirculation air

SQP sequential quadratic programming

SUP supply air

TB traction battery

TTO train trajectory optimizer

Chapter 1

Overview

Urban rail is facing increasing pressure to analyze and minimize its energy consumption to reduce operational costs and environmental impact [4]. A holistic energy simulation and optimization framework for urban rail vehicles has been developed and implemented in a software tool with user-friendly GUI.

In Chap. 1 a motivation, the proposed concepts/methods/models and related research are presented, the implementation of the developed methodologies in a software tool with user-friendly GUI is shown, and the main contribution of the selected journal articles is described. The publications itself and my own contribution can be found in Chap. 2.

1.1 Motivation and problem statement

Rail vehicles providing public transport services within metropolitan areas (urban rail vehicles) include tramways, light rail, rail rapid (metro), and regional or commuter rail vehicles [5]. These vehicles are operated in railway systems with relatively short distance between stations and are electrically powered [4]. Due to their electrification (electric drive train) and great capacity they are considered as an ideal solution to reduce the impact of urban mobility [5]. However, urban rail is facing increasing pressure to analyze and minimize its energy consumption to reduce operational costs and environmental impact [4]. In that regard rail vehicle manufacturers have to improve the overall design of their vehicles and deliver appropriate warranties on energy consumption already in the bidding phase. Thereby a multitude of on-board electrical components affecting thermal comfort, possible train trajectories, and energy efficiency exist. Due to the inherent interaction of these components and therefore all main design variables it is difficult for experts to obtain a satisfying design result for a train. The design must typically meet contradicting goals (low cost, high efficiency, high thermal comfort, etc.) in the presence of many constraints like travel schedule, comfort parameters, overall weight, etc.

The work presented here aims at supporting the designer by providing the following features: The overall urban rail vehicle model is modular structured and consists of easy and robust to parameterize validated subsystems. Thereby all essential energy consuming subsystems (traction system and auxiliaries) can be considered via fast executable models of adequate detail level (i.e. dynamic models, characteristic diagrams, etc.). Interaction between the subsystem is simulated and driven by the operational conditions and state of the art (state machines, PID) or sophisticated controllers (model

predictive controllers). Apart from power signals the holistic energy simulation and optimization framework provides many other high resolution time signals (e.g.: state of the indoor air, state of HVAC equipment, heat loss through the vehicle outer shell, pressure in the main container pipe, brake force, heat emission of a brake resistor, etc.), which contain valuable information for the vehicle manufacturer for design, sizing, testing, and operation of the vehicle. Different work flow variants of the framework (i.e. with/without train trajectory optimizer (TTO), virtual driver, optimized interaction of components) enable a case specific optimization. Furthermore a superordinated multi-objective mixed-integer optimization (MOMIO) can be applied to optimize the urban rail vehicle with respect to a multitude of design parameters and operational conditions. Additionally a Brute-Force-Method (BFM) simulating all possible combinations enables to analyze the sensitivity of objectives (e.g. total energy, key performance indicators (KPIs), etc.) with respect to those degrees of freedom (DOFs). Last but not least, the framework is embedded in a software tool with user-friendly GUI for robust parametrization and visualization.

1.1.1 State-of-the-art review

The need for methods and tools to analyze, simulate and optimize the energy flows in urban rail was already emphasized by the authors in [4, 6, 7, 8]. The authors in [9] present a review of hundred and twenty-five simulation tools for modeling and managing electric road vehicle energy requirements. Only two tools are reported that can cope with rail vehicles.

In metropolises where urban rail is not developing further it may lose its position at the forefront of economic and sustainable solutions for urban mobility [10], since new individual electrical transportation modes (like e-bikes, e-scooters, hybrid/electric cars) are arising and improving. The great benefit of an electric drive train beside its inherent efficiency is that it enables recuperative braking. Thereby due to higher mass, connection to an electric grid (with possibly other vehicles accelerating, stationary ESSs, reversible substations), and many on-board electric auxiliaries the possible benefit of regenerative braking for urban rail vehicles is higher than for plug-in electric automotive vehicles.

A thorough analysis of the energy flows and possible measures to improve efficiency in urban rail systems and different rail way networks is given in [6] and [8], respectively.

In [4] the authors use a holistic approach to produce a comprehensive set of key performance indicators (KPIs) for assessing and optimizing the energy consumption in urban rail systems. The authors conclude that energy saving measures will generally have to be evaluated at unit level before their implementation at system level. Given the difficulty and costs involved in testing measures at large scale, this process will normally need the use of simulation programs. Although the presented framework focuses on the vehicle many of those KPIs can be computed by simulation, their sensitivity with respect to DOFs analyzed via the BFM, and optimized by the subordinated MOMIO.

[7] focus on a comprehensive overview of the currently available strategies and technologies for recovery and management of braking energy in urban rail, covering timetable optimization, on-board and way-side energy storage systems (ESSs) and reversible substations. In this work a battery model which specifically addresses the pulse power charging/discharging possibility of traction batteries was developed and included

to the holistic energy simulation and optimization framework. Although the presented framework focuses on the systems of the rolling stock the interaction with reversible sub-stations/way-side ESSs can be simulated/optimized given the time and distance dependent receptivity and efficiency as environmental influences.

In [11] the optimal sizing of stationary ESSs to save regenerative braking energy in a metro line is based on the predicted maximum instantaneous regenerative energy. Although the framework of this work focuses on the rail vehicle, it can help to minimize transmission losses by determining the optimal positions of new stationary/way-side ESSs along the line.

In case of multiple energy/power sources an energy management system (EMS) is required to optimize operation. The authors in [12] focus on the performance evaluation of meta-heuristics to deal with power management of a dual ESS for electric vehicles. Both, [13] and [14] test a hybrid tram composed by a fuel cell and different on-board ESSs for catenary free operation. Furthermore an EMS is proposed to optimize power consumption. Also the holistic framework of this work comprises an EMS optimizing the power flow from/to supply grid (receptivity and efficiency), on-board ESS, auxiliaries, and brake resistor and can be used to test catenary free operation.

The authors in [15] develop an electric train energy consumption modeling framework considering instantaneous regenerative braking efficiency, described by an exponential function. However, the model does not consider internal engine data. This work not only considers the operating point dependent power losses of the traction components given by validated static lookup tables, but also enables to simulate/optimize the possible reuse of regenerative braking energy by auxiliaries/on-board ESS (dynamic models) and way-side ESS/reversible substations (receptivity and efficiency). Furthermore the built in TTO enables energy-efficient driving (matching the operating point dependent power losses of the traction system, the route, operational parameters, passenger loading, etc.) and can be used to optimize the speed profile in that regard.

[16] develop a model for the interactions between the motion of a high-speed train and the electrical line in case of regenerative braking. For the power consumption of the train's auxiliary systems a mean constant was assumed. However, for urban rail power consumption of the auxiliaries can rise up to about 35 % of the total energy entering the rolling stock [17, 18]. In this work not only for the components of the traction system (input choke, inverter, motor, etc.), but also for the main energy consuming auxiliary systems, their power consumption is obtained as time signals.

The authors in [19] show a thorough analysis of braking energy dispatch in the urban traction power supply system. One investigated strategy was to raise the power of heaters during regenerative braking and reduce it while driving. Also the study in [20] shows the interest in developing an advanced EMS that couples traction and heating functions of an (hybrid) electric vehicle. In this work, the presented framework incorporates a mixed-integer predictive hierarchical HVAC controller, which time-varying tuning weights can be used to demand high tracking performance (of the indoor air temperature) when regenerative braking energy is available.

The novel contribution of this work is that it enables a sensitivity analysis and a holistic multi-objective optimization of the system configuration based on a variety of lower-level time simulations and operation optimizations. To the author's knowledge none of the aforementioned references utilizes such a framework.

1.1.2 Problem definition

Fig. 1.1 shows a schematic illustration of a fully equipped urban rail vehicle operating on a DC net. Subsystems, environmental influences, and the main interdependencies are depicted as blocks and arrows, respectively. The presented holistic energy simulation and optimization framework for urban rail vehicles considers all these blocks and arrows via dynamic models, characteristic diagrams, controllers, and simulation-based optimization methods. This will be the topic of Section 1.3

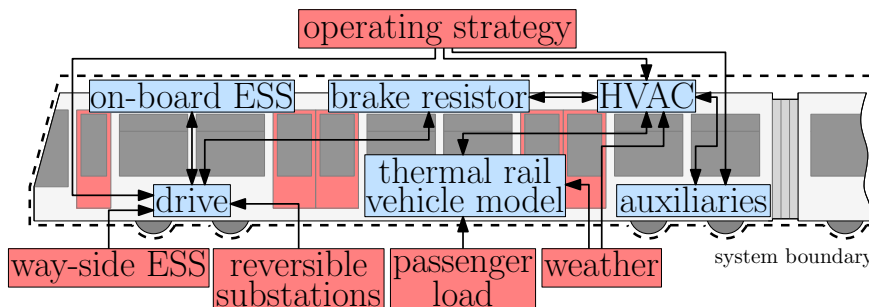


Figure 1.1: Overview of the urban rail vehicle and the individual subsystems (blue) and environmental influences (red).

1.2 Goals

The overall goal is a universal, modular structured, easy and robust to parameterize model for the energy flows in the urban rail vehicle. All essential energy consuming subsystems are capable of being integrated via models of adequate detail level. Interaction between subsystems shall be simulated and driven by the operational conditions and controllers. Furthermore, the overall model of the urban rail vehicle shall be suitable to analyze the sensitivity of objectives (e.g. total energy) with respect to design parameters and operational conditions. Moreover, due to its appropriate detail level and therefore fast execution time, the overall model of the urban rail vehicle shall be usable for a (mixed-integer) design optimization with respect to multiple conflicting objectives.

1.3 Methodology

In this Section the developed system component models (Section 1.3.1) of the urban rail vehicle depicted in Fig. 1.1 and the optimization methods and controllers (Section 1.3.2) are presented.

1.3.1 System component models

Traction system components

The traction system of a state of the art traction vehicle operating on a DC net basically consists of input chokes, the three-phase pulse width modulated power inverters, three-phase motors, gears, the mechanical braking system, and wheels. Figs 1.2a and 1.2b

depict the mechanical and electrical powers and power losses if the train is currently operated in traction and braking mode, respectively.

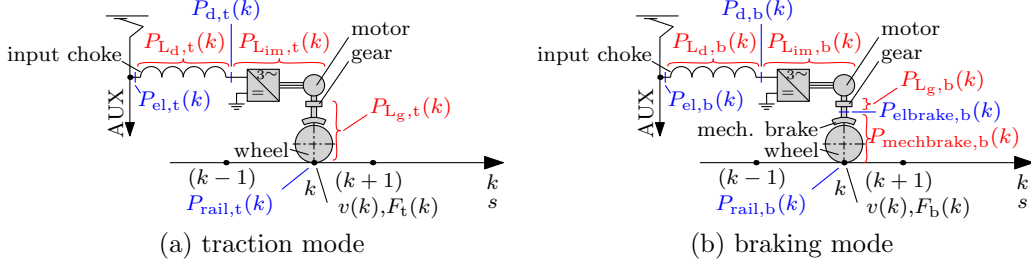


Figure 1.2: Sketch: mechanical and electrical powers and power losses at sampling instance k ; adopted from [1] (Publication B)

In Fig. 1.2 $v(k)$ is the train speed at sampling instance k , F_t/F_b is the traction/braking force, $P_{rail,t}/P_{rail,b}$ is the traction/total braking power, $P_{Lg,t}/P_{Lg,b}$ are the power losses of the gears, $P_{Lim,t}/P_{Lim,b}$ are the power losses of all three-phase pulse width modulated power inverters and three-phase motors, $P_{Ld,t}/P_{Ld,b}$ are the power losses of the input choke, and $P_{mechbrake,b}$ is the dissipated power due to mechanical braking.

Thermal model of the brake resistor

The proportion of the electrical energy provided by the electrical braking system which can neither be used within the vehicle nor fed back to the electrical net has to be dissipated in the brake resistors. Heat emission to the environment is given by free convection and radiation. For the usual temperature range of the brake resistor the heat emission is dominated by free convection. The hot surface of the brake resistor heats up the surrounding air, so that the density decreases and the air rises, resulting in a vertical air stream.

Fig. 1.3 shows the thermal model of the brake resistor with temperature $T_{br}(k)$, heat capacity C_{br} , and effective surface of free convection A_{fc} / radiation A_{rad} . The quantities $\dot{Q}_{conv}/\dot{Q}_{rad}$, $P_{el,in}$, and T_{env} are the heat emission through free convection/radiation, the electrical power to be dissipated, and the temperature of the environment, respectively.

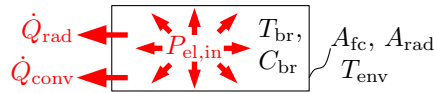


Figure 1.3: Thermal model brake resistor

The time-discrete time-variant nonlinear state space model for the temperature of the brake resistor T_{br} reads

$$T_{br}(k+1) = \frac{P_{el,in}(k) - \dot{Q}_{rad}(k) - \dot{Q}_{conv}(k)}{C_{br}} \cdot \Delta t(k) + T_{br}(k) \quad (1.1)$$

where

$$\dot{Q}_{rad}(k) = \varepsilon \cdot \sigma \cdot A_{rad} \cdot (T_{br}^4(k) - T_{env}^4(k)) \quad (1.2)$$

and

$$\dot{Q}_{\text{conv}}(k) = \alpha_m(k) \cdot A_{\text{fc}} \cdot (T_{\text{br}}(k) - T_{\text{env}}(k)). \quad (1.3)$$

In (1.1) $\Delta t(k)$ is the time step at sampling instance k . In (1.2) ε is the radiation emission factor of the surface and σ is the Stefan–Boltzmann constant. In (1.3) $\alpha_m(k)$ is the quasi-static mean heat transfer coefficient.

Traction batteries

The model of the traction battery (see Fig. 1.4) consists of an electrical model, a model which describes the energy content, a thermal model, and a model which considers the high-current capability of traction batteries for a short time period. Based on these models the battery management sets the charging/discharging strategy.

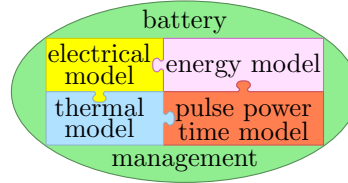


Figure 1.4: Traction battery (TB) submodels

The electrical model of the traction battery is a quasi static model. The irreversibly of the charging/discharging process is described by the internal resistance of the battery $R_i(k)$. The input to the model is the terminal power (P_{tc} for charging and P_{td} for discharging). In charging mode the relationship between the terminal power P_{tc} and the terminal voltage U_{tc} is given by

$$U_{\text{tc}} = \frac{U_q}{2} + \sqrt{\frac{U_q^2}{4} + R_i P_{\text{tc}}} \quad (1.4)$$

In (1.4) U_q is the no-load voltage. The charging current is then $I(k) = \frac{P_{\text{tc}}(k)}{U_{\text{tc}}(k)}$. The electrical energy stored by the battery $E_q(k)$ is considered a state. The input to this state equation is the reversibly supplied/withdrawn electric power $P_q(k) = U_q \cdot I(k)$.

The temperature of a traction battery $T_{\text{tb}}(k)$ is described by its state equation. The inputs to this state equation are the thermal power dissipated to heat at the internal resistance $P_{\text{th}}(k) = R_i(k) \cdot I^2(k)$ and the applied cooling power $\dot{Q}_c(k)$ of the cooling system.

Most traction batteries allow high currents and powers for a short time span, called pulse power charging/discharging. This fact is modeled by the following approach: The pulse power time span $t_{\text{pp}}(k)$ is considered a state with state equation

$$t_{\text{pp}}(k+1) = t_{\text{pp}}(k) + W_{\text{pp}}(k) \cdot \Delta t(k) \quad (1.5)$$

In (1.5) $W_{\text{pp}}(k)$ is used to rate the current time step $\Delta t(k)$. With I_l being the nominal continuous current and I_h being the pulse power current which can only be conducted for a maximum time span $T_{\text{pp,max}}$, the rating function is chosen as

$$W_{\text{pp}}(k) = \left(\max \left\{ 0, \frac{I(k) - I_l}{I_h - I_l} \right\} \right)^2. \quad (1.6)$$

Note that between the nominal continuous current and the pulse power current a quadratic weighting is used. This respects that the thermal power is a quadratic function of the current.

Compressed air system and power consumption of air compressor

Each train is equipped with two redundantly designed air compressors. These centrifugal compressors supply the main container pipe (MCP) with compressed air. The power consumption of an air compressor is about 7 kW and depends on the back pressure i.e. the pressure in the MCP. The on/off mode of the air compressor is controlled by a two-point controller which reacts on the pressure in the MCP p_{MCP} . By this means p_{MCP} stays between the lower and the upper threshold ($p_{\text{MCP,min}}/p_{\text{MCP,max}}$) of the two-point controller.

The power consumption of the air compressor $P_{\text{el,c}}$ was measured as a function of the back pressure p_{back} and stored in a characteristic diagram $P_{\text{el,c}} = P_{\text{el,c}}(p_{\text{back}})$. For the back pressure (i.e. $p_{\text{back}} = p_{\text{MCP}}$) a dynamic simulation model was developed. Fig. 1.5 shows the closed-loop simulation model for the power consumption of the air compressor $P_{\text{el,c}}(t) = P_{\text{el,c}}(u_c(t), p_{\text{MCP}}(t))$. The blocks are the two-point controller, the dynamic model of the pressure in the MCP p_{MCP} , and the characteristic diagram of the power consumption of the air compressor $P_{\text{el,c}}(p_{\text{back}})$. In the following the dynamic model for the pressure in the MCP $p_{\text{MCP}}(t)$ subject to the compressor on/off signal $u_c(t)$ and the disturbances $z_m(t)$ is explained.

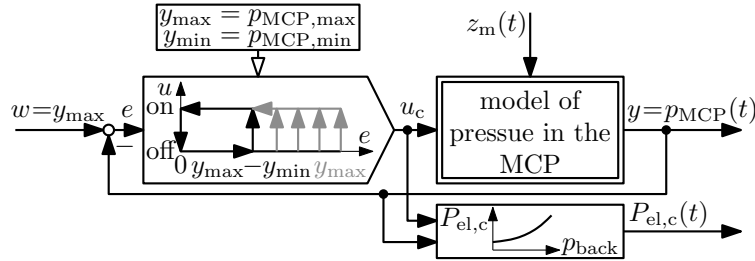


Figure 1.5: Simulation model for the power consumption of air compressor

Essential compressed air consumers are compressed-air springs, the air brakes, and leakage.

Leakage depends on the pressure in the MCP. Starting at the upper pressure limit $p_{\text{MCP,max}}$ the time signal $p_{\text{MCP}}(t)$ of air spillage was measured. Using Euler's method the first time derivative as a function of the pressure in the MCP i.e. $\frac{dp_{\text{MCP}}}{dt} = \frac{dp_{\text{MCP}}}{dt}(p_{\text{MCP}})$ was numerically computed and stored in a map. The same method was used to obtain a map of the pressure increase if the air compressor is switched on and supplies the main container pipe.

An increase in the brake force of an air brake results in a proportional pressure drop in the MCP. A steady or decreasing brake force does not affect the MCP. The simulation tool computes the brake force of the air brakes $F_{\text{mechbrake}}(k)$ by subtracting the electrical brake force $F_{\text{elbrake}}(k)$ from the total brake force $F_b(k)$. Thereby the amount of $F_{\text{elbrake}}(k)$ is maximized and has to stay below its maximum $F_{\text{elbrake,max}}(v(k))$, which is a function of the train speed. The total brake force $F_b(k)$ is either obtained from the TTO or computed for a given speed trajectory.

For the air consumption of the compressed-air springs during the operation a mean pressure drop per time unit was determined from measurement data. Moreover, the air springs vary their inner pressure proportional to the passenger load to keep the vehicle level. The respective proportional gain has to be determined from measurement data.

Thermal rail vehicle model

Fig. 1.6 shows a schematic illustration of the dynamic thermal rail vehicle model. The thermal vehicle model is extracted from input-output data, and both the model order and the model parameters are obtained from the Prediction Error Method (PEM). PEM uses numerical optimization algorithms, see [21, 22]. If, however, a physical parameter interpretation is sought-after, the following model structure can be assumed: The thermal vehicle model consists of two subsystems (since it is a second-order system) defined by two system boundaries, which exchange the heat flow \dot{Q}_{veh} . System 1 has the heat capacity C_{IDA} (assumed constant) with temperature ϑ_{IDA} . System 2 has the heat capacity C_{VEH} with temperature ϑ_{VEH} . For a further interpretation of this gray-box model and the specific experiment to gather measurement data for the PEM, see [2] (Publication A) and [23].

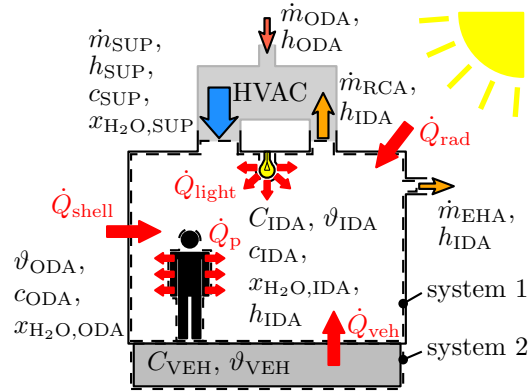


Figure 1.6: Schematic illustration of the thermal rail vehicle model; adopted from [2] (Publication A)

The state space model of the thermal vehicle model with state vector

$$\mathbf{x}_{tv}(k) = \begin{bmatrix} \vartheta_{IDA}(k) \\ \vartheta_{VEH}(k) \\ c_{IDA}(k) \\ x_{H_2O,IDA}(k) \end{bmatrix} \quad (1.7)$$

is obtained by transient energy and stationary mass balances for the system 1 and 2, see [2] (Publication A). Thereby the state of the wet air with subscript “A” (indoor air (IDA), outdoor air (ODA), supply air (SUP), recirculation air (RCA), exhaust air (EHA)) in terms of temperature ϑ_A , enthalpy h_A , CO_2 level c_A , and water content $x_{H_2O,A}$ are considered. Furthermore the heat flow through the outer shell of the vehicle \dot{Q}_{shell} , the heat flow entering the passenger cabin due to sun radiation \dot{Q}_{rad} , the heat flow due to electric lighting/equipment \dot{Q}_{light} , and the heat, water, and CO_2 production of the passengers are taken into account. For solar radiation calculations the ASHRAE

clear-sky model was implemented to the tool to automatically compute based on the day, the time, and the global position the solar angles (azimuth and elevation), the normal direct irradiation, and the diffuse irradiation. The train's position on the line and its azimuth angle are obtained from the train trajectory optimization/simulation. These time signals are combined to compute the angle of incidence and the total insulation for each surface of the vehicle at each time step. The heat flow \dot{Q}_{rad} is then computed considering the transmission factors of windows and absorption factors of walls. Track shading, the reflection of the ground, and tunnels can be considered by additional factors.

HVAC model

The tool uses a modular structured HVAC model. This approach enables a quick adaptation of the HVAC model to fit the structure of different HVAC system by adding or removing components. Fig. 1.7 shows a schematic illustration of the assumed HVAC system. Multiplicities of components are depicted aggregated.

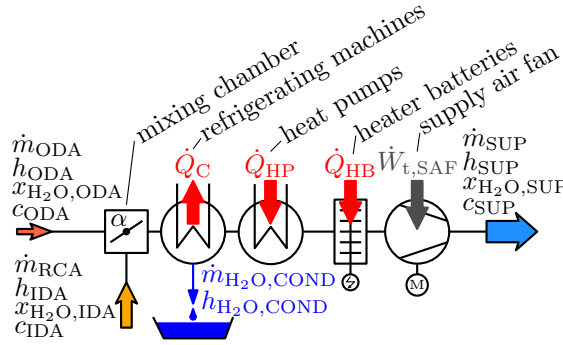


Figure 1.7: Conceptual HVAC system; adopted from [3] (Publication C)

In the mixing chamber the fresh ODA mass flow \dot{m}_{ODA} is isobarically mixed with the RCA mass flow \dot{m}_{RCA} from the plant interior. In Fig. 1.7 the quantities $h_{\text{ODA}}/h_{\text{IDA}}$, $x_{\text{H}_2\text{O,ODA}}/x_{\text{H}_2\text{O,IDA}}$, and $c_{\text{ODA}}/c_{\text{IDA}}$ are the specific enthalpy, the water content, and the volume fraction of CO_2 in air (in ppmv) of the wet ODA/IDA.

In the refrigerating machines the total heat flow \dot{Q}_{C} is isobarically withdrawn from the wet air mass flow. If due to cooling the temperature falls below the dew point temperature the condensate is removed. In this case the leaving air is saturated air.

In heat pumps and heater batteries the total heat flows \dot{Q}_{HP} and \dot{Q}_{HB} , respectively, are isobarically introduced.

The supply air fan delivers the conditioned wet air mass flow \dot{m}_{SUP} to the plant. Thereby it introduces the power $\dot{W}_{\text{t,SAF}}$ to the air mass flow. The SUP has the specific enthalpy h_{SUP} , water content $x_{\text{H}_2\text{O,SUP}}$, and volume fraction of CO_2 in air c_{SUP} . A typical HVAC model was derived and validated in [2] (Publication A).

1.3.2 Optimization methods and controllers

Train trajectory optimizer (TTO)

The train trajectories are defined as function of the discretized track position s . The position increment $\Delta s(k)$ is non equidistant, i.e. it depends on the sampling instance

k . The discretized nonlinear position-varying state space model used by the simulation based train trajectory optimization was derived in [1] (Publication B) and is given by

$$\begin{bmatrix} x_1(k+1) \\ x_2(k+1) \end{bmatrix} = \begin{bmatrix} x_1(k) \\ x_2(k) \end{bmatrix} + \begin{bmatrix} \frac{1}{x_2(k)} \\ \frac{u(k) - F_r(x_2(k)) - mg \sin \alpha(k)}{m_t x_2(k)} \end{bmatrix} \Delta s(k). \quad (1.8)$$

The states are the time $x_1(k) = t(k)$ and the train speed $x_2(k) = v(k)$. The input to the system $u(k)$ is the traction/braking force. The input sequence $u(k)$ constitutes the decision vector of the trajectory optimization problem, solved by a sequential quadratic programming (SQP) algorithm (see [24, 25]). In (1.8) m is the gravitational mass of the train whereas m_t is the total mass to be accelerated (i.e. including rotatory masses). The quantities F_r , g , and α , are the resistance force as a function of the velocity, the gravitational acceleration, and the gradient angle of the track.

The basic workflow of the TTO is depicted in Fig. 1.8. Details are found in [1] (Publication B).

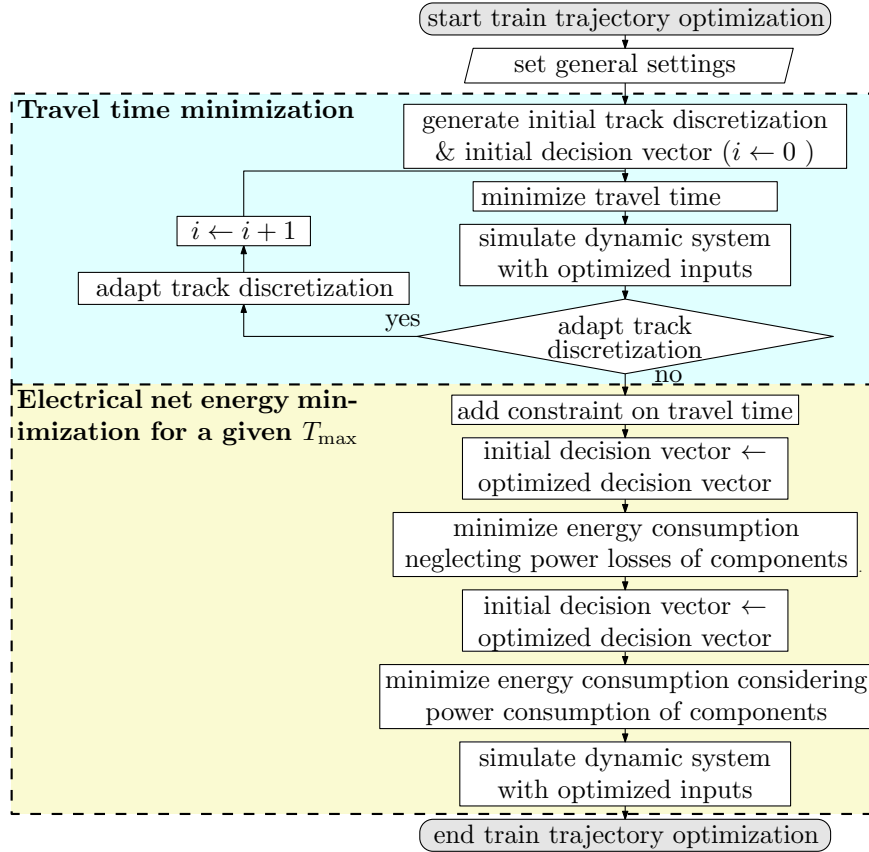


Figure 1.8: Workflow of the train trajectory optimizer (TTO); adopted from [1] (Publication B)

HVAC controllers

Finite state machine (FSM) controller The FSM HVAC controller is hierarchically structured and operates on two different levels, see Fig. 1.9.

On the top level the controller of the HVAC unit consists of one FSM. It is used to model the so called “global state” of the HVAC system like “electrical heating”, “ventilation”, “cooling”, etc.. On the bottom level the controller is a variety of FSMs each describing an HVAC component within a global state, see Fig. 1.9. The top level

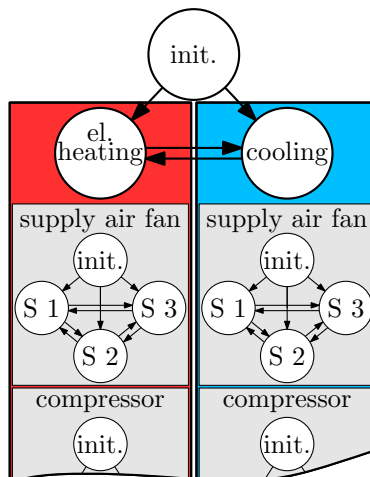


Figure 1.9: Excerpt of the FSM HVAC controller of the Viennese Ultra Low Floor tram (with global states electrical heating and cooling); adopted from [2] (Publication A)

FSM and the bottom level FSMs are in only one state at a time, the so called “current state”. For each FSM, at each time step k all transitions of the “current state” are evaluated. The state is changed from one state to another when the corresponding transition leading there is logically “true”. If all transitions from the “current state” are logically “false” the state of the FSM is not changed. The transitions of the FSMs are updated at each time step k . The transitions are logical expressions of constants and variables of the simulation model (like the indoor air temperature ϑ_{IDA} , the outdoor air temperature ϑ_{ODA} , the set point temperature $\vartheta_{set}(\vartheta_{ODA})$, etc.). This effectively constitutes a rule based control with well-defined switching transitions between constant operating modes.

This approach can describe a variety of logic circuits implemented by HVAC manufacturers. Furthermore, this method enables an easy modification of an implemented control strategy by the user. Background on FSMs is found in [26].

More insights into the FSM HVAC controller and a validation using on-site measurement data of a whole year is found in [2] (Publication A).

Advanced HVAC controller (AHC) The AHC is a highly versatile and numerically tractable hierarchical multi-input multi-output (MIMO) model predictive control (MPC) framework (see Fig. 1.10). It enables HVAC operation optimized for energy, comfort, and wear and was published in [3] (Publication C). With the AHC temperature, CO_2 level, and humidity can be controlled simultaneously in a decoupled fashion.

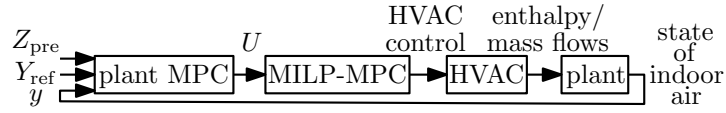


Figure 1.10: Basic control architecture of the AHC; taken from [3] (Publication C)

On the upper-level a computationally inexpensive plant MPC enables large horizons to take care of the slow dynamics of the thermal rail vehicle model. It can effectively incorporate available disturbance forecasts (e.g.: passenger load, ambient temperature/humidity/CO₂ level, heat flow due to sun radiation, etc.). Because the plant MPC considers the heat capacities and heat transfer coefficients of the rail vehicle it enables a versatile application for different rail vehicles.

On the lower-level a MILP-MPC based on a flexible and modular mixed-integer linear programming (MILP) model which can represent a variety of different HVAC systems optimizes the HVAC operation. The MILP-MPC considers the control trajectory of the plant MPC as its reference trajectory. It minimizes power consumption and switching. Thereby it obeys the technological limitations and solves a unit commitment problem. No heuristics have to be applied to account for discrete or switching HVAC components. Due to its prediction horizon the MILP-MPC can oversee the dwell times of HVAC components achieving optimized switching times. The mixed-integer linear formulation of the HVAC ensures a (near) global optimality.

Energy management system (EMS)

A central goal of the EMS is that recuperated power is provided to the auxiliaries (HVACs, air compressor, lightning and entertainment systems, etc.) first. In case the recuperated power is not used up by the auxiliaries the remaining part might be sent to the traction batteries/the overhead line, or has to be dissipated in the brake resistors. Four different strategies result from combinations the user can choose to meet a power demand. The request/offer is either first sent to the traction batteries and then the remaining power is provided by/sent to the electrical net or vice versa.

A fifth strategy optimizes the power split between electrical net and traction batteries. The decision variables (DVs) of this nonlinear optimization problem are the current of the traction batteries and the power of their cooling system.

All strategies consider time and distance dependent power capabilities of the line, efficiencies for supply/reutilization within the electrical net, and the submodel of the traction batteries (see Fig. 1.4).

Multi-objective mixed-integer optimization (MOMIO) of the system configuration

In Fig. 1.11 the flowchart of the multi-objective mixed-integer component configuration optimization solved by a controlled elitist genetic algorithm (GA) (a variant of NSGA-II, see [27]) is depicted. The decision vector of this optimization represents a specific system configuration in terms of parameters, characteristic maps, constraints, etc..

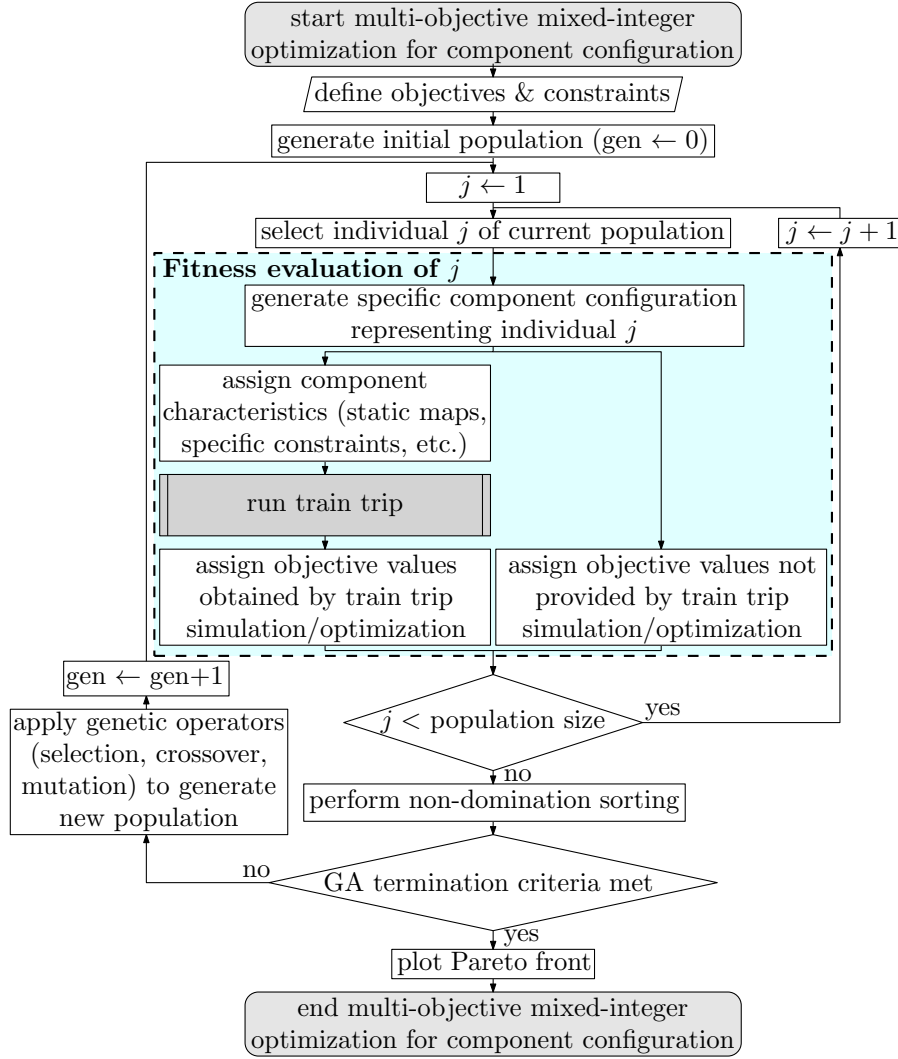


Figure 1.11: Multi-objective mixed-integer optimization (MOMIO) of system configuration; adopted from [1] (Publication B)

First the vector of objectives $\mathbf{F}(\boldsymbol{\theta}) = [F_1(\boldsymbol{\theta}), \dots, F_j(\boldsymbol{\theta}), \dots, F_m(\boldsymbol{\theta})]^T$ has to be defined by choosing the objectives of interest (e.g. energy consumption, investment costs, etc.). In accordance with the constraints a random initial population is generated.

The specific system configuration representing the individual j is generated and the train trip is simulated for this configuration. Thereby the operation and interaction of subsystems is optimized (e.g.: HVAC, traction system and traction batteries, etc.). For individual j the objective values are assigned.

The fitness evaluation continues until the fitness of all individuals of the current population has been evaluated. Then the GA performs the non-domination sorting and applies the genetic operators (selection, crossover, and mutation) to generate a new generation. The algorithm starts evaluating the individuals of the new population. The multi-objective GA stops if the spread, a measure of the movement of the Pareto front, is smaller than a threshold or the maximum number of generations is reached.

1.4 Implementation of the methodologies in a software tool

In a follow-up of the research project the developed methodologies were implemented in an extensive software tool with user-friendly graphical user interface (GUI) and handed to the industrial partner to be utilized in business processes and projects.

Fig 1.12 shows the main work flow variants of the tool.

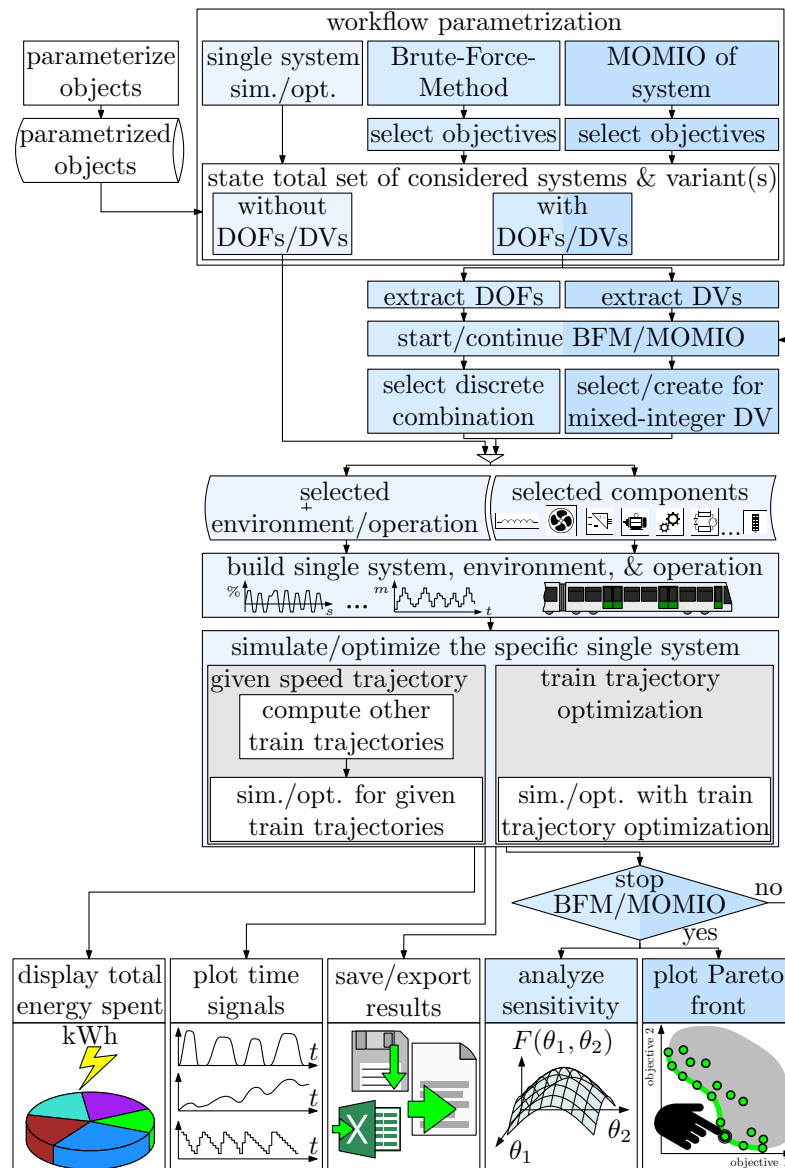


Figure 1.12: Work flow variants of the simulation/optimization software tool.

Parametrization is carried out via property tables. These property tables set the properties of MATLAB[®] objects.

In the work flow parametrization property table the user states the main work flow and the total set of considered objects (subsystems, controllers, operation conditions, etc.). For a specific (fixed) single system the tool allows to simulate and optimize the

operation of subsystems and the whole vehicle. Thereby the user can choose between simulating and optimizing for a given speed trajectory or including a train trajectory optimization. Furthermore the superordinated multi-objective mixed-integer optimization (MOMIO) can be applied to optimize the system with respect to a multitude of design parameters and environmental/operational conditions. Additionally the superordinated Brute-Force-Method (BFM) simulating all possible combinations enables to analyze the sensitivity of objectives with respect to the selected degrees of freedom (DOFs).

1.5 Summary of scientific approaches

In **Publication A**, see Sec. 2.1, a method and its implementation for computing the annual energy consumption of the HVAC unit of a tram is presented. It comprises a dynamic thermal vehicle model, a modular structured HVAC model, and a hierarchically structured finite state machine (FSM)-HVAC controller and includes operational and weather inputs. Thereby the state-space model of the thermal vehicle model is parameterized by applying the PEM utilizing measurement data obtained by a specific experiment in a climatic wind tunnel. Due to a gray-box modeling approach its parameters can be physically interpreted. To speed up computation time a method for extrapolating the annual energy consumption based on classified days utilizing the clustering algorithm K-Means is developed. A tram line in Vienna was used to obtain real measurements for validation of the simulation model.

In **Publication B**, see Sec. 2.2, a holistic framework for multi-objective optimization of the traction system configuration of rail vehicles operating on a DC net with mixed-integer decision variables is presented. The overall optimization is achieved by a two level approach: The Pareto front of optimal system configurations is obtained by a multi-objective mixed-integer elitist genetic algorithm (GA) on the upper-level. To capture the influence of a specific traction system configuration on travel time and energy a subordinated train trajectory optimizer (TTO) is developed, validated, and employed in the lower-level. The TTO considers the power losses of the components given as validated static look up tables and is solved by SQP. Speed limits, technological constraints, and constraints ensuring passenger comfort are observed. Furthermore, the effects of regenerative braking on the optimal train trajectory are considered. The BFM simulating all possible combinations of discretized DVs is utilized to validate the obtained Pareto front.

In **Publication C**, see Sec. 2.3, a highly versatile and numerically tractable hierarchical MIMO MPC framework for energy-, wear-, and comfort-optimized operation of HVACs is proposed. On the upper-level a computationally inexpensive plant MPC enables large horizons to take care of the slow dynamics of a thermal plant (e.g. rail vehicle) and effectively incorporate available disturbance forecasts. On the lower-level a MILP-MPC based on a flexible and modular MILP optimization model of an HVAC system optimizes the HVAC operation. The MILP-MPC considers the first few samples of the control trajectory of the plant MPC as its reference trajectory. It minimizes power consumption and switching of the HVAC. Thereby it has to obey constraints, consider

component characteristics by nonlinearity approximation, and solve a unit commitment problem. The fact that the plant MPC can be based on an almost arbitrary plant model and the MILP model of the MILP-MPC can represent a variety of different HVAC systems unifies HVAC control.

1.6 Scientific contributions of this work

The novel scientific contribution of this work is that it enables a sensitivity analysis and a holistic multi-objective optimization of the system configuration based on a variety of lower-level time simulations and operation optimizations.

The scientific contributions of this work can be summarized as follows:

- Development of models for all essential energy consuming subsystems.
 - These validated models are easy and robust to parameterize.
 - The adequate detail level of the models ensures a fast execution time of the overall vehicle model.
 - The interaction between the individual subsystems is modeled.
 - Subsystems are simulated in the time domain.
 - Apart from energy signals many other high resolution output signals are computed also for the subsystems.
 - Operation and interaction between subsystems is driven by the operational conditions and state of the art or sophisticated controllers (MPCs) and optimizations.
- Flexibility of the overall modular urban rail vehicle model.
 - Flexibility for adding or removing of subsystems is given due to the modular approach.
 - Adaptive non equidistant time/space sampling to trade precision versus computation time.
 - Different work flow variants enable a case specific simulation or optimization.
- Holistic approach for design and operation optimization and sensitivity analysis.
 - The developed superordinated MOMIO can be applied to optimize the system with respect to a multitude of design parameters and operational conditions.
 - The developed superordinated BFM simulating all possible discrete combinations enables to analyze the sensitivity of objectives (e.g. total energy) with respect to parameters.
- Implementation in an extensive software tool with user-friendly GUI.
 - For easy and robust parametrization of subsystems, operational conditions, controllers, and optimization methods.

- For convenient parametrization of the overall urban rail vehicle model and the simulation and optimization work flow.
- For analyzing, visualizing, saving, and exporting the results.

Bibliography

- [1] C. Dullinger, W. Struckl, M. Kozek, Simulation-based multi-objective system optimization of train traction systems, *Simulation Modelling Practice and Theory* 72 (2017) 104 – 117. doi:<http://dx.doi.org/10.1016/j.simpat.2016.12.008>.
- [2] C. Dullinger, W. Struckl, M. Kozek, A modular thermal simulation tool for computing energy consumption of HVAC units in rail vehicles, *Applied Thermal Engineering* 78 (2015) 616 – 629. doi:<http://dx.doi.org/10.1016/j.applthermaleng.2014.11.065>.
- [3] C. Dullinger, W. Struckl, M. Kozek, A general approach for mixed-integer predictive control of HVAC systems using MILP, *Applied Thermal Engineering* 128 (2018) 1646 – 1659. doi:<https://doi.org/10.1016/j.applthermaleng.2017.09.104>.
- [4] A. González-Gil, R. Palacin, P. Batty, Optimal energy management of urban rail systems: Key performance indicators, *Energy Conversion and Management* 90 (2015) 282 – 291. doi:<https://doi.org/10.1016/j.enconman.2014.11.035>.
- [5] V. Vuchic, *Urban Transit Systems and Technology*, Wiley, 2007.
- [6] A. González-Gil, R. Palacin, P. Batty, J. Powell, A systems approach to reduce urban rail energy consumption, *Energy Conversion and Management* 80 (2014) 509 – 524. doi:<https://doi.org/10.1016/j.enconman.2014.01.060>.
- [7] A. González-Gil, R. Palacin, P. Batty, Sustainable urban rail systems: Strategies and technologies for optimal management of regenerative braking energy, *Energy Conversion and Management* 75 (2013) 374 – 388. doi:<https://doi.org/10.1016/j.enconman.2013.06.039>.
- [8] H. Douglas, C. Roberts, S. Hillmansen, F. Schmid, An assessment of available measures to reduce traction energy use in railway networks, *Energy Conversion and Management* 106 (2015) 1149 – 1165. doi:<https://doi.org/10.1016/j.enconman.2015.10.053>.
- [9] K. Mahmud, G. E. Town, A review of computer tools for modeling electric vehicle energy requirements and their impact on power distribution networks, *Applied Energy* 172 (2016) 337 – 359. doi:<https://doi.org/10.1016/j.apenergy.2016.03.100>.
- [10] D. A. Nicola, M. A. Rosen, C. A. Bulucea, C. Brandusa, Some sustainability aspects of energy conversion in urban electric trains, *Sustainability* 2 (5) (2010) 1389–1407. doi:[10.3390/su2051389](https://doi.org/10.3390/su2051389).

-
- [11] R. Teymourfar, B. Asaei, H. Iman-Eini, R. N. fard, Stationary super-capacitor energy storage system to save regenerative braking energy in a metro line, *Energy Conversion and Management* 56 (2012) 206 – 214. doi:<https://doi.org/10.1016/j.enconman.2011.11.019>.
- [12] J. P. Trovão, C. H. Antunes, A comparative analysis of meta-heuristic methods for power management of a dual energy storage system for electric vehicles, *Energy Conversion and Management* 95 (2015) 281 – 296. doi:<https://doi.org/10.1016/j.enconman.2015.02.030>.
- [13] L. M. Fernandez, P. Garcia, C. A. Garcia, F. Jurado, Hybrid electric system based on fuel cell and battery and integrating a single dc/dc converter for a tramway, *Energy Conversion and Management* 52 (5) (2011) 2183 – 2192. doi:<https://doi.org/10.1016/j.enconman.2010.12.028>.
- [14] W. Zhang, J. Li, L. Xu, M. Ouyang, Optimization for a fuel cell/battery/capacity tram with equivalent consumption minimization strategy, *Energy Conversion and Management* 134 (2017) 59 – 69. doi:<https://doi.org/10.1016/j.enconman.2016.11.007>.
- [15] J. Wang, H. A. Rakha, Electric train energy consumption modeling, *Applied Energy* 193 (2017) 346 – 355. doi:<https://doi.org/10.1016/j.apenergy.2017.02.058>.
- [16] A. Frilli, E. Meli, D. Nocciolini, L. Pugi, A. Rindi, Energetic optimization of regenerative braking for high speed railway systems, *Energy Conversion and Management* 129 (2016) 200 – 215. doi:<https://doi.org/10.1016/j.enconman.2016.10.011>.
- [17] W. Struckl, A. Stribersky, W. Günselmann, Life cycle analysis of the energy consumption of a rail vehicle, in: *International workshop of allianz pro schiene: improvement of the environmental impacts of rail transport - challenges, good practices and future challenges*, Berlin, Germany, 2006.
- [18] W. Struckl, *Green Line : Environmental related product development strategies for railway vehicles based on the life cycle assessment of a metro in Oslo (in German)*, Vienna University of Technology, Vienna, Austria, 2007.
- [19] M. Bartłomiejczyk, M. Polom, Multiaspect measurement analysis of braking energy recovery, *Energy Conversion and Management* 127 (2016) 35 – 42. doi:<https://doi.org/10.1016/j.enconman.2016.08.089>.
- [20] L. Horrein, A. Bouscayrol, Y. Cheng, C. Dumand, G. Colin, Y. Chamailard, Influence of the heating system on the fuel consumption of a hybrid electric vehicle, *Energy Conversion and Management* 129 (2016) 250 – 261. doi:<https://doi.org/10.1016/j.enconman.2016.10.030>.
- [21] L. Ljung, *System Identification: Theory for the User*, Pearson Education, New Jersey, USA, 1998.

-
- [22] L. Ljung, Prediction error estimation methods, *Circuits, Systems and Signal Processing* 21 (1) (2002) 11–21. doi:10.1007/BF01211648.
- [23] R. N. Hofstädter, T. Zero, C. Dullinger, G. Richter, M. Kozek, Heat capacity and heat transfer coefficient estimation for a dynamic thermal model of rail vehicles, *Mathematical and Computer Modelling of Dynamical Systems* 0 (0) (2017) 1–14. arXiv:<http://dx.doi.org/10.1080/13873954.2016.1263670>, doi:10.1080/13873954.2016.1263670.
- [24] J. Nocedal, S. Wright, *Numerical Optimization*, Springer Series in Operations Research and Financial Engineering, Springer New York, 2006.
- [25] J. Bonnans, J. Gilbert, C. Lemarechal, C. Sagastizábal, *Numerical Optimization: Theoretical and Practical Aspects*, Universitext, Springer Berlin Heidelberg, 2013.
- [26] F. Wagner, R. Schmuki, T. Wagner, P. Wolstenholme, *Modeling Software with Finite State Machines: A Practical Approach*, Taylor & Francis, Boca Raton, USA, 2006.
- [27] K. Deb, *Multi-Objective Optimization Using Evolutionary Algorithms*, Wiley Interscience Series in Systems and Optimization, Wiley, 2001.

Chapter 2

Publications

List of journal publications:

Publication A

Christian Dullinger, Walter Struckl, and Martin Kozek.

A modular thermal simulation tool for computing energy consumption of HVAC units in rail vehicles.

Applied Thermal Engineering, Volume 78, 2015, Pages 616-629.

DOI: 10.1016/j.applthermaleng.2014.11.065

Publication B

Christian Dullinger, Walter Struckl, and Martin Kozek.

Simulation-based multi-objective system optimization of train traction systems.

Simulation Modelling Practice and Theory, Volume 72, 2017, Pages 104-117.

DOI: 10.1016/j.simpat.2016.12.008

Publication C

Christian Dullinger, Walter Struckl, and Martin Kozek.

A general approach for mixed-integer predictive control of HVAC systems using MILP.

Applied Thermal Engineering, Volume 128, 2018, Pages 1646-1659.

DOI: 10.1016/j.applthermaleng.2017.09.104

2.1 Publication A

Christian Dullinger, Walter Struckl, and Martin Kozek.

A modular thermal simulation tool for computing energy consumption of HVAC units in rail vehicles.

Applied Thermal Engineering, Volume 78, 2015, Pages 616-629.

DOI: 10.1016/j.applthermaleng.2014.11.065

Own contribution

Problem analysis, selection of methods, execution of the solution, development and programming of algorithms, consideration of implementation aspects, performing simulations studies, and structuring, writing, and editing of the manuscript was done by the applicant. Problem statement and discussion was done by the second author. Problem statement, discussion and editing was done by the third author.

Applied Thermal Engineering 78 (2015) 616–629



Contents lists available at ScienceDirect

Applied Thermal Engineering

journal homepage: www.elsevier.com/locate/apthermeng

Research paper

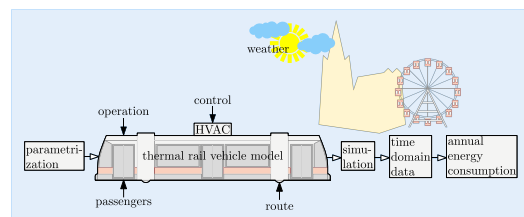
A modular thermal simulation tool for computing energy consumption of HVAC units in rail vehicles

Christian Dullinger^{a,*}, Walter Struckl^b, Martin Kozek^a^a Institute of Mechanics and Mechatronics, Division of Control and Process Automation, Getreidemarkt 9/325-A5, A-1060 Vienna, Austria^b Siemens AG Österreich, Austria

HIGHLIGHTS

- Data-based dynamic thermal rail vehicle model.
- Validated dynamic thermal simulation tool embedded in user-friendly GUI.
- GUI enables model parametrization, processing of weather/route data, & visualization.
- Computation of fast sampled time domain signals and the annual energy consumption.

GRAPHICAL ABSTRACT



ARTICLE INFO

Article history:

Received 29 September 2014
 Accepted 28 November 2014
 Available online 9 December 2014

Keywords:

Rail vehicle
 Data-based vehicle model
 HVAC
 Dynamic thermal simulation tool
 Energy consumption

ABSTRACT

A method and its implementation for computing the energy consumption of the heating, ventilation and air conditioning (HVAC) unit of a light rail vehicle is presented. In order to simulate the energy consumption of the HVAC a modular structured simulation model is generated which provides access to the essential HVAC parameters. The simulation combines the HVAC system with a dynamic thermal vehicle model and includes operational and weather inputs. The vehicle model is obtained by a data-based system identification utilizing data from climatic wind tunnel experiments. Due to a gray-box modeling approach its parameters can be physically interpreted. Because of the small sampling time ($T_s = 10$ s) effects of transient switching operations can be observed. The holistic thermal simulation model is integrated in a user-friendly tool with graphical user interface (GUI). The tool enables an efficient processing of simulation data sets, visualization of time-domain results and computation of the annual energy consumption of the HVAC system. A tram line in Vienna was used to obtain real measurements for validation of the simulation model. The results of both short-time and long-time simulations yield realistic statements.

© 2014 Elsevier Ltd. All rights reserved.

1. Introduction

Urban rail plays an important role in reducing traffic volume, air pollution and energy consumption in urban areas. Nowadays,

increased thermal comfort demands of passengers require modern trams to be equipped with heating, ventilation and air conditioning (HVAC) units. These systems consume up to 30% of the total operational energy [1]. On the technical side, this poses the challenge of reducing the energy consumption for heating, ventilation and air conditioning, while still ensuring a comfortable indoor climate in the passenger cabin.

Analysis of data gathered from one tram during daily use over 13 months in Ghent (Belgium) revealed that it is possible to reduce

* Corresponding author. Tel.: +43 1 58801 325514.

E-mail addresses: christian.dullinger@tuwien.ac.at (C. Dullinger), walter.struckl@siemens.com (W. Struckl), martin.kozek@tuwien.ac.at (M. Kozek).

Nomenclature	
A_{shell}	surface of the vehicle's outer shell
C_{IDA}	heat capacity system 1
C_{VEH}	heat capacity system 2
c_i	volume fraction of CO ₂ in air mass/mass flow i (in ppmv)
$c_{p,a}, c_{p,l}, c_{p,v}$	specific heat capacity of dry air, liquid water, water vapor
c_s	weather class defining a season s
E_d	energy consumption for HVAC of the simulated day d
E_{dc}	energy consumption simulated day d in class c
$E_{\text{HVAC},c}$	energy consumption of one HVAC unit extrapolated for weather class c
$E_{i,dc}$	energy consumption of component i of simulated representative day d of class c
$E(k)$	overall electrical energy consumption of the HVAC system(s) up to time step k
E_y	annual energy consumption of the HVAC unit(s)
$E_{y,i}$	annual energy consumption for HVAC component i
H_c	number of days in class c
$h_{\text{H}_2\text{O},\text{COND}}$	specific enthalpy of the removed condensed water
h_m	specific enthalpy of the (wet) air mass/mass flow
k_{shell}	heat transfer coefficient (in W/m ² K)
K_{trans}	heat transfer coefficient between system 1 & system 2
\dot{m}_i	air mass flow i
$\dot{m}_{\text{H}_2\text{O},\text{COND}}$	mass flow of the removed condensed water
$P_{\text{COM},i}^{\text{m}}$	measured power consumption of compressor i
$P_i(k)$	power consumption of HVAC component i at time step k
$P(k)$	overall electrical power consumption of the HVAC system(s) at time step k
P_{SAF}	power consumption of the supply air fan
\dot{Q}_i	heat flow i
\dot{Q}_{light}	heat flow due to electric lighting
\dot{Q}_{rad}	heat flow entering passenger cabin due to sun radiation
\hat{q}_{rad}	radiation vector of the sun (in W/m ²)
$ \hat{q}_{\text{rad},sd}(k) $	magnitude of the sun radiation vector at time step k of day d in a weather class
\dot{Q}_{shell}	heat flow through the vehicle's outer shell
\dot{Q}_{veh}	heat flow between system 1 & system 2
$W_{t,\text{SAF}}$	power introduced by the supply air fan
$x_{\text{H}_2\text{O},i}$	water content of the wet air mass/mass flow i
x_{vi}	vapor content of the wet air mass/mass flow i
<i>Greek letters</i>	
$\epsilon(k \theta)$	prediction error vector (at time step k)
ϵ_{rad}	ratio of sun heat flow that enters the passenger cabin factor considering shading along the track
ϵ_{shad}	factor considering shading along the track
ϵ_{trans}	transmission factor of the vehicle
ϑ_i	temperature of the wet air mass/mass flow i
ϑ_{IDA}	indoor air temperature/temperature of C_{IDA}
ϑ_{set}	set point temperature
ϑ_{VEH}	temperature of C_{VEH}
<i>Subscripts</i>	
AC	air condition
BYP	bypass valve
COM	compressor
EHA	exhaust air
HB	heater battery
IDA	indoor air
MIA	mixed air
ODA	outdoor air
RCA	recirculation air
SAF	supply air fan
SUP	supply air

energy consumption of the HVAC systems and improve the thermal comfort of the passengers by using an outdoor air temperature dependent set point temperature, with estimated energy savings ranging from 15% to 42%, depending on the type of rolling stock, see Ref. [2]. In Ref. [3] a methodology and results of an experimental investigation in Newcastle upon Tyne (UK) is presented that aimed to assess the energy use of stabled rail vehicles also stating that on-board auxiliaries have a high potential for energy reduction. It was found that heating is responsible for the greatest portion of this consumption.

In order to identify such energy saving potentials existing systems can be examined in terms of changes in structure, components, materials, control software, and set point curves, respectively. However, the experimental implementation of such measures in operation is time-consuming and expensive. For these reasons a flexible simulation tool is of great value that enables investigating such measures with respect to the energy consumption and fulfillment of thermal comfort requirements.

The main contribution of this work is a validated dynamic ($T_s = 10$ s) thermal model and simulation tool for rail vehicles with:

- a modular and easy to parameterize HVAC model
- a data-based dynamic thermal vehicle model
- a user-friendly GUI for model parametrization, processing of real weather/route data, computation/visualization of time domain

signals and calculation of the annual energy consumption of the HVAC system

Thermal simulations of HVAC systems have long been state of the art in the automotive sector. A simplified and dynamic thermal model for the cabin of a car is proposed and validated in Ref. [4], which can be used for the design and testing of the HVAC system. The authors present a thermal model that is based on theoretical heat transfer, thermal inertia, and radiation treatment equations. Similar to the model presented in this work it consists of two heat capacities – one heat capacity is the indoor air and one heat capacity is the thermal inertia of the base elements (dashboard, seats and panels). However, the numerical values of these two heat capacities are obtained analytically and not from data. In Ref. [5] an exergy based simulation model for automotive vehicle HVAC operation is presented. The authors present a simulation tool (with a comprehensive GUI) of modular structure. Like the presented simulation tool of this work simulations are carried out in transient mode which makes it possible to evaluate the performance of various solutions for the thermal management of the vehicle. By this means, both tools avoid expensive experimental tests and permit the vehicle manufacturer to look at optimal solutions for vehicle's air conditioning. In Ref. [6] a completely dynamic thermal model of a vehicle's cabin validated under variable ambient conditions is presented. The authors show a lumped-parameter

thermal model of the passengers' compartment of a minibus that can help analyze capacity reduction actions for air-conditioning systems. However, a model of an air conditioning system is not yet integrated. In Ref. [7] a comparative analysis of an automotive air conditioning (AC) system operating with CO₂ and R134a is carried out using semi-theoretical cycle models. The authors use a complex model of the AC system that includes its components in detail. In contrast the simulation tool of this work uses a sufficiently accurate HVAC model which enables an efficient fast sampled simulation together with the thermal vehicle model. For the interested reader a review of modeling methods for HVAC systems is given in Ref. [8] and a review of alternative cooling technologies is given in Ref. [9].

For automotive applications the software package KULI can be used for simulating and optimizing the thermal management system [10]. It supports the engineer in setting up system components and control strategies regarding the optimization of performance, comfort, and operating reliability. In Ref. [11] the initial results of air conditioning, passenger compartment, and power electronics KULI models of an electric vehicle are presented. The authors assess various concepts for combining different system components and compare the performance to a baseline system. For rail vehicles a similar flexible thermal simulation tool like KULI is not known to the authors. Existing thermal simulation tools are either highly specialized for a specific rail vehicle and/or have a long sampling time. In Ref. [12] the dynamic cooling loads of the YZ_{25C} train compartment are investigated under the average ambient conditions during the hottest month. The authors show that using the Chinese national standard (TB1951-87) it is likely to overestimate the actual cooling load of a train, which can lead to a waste of energy. The air cycle refrigeration system used in Chinese train air conditioning engineering is investigated in Ref. [13]. The authors perform a sensitivity analysis of the thermodynamic model in order to identify parameters affecting system performance. In Ref. [14] the variation of cooling load in a compartment of a railway car is numerically investigated considering ambient and inside conditions, car speed, fresh air volume, solar time and the number of passengers. The authors claim that the simulations provide useful information concerning the different thermal loads.

The last three works have in common that they use a vehicle model obtained by a first-principles modeling approach tailored for a specific rail vehicle. As opposed to this, the vehicle model of the presented simulation tool is obtained by a data-based gray-box modeling approach. This simple second-order vehicle model with only four parameters (two heat capacities and two heat transfer coefficients) can adequately describe the thermodynamic behavior of different rail vehicles and is well suited for integration into fast sampled thermal simulations. It can be shown that the vehicle model can also be parametrized based on expertise if measurement data of the rail vehicle is not available for parameter identification. In the two prior works of the work group [15,16] an energy efficient design and simulation of a demand controlled heating and ventilation unit in a metro vehicle and a holistic thermal simulation model of a tram are presented, respectively.

In contrast to the aforementioned publications, a validated thermal simulation model comprising an HVAC model and a dynamic thermal vehicle model is presented in this work. The model is integrated in a user-friendly tool that enables an efficient processing of simulation data sets (real weather, route data, HVAC parameters, etc.), visualization of time-domain results (condition of indoor air, power and energy consumption, state of HVAC components, etc.) and computation of the annual energy consumption of the HVAC system.

The HVAC model is structured in modules, which enables a quick adaption to fit the structure of a real or fictitious HVAC

system, by adding, removing or changing the order of its components. For a given or fictitious rail vehicle the parametrization of the thermal vehicle model can be performed using the tool.

The remainder of this paper is structured as follows: In Sections 2 and 3 modeling of the vehicle and the HVAC is presented, respectively. In Section 4 preprocessing and parametrization within the thermal simulation tool is discussed. Simulation and visualization of time domain signals and the annual energy consumption of the HVAC units is described in Section 5. In Section 6 first a specific experiment in a climatic wind tunnel is described used for data-based vehicle parametrization. Then measurement data is obtained from a tram in Vienna and used for validation of the thermal simulation tool. In Section 7 the annual energy consumption needed for heating, ventilation and air conditioning of the ULF tram is obtained by extrapolating the energy consumption of nine simulated days. A summary and possible applications of the presented thermal simulation tool are discussed in Section 8 and an acknowledgment is given in Section 9.

2. Vehicle model

In the following basic equations of thermodynamics are utilized to derive the thermal vehicle model (Section 2.1), and a data-based method for its parametrization is presented (Section 2.2). The equations for computing humidity and CO₂ concentration of the indoor air are obtained in Sections 2.3 and 2.4, respectively.

2.1. Thermal vehicle model

Fig. 1 shows a schematic illustration of the thermal vehicle model. It is important to note that the thermal vehicle model is extracted from input–output data, and both the model order and the model parameters are a result from a mathematical optimization algorithm (see Section 2.2). If, however, a physical parameter interpretation is sought-after, the following model structure can be assumed: The thermal vehicle model consists of two subsystems (since it is a second-order system) defined by two system boundaries, which exchange the heat flow \dot{Q}_{veh} . System 1 has the heat capacity C_{IDA} (assumed constant) with temperature ϑ_{IDA} . System 2 has the heat capacity C_{VEH} with temperature ϑ_{VEH} .

The two heat capacities can be interpreted in the following way: The heat capacity C_{IDA} not only consists of the heat capacity of the indoor air, but also of the heat capacity of those parts of the passenger cabin which are in thermal equilibrium with the indoor air (presumably: seats, handholds, etc.). The heat capacity of the air inside the passenger cabin alone is not large enough to describe the dynamic behavior adequately. The heat capacity C_{VEH} consists of

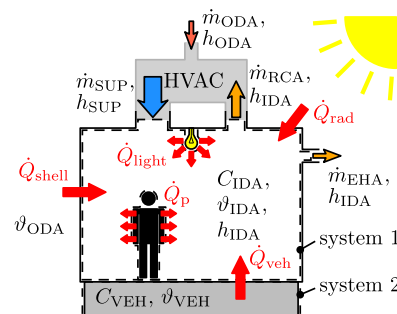


Fig. 1. Schematic illustration of the thermal vehicle model.

those parts of the vehicle which exchange heat with the heat capacity C_{IDA} , but do not have a heat exchange with the environment. By incorporating C_{VEH} into the vehicle model it significantly improves the dynamic behavior of the model. However, a clear assignment of vehicle masses to C_{VEH} is not possible since it is a parameter of a gray-box model.

The non-stationary energy balance for the open system 1 is given by

$$C_{IDA} \frac{d\vartheta_{IDA}}{dt} = \sum_i \dot{H}_i + \sum_j \dot{Q}_j \quad (1)$$

and the non-stationary energy balance for the closed system 2 is given by

$$C_{VEH} \frac{d\vartheta_{VEH}}{dt} = -\dot{Q}_{veh}. \quad (2)$$

In (1) $\sum_i \dot{H}_i$ is the sum enthalpy flow due to mass flows and $\sum_j \dot{Q}_j$ is the sum heat flow.

Assuming that the air mass inside the passenger cabin does not change (i.e. $dm/dt = 0$) the mass balance of air for system 1 is given by

$$0 = \dot{m}_{SUP} - \dot{m}_{RCA} - \dot{m}_{EHA}. \quad (3)$$

In (3) \dot{m}_{SUP} is the supply air (SUP) mass flow of the HVAC system, \dot{m}_{RCA} is the recirculation air (RCA) mass flow going back to the HVAC system and \dot{m}_{EHA} is the exhaust air (EHA) mass flow blown into the environment. Assuming a stationary mass balance for the combined system HVAC plus passenger cabin the latter equals the fresh air mass flow \dot{m}_{ODA} sucked in by the HVAC system:

$$\dot{m}_{EHA} = \dot{m}_{ODA} \quad (4)$$

By defining the fresh air ratio

$$\alpha = \frac{\dot{m}_{ODA}}{\dot{m}_{SUP}} \leq 1 \quad (5)$$

the exhaust air mass flow and the recirculation air mass flow can be computed by (6) and (7), respectively:

$$\dot{m}_{EHA} = \alpha \cdot \dot{m}_{SUP} \quad (6)$$

$$\dot{m}_{RCA} = (1 - \alpha) \cdot \dot{m}_{SUP} \quad (7)$$

The sum enthalpy flow due to mass flows in (1) is given by

$$\sum_i \dot{H}_i = \dot{m}_{SUP} \cdot h_{SUP} - \dot{m}_{RCA} \cdot h_{IDA} - \dot{m}_{EHA} \cdot h_{IDA}. \quad (8)$$

In (8) h_{SUP} is the specific enthalpy of the supply air and h_{IDA} is the specific enthalpy of the indoor air. In this work specific enthalpies of air are computed applying the formula for wet air given by

$$h_m = (c_{p,a} + x_{v,m} \cdot c_{p,v} + x_{l,m} \cdot c_{p,l}) \cdot \vartheta_m + x_{v,m} \cdot r_0. \quad (9)$$

In (9) $c_{p,a}$, $c_{p,v}$ and $c_{p,l}$ are the assumed constant specific heat capacities of dry air, water vapor and liquid water, respectively. The quantities $x_{v,m}$ and $x_{l,m}$ denote the vapor content and the liquid water content. In (9) r_0 is the enthalpy of evaporation and ϑ_m is the temperature in degrees Celsius. The water content of the wet air mass is given by

$$x_{H_2O,m} = x_{v,m} + x_{l,m} \quad (10)$$

The sum heat flow in (1) is given by

$$\sum_j \dot{Q}_j = \dot{Q}_{shell} + \dot{Q}_{veh} + \dot{Q}_{rad} + \dot{Q}_p + \dot{Q}_{light}. \quad (11)$$

The heat flow through the outer shell of the vehicle \dot{Q}_{shell} is given by

$$\dot{Q}_{shell} = k_{shell} \cdot A_{shell} \cdot (\vartheta_{ODA} - \vartheta_{IDA}). \quad (12)$$

It is driven by the temperature difference between the outdoor air (ODA) temperature ϑ_{ODA} and the indoor air (IDA) temperature ϑ_{IDA} . The heat transfer coefficient k_{shell} (in W/m^2) is a key parameter obtained by manufacturer's software tools or by climatic wind tunnel experiments. In (12) A_{shell} denotes the surface of the vehicle's outer shell.

The heat flow \dot{Q}_{veh} (i.e. the heat transfer) driven by the temperature difference between the two heat capacities C_{IDA} and C_{VEH} is described by

$$\dot{Q}_{veh} = K_{trans} \cdot (\vartheta_{VEH} - \vartheta_{IDA}). \quad (13)$$

In (13) K_{trans} can be interpreted as the product of the heat transfer coefficient between the heat capacity C_{VEH} and the passenger cabin and the surface through which this heat is exchanged. However, a split-up in these two multipliers is not reasonable since neither the surface nor the heat transfer coefficient can be properly chosen as K_{trans} is parametrized by a gray-box identification (see Section 2.2).

For considering the heat flow entering the passenger cabin due to sun radiation \dot{Q}_{rad} the following approach was chosen: The vehicle is simplified to a cuboid depicted in Fig. 2. Equation (14) describes the radiation vector of the sun with magnitude $|\dot{q}_{rad}|$ (in W/m^2) in the frame of reference of the moving vehicle:

$$\dot{q}_{rad}^T = |\dot{q}_{rad}| \cdot [|\cos\beta\cos\alpha| \quad |\cos\beta\sin\alpha| \quad |\sin\beta|] \quad (14)$$

with that defined \dot{Q}_{rad} is given by

$$\dot{Q}_{rad} = \underbrace{\epsilon_{shad} \cdot \epsilon_{trans}}_{\epsilon_{rad}} \cdot \dot{q}_{rad}^T \cdot A_{rad}. \quad (15)$$

with

$$A_{rad} = \begin{bmatrix} h \cdot w \\ h \cdot l \\ l \cdot w \end{bmatrix}. \quad (16)$$

In (15) the factor $\epsilon_{rad}(kT_s) < 1$ is the ratio between the heat flow that actually enters the passenger cabin and the incoming heat flow. It is

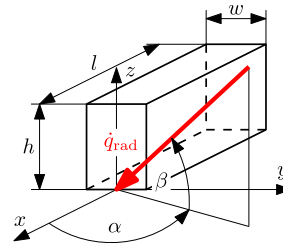


Fig. 2. Vehicle model for considering radiation input from the sun \dot{q}_{rad} .

620

C. Dullinger et al. / Applied Thermal Engineering 78 (2015) 616–629

the product of the time function $\varepsilon_{\text{shad}}(kT_s)$ which allows to consider shading along the track and the assumed constant transmission factor of the vehicle $\varepsilon_{\text{trans}}$, which can be used to study the effects of anti-radiation measures like radiation reflecting paints or films.

In (11) \dot{Q}_p is the emitted sensible heat of the passengers. It is computed by

$$\dot{Q}_p = \dot{Q}_{\text{sensible}} \cdot n_p, \quad (17)$$

where n_p is the number of passengers and $\dot{Q}_{\text{sensible}}$ is the sensible heat emitted by one person which is given by

$$\dot{Q}_{\text{sensible}} = \dot{Q}_{\text{human}} - \dot{Q}_{\text{latent}}. \quad (18)$$

Equation (17) does not consider the latent heat \dot{Q}_{latent} because state of the art vehicles are equipped with HVAC units which ensure that water vapor does not condense inside the passenger cabin. Therefore, this part of the emitted heat is transferred out of the passenger cabin and does not contribute to the heat inside the vehicle.

In (18) the total emitted heat of one person $\dot{Q}_{\text{human}} = 120\text{W}$ was assumed to be independent of the indoor air temperature, whereas the latent heat of one person was approximated using the piecewise linear function (see Ref. [17])

$$\dot{Q}_{\text{latent}}(\vartheta_{\text{IDA}}) = \begin{cases} 20 & \vartheta_{\text{IDA}} < 18 \\ \frac{10}{3}\vartheta_{\text{IDA}} - 40 & 18 \leq \vartheta_{\text{IDA}} < 24 \\ 5\vartheta_{\text{IDA}} - 80 & 24 \leq \vartheta_{\text{IDA}} < 35 \\ 95 & 35 \leq \vartheta_{\text{IDA}} \end{cases}. \quad (19)$$

In (11) \dot{Q}_{light} is heat flow due to electric lighting given by

$$\dot{Q}_{\text{light}} = (1 - \eta_{\text{lamp}}) \cdot P_{\text{lamp}} \cdot n_{\text{lamp}}, \quad (20)$$

where η_{lamp} and P_{lamp} are the efficiency and the electrical power consumption of one lamp and n_{lamp} is the number of lamps.

2.2. Parametrization of the thermal vehicle model based on measured data

Omitting $\sum \dot{H}_i^{(m)}$, \dot{Q}_{rad} , \dot{Q}_p , and \dot{Q}_{light} as external inputs in Fig. 1 and additionally considering the heat flow of specific heaters and fans (temporary) installed in the passenger cabin \dot{Q}_{hf} , see Fig. 3, the non-stationary energy balance for system 1 changes to

$$C_{\text{IDA}} \frac{d\vartheta_{\text{IDA}}}{dt} = \dot{Q}_{\text{shell}} + \dot{Q}_{\text{veh}} + \dot{Q}_{\text{hf}}. \quad (21)$$

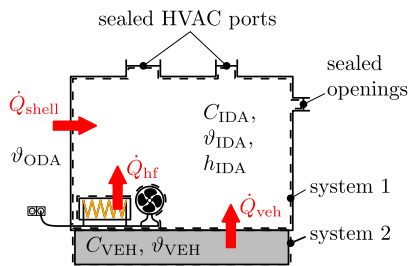


Fig. 3. Schematic illustration of the relevant influencing factors for the experiment performed in the climatic wind tunnel (CWT) utilized to obtain measurement data for parameter estimation of the thermal vehicle model.

By choosing the state vector $\mathbf{x} = [\vartheta_{\text{IDA}} \quad \vartheta_{\text{VEH}}]^T$ and defining $\mathbf{u} = [\vartheta_{\text{ODA}} \quad \dot{Q}_{\text{hf}}]^T$ and $y = \vartheta_{\text{IDA}}$ as input vector respectively output, the differential Equations (21) and (2) can be represented by the linear state-space system

$$\dot{\mathbf{x}} = \underbrace{\begin{bmatrix} \frac{K_{\text{trans}} + k_{\text{shell}} \cdot A_{\text{shell}}}{C_{\text{IDA}}} & \frac{K_{\text{trans}}}{C_{\text{IDA}}} \\ \frac{K_{\text{trans}}}{C_{\text{VEH}}} & -\frac{K_{\text{trans}}}{C_{\text{VEH}}} \end{bmatrix}}_{\mathbf{A}} \mathbf{x} + \underbrace{\begin{bmatrix} \frac{k_{\text{shell}} \cdot A_{\text{shell}}}{C_{\text{IDA}}} & \frac{1}{C_{\text{IDA}}} \\ 0 & 0 \end{bmatrix}}_{\mathbf{B}} \mathbf{u} \quad (22)$$

$$y = \underbrace{[1 \quad 0]}_{\mathbf{C}} \mathbf{x}. \quad (23)$$

Note that (22) reflects the structural assumptions made in Section 2.1, and ϑ_{VEH} and C_{VEH} are fictitious quantities which guarantee an accurate model. Utilizing measurement data obtained by a specific experiment (see Section 6.1) in a climatic wind tunnel the parameters of the state-space system (22) can be identified by applying the Prediction Error Method (PEM) [18] according to the following criterion

$$J(\theta) = \mathbf{e}^T \mathbf{e} \rightarrow \min_{\theta}, \quad (24)$$

where

$$\mathbf{e} = \begin{bmatrix} \varepsilon(k|\theta) \\ \vdots \\ \varepsilon(k+N-1|\theta) \end{bmatrix} \text{ with } \varepsilon(k|\theta) = y(k) - \hat{y}(k|\theta). \quad (25)$$

In (25) $\varepsilon(k|\theta)$ is the prediction error (at time step k), which is the difference between the measured output $y(k)$ and the predicted output of the model $\hat{y}(k|\theta)$. With $K_{\text{shell}} = k_{\text{shell}} \cdot A_{\text{shell}}$ the parameter vector is defined as

$$\theta = [K_{\text{trans}} \quad K_{\text{shell}} \quad C_{\text{IDA}} \quad C_{\text{VEH}}]^T \quad (26)$$

and N is the number of training data samples. For minimizing the cost function given in (24) PEM uses numerical optimization algorithms, see Refs. [18,19].

2.3. Humidity of the indoor air

In order to compute the specific enthalpy of the (wet) indoor air h_{IDA} , using Equation (9) for wet air, the quantities $x_{v,\text{IDA}}$ and $x_{\text{H}_2\text{O},\text{IDA}}$ have to be computed by the vehicle model. With the assumption that air in the passenger cabin always stays in the region of unsaturated air (i.e. $x_{\text{H}_2\text{O},\text{IDA}} = 0$) the water content of the indoor air is given by

$$x_{\text{H}_2\text{O},\text{IDA}} = x_{v,\text{IDA}}. \quad (27)$$

For the passenger cabin the non-stationary mass balance for water is given by

$$\rho_{\text{air}} \cdot V_{\text{cabin}} \cdot \frac{dx_{\text{H}_2\text{O},\text{IDA}}}{dt} = \sum_i \dot{m}_{\text{H}_2\text{O},i}, \quad (28)$$

with

$$\sum_i \dot{m}_{\text{H}_2\text{O},i} = \dot{m}_{\text{SUP}} \cdot (x_{\text{H}_2\text{O},\text{SUP}} - x_{\text{H}_2\text{O},\text{IDA}}) + \dot{m}_{\text{H}_2\text{O},\text{human}} \cdot n_p \quad (29)$$

In (28) V_{cabin} is the volume of the passenger cabin and ρ_{air} is the density of air. For simplicity ρ_{air} is assumed constant. In (29)

$\dot{m}_{\text{H}_2\text{O, human}}$ is the mass of water due to one person's perspiration. It is computed by

$$\dot{m}_{\text{H}_2\text{O, human}}(\vartheta_{\text{IDA}}) = \frac{\dot{Q}_{\text{latent}}(\vartheta_{\text{IDA}})}{r_0}, \quad (30)$$

where r_0 is the enthalpy of evaporation of water.

2.4. CO₂ concentration of the indoor air

In order to be able to study the effects of CO₂ based control strategies on the energy consumption of the HVAC system, the vehicle model additionally computes the CO₂ concentration of the indoor air.

For the passenger cabin the non-stationary mass balance for CO₂ is given by

$$\frac{\mathcal{M}_{\text{CO}_2}}{\mathcal{M}_{\text{air}}} \cdot \rho_{\text{air}} \cdot V_{\text{cabin}} \cdot \frac{dc_{\text{IDA}}}{dt} = \sum_i \dot{m}_{\text{CO}_2, i}, \quad (31)$$

where c_{IDA} is the volume fraction of CO₂ in air (in ppmv) inside the passenger cabin. The molar mass of air and CO₂ is $\mathcal{M}_{\text{air}} = 28.97$ kg/kmol and $\mathcal{M}_{\text{CO}_2} = 44.01$ kg/kmol, respectively. The sum mass flow of CO₂ $\sum \dot{m}_{\text{CO}_2, i}$ in (31) is given by

$$\sum_i \dot{m}_{\text{CO}_2, i} = \frac{\mathcal{M}_{\text{CO}_2}}{\mathcal{M}_{\text{air}}} \cdot \dot{m}_{\text{SUP}} \cdot (c_{\text{SUP}} - c_{\text{IDA}}) + \dot{m}_{\text{CO}_2, \text{human}} \cdot n_p. \quad (32)$$

In (32) c_{SUP} and $\dot{m}_{\text{CO}_2, \text{human}}$ denote the volume fraction of CO₂ in the supply air (SUP) and the CO₂ production rate of one person ($\dot{m}_{\text{CO}_2, \text{human}} = 6 \cdot 10^{-6}$ kg/s), respectively.

3. HVAC model

The thermal simulation utilizes a modular structured HVAC model. This approach enables a quick adaption of the HVAC model to fit the structure of a different (real or fictitious) HVAC system, by adding, removing or changing the order of its components. By this means novel ideas in air-conditioning technology of rail vehicles, like adding a heat pump, can be investigated in terms of energy consumption and fulfillment of thermal comfort criteria with a temporal resolution of only 10 s.

Fig. 4 shows a schematic illustration of the HVAC system implemented in the Ultra Low Floor (ULF) tram used for validation of the thermal simulation model.

The air conditioning unit of the ULF Tram uses the refrigerant fluid R407C. Since the simulation tool does not utilize a dynamic model of the vapor compression plant (see Remark in Section 3.2), the refrigerant fluid respectively its physical/chemical properties are not an input to the simulation tool. The focus of this work is not

a detailed HVAC model, but a sufficiently accurate HVAC model which enables an efficient fast sampled simulation together with the thermal vehicle model.

For HVAC units there is no European regulation that specifies which tests have to be carried out for a mobile air conditioning plant. However, client and contractor agree on which standardized tests (e.g. fire safety regulation test, IP-classification, etc.) to be performed.

For the components of the HVAC unit depicted in Fig. 4 the energy balances, mass balances for air, water and CO₂, respectively, are obtained in the following.

3.1. Mixing chamber

In the mixing chamber the fresh outdoor air (ODA) mass flow \dot{m}_{ODA} is isobarically mixed with the recirculation air (RCA) mass flow \dot{m}_{RCA} from the vehicle interior. The stationary mass balances for air, water and CO₂ is given by

$$0 = \dot{m}_{\text{ODA}} + \dot{m}_{\text{RCA}} - \dot{m}_{\text{MIA}}, \quad (33)$$

$$0 = \dot{m}_{\text{ODA}} \cdot x_{\text{H}_2\text{O, ODA}} + \dot{m}_{\text{RCA}} \cdot x_{\text{H}_2\text{O, IDA}} - \dot{m}_{\text{MIA}} \cdot x_{\text{H}_2\text{O, MIA}}, \quad (34)$$

and

$$0 = \frac{\mathcal{M}_{\text{CO}_2}}{\mathcal{M}_{\text{air}}} \cdot (\dot{m}_{\text{ODA}} \cdot c_{\text{ODA}} + \dot{m}_{\text{RCA}} \cdot c_{\text{IDA}} - \dot{m}_{\text{MIA}} \cdot c_{\text{MIA}}), \quad (35)$$

respectively. The stationary energy balance is given by

$$0 = \dot{m}_{\text{ODA}} \cdot h_{\text{ODA}} + \dot{m}_{\text{RCA}} \cdot h_{\text{IDA}} - \dot{m}_{\text{MIA}} \cdot h_{\text{MIA}}. \quad (36)$$

3.2. Refrigerating machine

In the refrigerating machine the heat flow \dot{Q}_{AC} is isobarically withdrawn from the wet air mass flow. If due to cooling the temperature ϑ_{AC} of the wet air mass flow falls below the dew point $\vartheta_{\text{dew}}(x_{\text{H}_2\text{O, MIA}})$ the condensate is removed. Thus, the air mass flow leaving the air condition in this case is in the state of saturated air, with water content $x_{\text{H}_2\text{O, AC}} = x_{\text{v, AC}}$ and temperature $\vartheta_{\text{AC}} = \vartheta_{\text{dew}}(x_{\text{H}_2\text{O, AC}})$.

The stationary mass balance of air is given by

$$0 = \dot{m}_{\text{MIA}} - \dot{m}_{\text{AC}}. \quad (37)$$

The stationary energy balance is given by

$$0 = \dot{m}_{\text{MIA}} \cdot h_{\text{MIA}} - \dot{m}_{\text{AC}} \cdot h_{\text{AC}} - \dot{m}_{\text{H}_2\text{O, COND}} \cdot \underbrace{c_{\text{p, l}} \cdot \vartheta_{\text{AC}}}_{h_{\text{H}_2\text{O, COND}}} - \dot{Q}_{\text{AC}}, \quad (38)$$

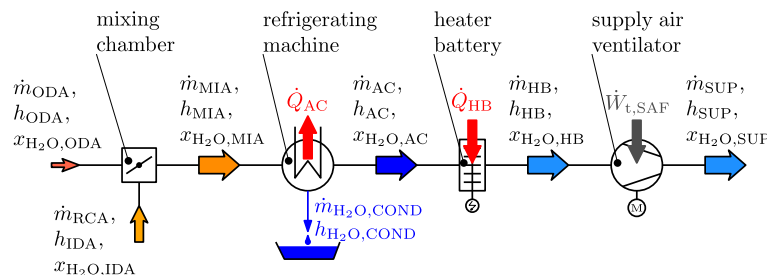


Fig. 4. Schematic illustration of the HVAC systems implemented in the Ultra Low Floor (ULF) trams in Vienna.

622

C. Dullinger et al. / Applied Thermal Engineering 78 (2015) 616–629

where $\dot{m}_{\text{H}_2\text{O,COND}}$ is the mass flow of the removed condensed water obtained by

$$\dot{m}_{\text{H}_2\text{O,COND}} = x_{\text{H}_2\text{O,MIA}} \cdot \dot{m}_{\text{MIA}} - x_{\text{H}_2\text{O,AC}} \cdot \dot{m}_{\text{AC}} \quad (39)$$

If no condensation takes place, $\dot{m}_{\text{H}_2\text{O,COND}} = 0$.

Remark: The HVAC model is a static model. The behavior of the vapor compression plant is described by its coefficient of performance (COP). The COP is given via a characteristic diagram specified by one of the user defined numerical look-up tables (see Section 4.3). This modeling approach assumes that all transient phenomena in the refrigerating circle decay faster than the sampling time $T_s = 10$ s so that a steady state is reached between two sampling instances.

3.3. Heater battery

In the heater battery the heat flow \dot{Q}_{HB} is isobarically introduced to the wet air mass flow. The stationary mass balance of air and the stationary energy balance are given by

$$0 = \dot{m}_{\text{AC}} - \dot{m}_{\text{HB}} \quad (40)$$

and

$$0 = \dot{m}_{\text{AC}} \cdot h_{\text{AC}} - \dot{m}_{\text{HB}} \cdot h_{\text{HB}} + \dot{Q}_{\text{HB}}, \quad (41)$$

respectively.

3.4. Supply air ventilator

The supply air ventilator delivers the conditioned air to the passenger cabin. Its stationary mass balance of air is given by

$$0 = \dot{m}_{\text{HB}} - \dot{m}_{\text{SUP}} \quad (42)$$

The stationary energy balance is given by

$$0 = \dot{W}_{\text{L,SAF}} + \dot{m}_{\text{HB}} \cdot h_{\text{HB}} - \dot{m}_{\text{SUP}} \cdot h_{\text{SUP}}, \quad (43)$$

where $\dot{W}_{\text{L,SAF}}$ is the power introduced to the air mass flow by the supply air fan.

3.5. HVAC controller

The HVAC controller of the ULF trams of Vienna is modeled as hierarchically structured finite state machine (FSM), which operates on two different levels, see Fig. 5. This effectively constitutes a rule based control with well-defined switching transitions between constant operating modes.

This approach was considered best to describe the logic circuit implemented by the HVAC manufacturer. Furthermore, this method enables a broad application of the presented simulation tool and ensures an easy modification of an implemented control strategy by the user. Background on FSM is found in Refs. [20–22].

On the top level the controller of the HVAC unit consists of one finite state machine. It is used to model the so called “global state” of the HVAC system. In case of modeling the HVAC system implemented in the ULF trams the state machine on the top level consists of the three global states, “electrical heating”, “cooling”, and “initialization”, respectively.¹ If necessary to describe a given HVAC

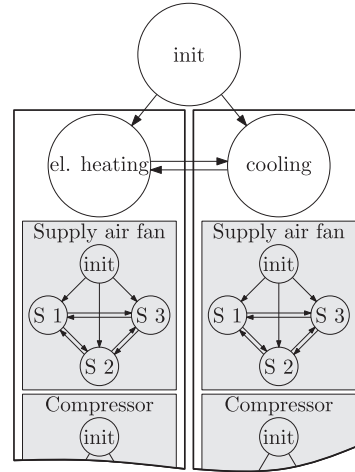


Fig. 5. Excerpt of the FSM used for modeling the HVAC controller of an ULF tram (with global states electrical heating and cooling).

system adequately additional global states like “dehumidifying”, “heating with heat pump”, “ventilation” and so on, can be added to the state machine on the top level by the user. On the bottom level the controller consists of a variety of finite state machines each describing an HVAC component within a global state, see Fig. 5. The top level FSM and the bottom level FSMs are in only one state at a time, the so called “current state”. For each FSM, at each time step k all transitions of the “current state” are evaluated. The state is changed from one state to another when the corresponding transition leading there (from the “current state”) is logically “true”. If all transitions leading away from the “current state” are logically “false” the state of the FSM is not changed. The transitions of the FSMs are updated at each time step k . The transitions are logical expressions of constants (numerical values assigned by the user) and variables of the simulation model updated in each time step k (like the indoor air temperature ϑ_{IDA} , the outdoor air temperature ϑ_{ODA} , the set point temperature $\vartheta_{\text{set}}(\vartheta_{\text{ODA}})$, the state of some component, the time spent in the same state of some component, etc.).

Remark: In principle all variables computed by the simulation model can be used in the transitions of the FSMs. By this means it is possible to perform case studies like a CO_2 dependent control of the fresh air mass flow \dot{m}_{ODA} or test other novel control strategies.

4. Preprocessing and parametrization

The simulation tool is a software with a user friendly graphical user interface (GUI) that is suitable for the efficient processing of data sets, with the ultimate goal to obtain the annual energy consumption needed for the HVAC system of a (light) rail vehicle.

Fig. 6 depicts the work flow of the simulation tool, described in the following sections.

4.1. Vehicle parametrization

The parametrization of a vehicle by its heat capacities and heat transfer coefficients (see Section 2.1) can be performed in three different ways:

¹ By switching off the heater battery the HVAC system of the ULF trams also uses the “heating” mode for pure ventilation.

1. If measurement data from a climatic wind tunnel experiment are available they can be imported to the simulation tool. Then the Prediction Error Method (PEM) (see Section 2.2) can be performed to obtain an estimate of the vehicle parameters. The PEM is applied on the training data to update the parameters of the initial parametrized linear state-space model (22).
2. Experiments on different rail vehicle classes (e.g. light rail, heavy rail, etc.) in the climatic wind tunnel of Vienna and the identification of the before mentioned parameters utilizing the presented simulation tool revealed that the parameters of distinct classes constitute separate clusters in parameter space. Therefore, for brand new vehicles or vehicles in the construction phase – with no measurements available yet – the following approach for parametrization can be performed: (i) Association of the vehicle to a rail vehicle class. (ii) Parametrization based on gathered expertise of the parameters of the vehicle class.
3. If the parameters of the linear state-space model (22) can be extracted from sophisticated numerical calculation programs (e.g. ANSYS[®] Fluent[®]) the presented tool enables a direct parametrization.

4.2. Configuration of the HVAC controller

In order to model a given HVAC system the user can choose between six “global states” by selecting the corresponding check boxes of the GUI. The available “global states” are: (i) heating with heat pump, (ii) electrical heating, (iii) electrical heating plus heating with heat pump, (iv) ventilation, (v) cooling, (vi) dehumidifying.

In the next step the user specifies for each HVAC component the number of its different states. For instance, the supply air fan (SAF) of the ULF HVAC system can be adjusted in three steps, thus the FSM used for modeling this component consists of three states (plus one initialization state). A check box for each component allows to specify if the transition of the component FSM depends on the “global state” of the HVAC or not. The predefined HVAC components are: (i) supply air fan, (ii) compressor, (iii) bypass valve of the compressor, (iv) heater battery, (v) mixing chamber.

Due to the modular structure of the HVAC model additional components can be added easily. For convenience templates for entering the transitions are generated automatically by the software tool for all FSMs.

4.3. Configuration of the HVAC parameters

For each component the tool automatically generates an empty table, which rows correspond to the states of the respective component. Additionally to the power consumption at a given state, other quantities like mass flows, heating power, cooling power, etc. have to be entered in these numerical look-up tables (LUTs). If the parameters of a component depend on the “global state” of the HVAC additional LUTs are provided for that component (by selecting a check box).

4.4. Processing of weather data

Because real weather data is frequently not available with a temporal resolution of only ten seconds the imported weather data (.csv or.xls data) are linearly interpolated by the software. A comprehensive meteorological database for Austria is provided by Ref. [23]. The simulation tool utilizes the following weather data:

- water content of the outdoor air $x_{\text{H}_2\text{O,ODA}}$ (in $\text{g}_{\text{H}_2\text{O}}/\text{kg}_{\text{air}}$)
- temperature of the outdoor air ϑ_{ODA} (in °C)
- sun radiation $|\dot{q}_{\text{rad}}|$ (in W/m^2 , see Fig. 2)

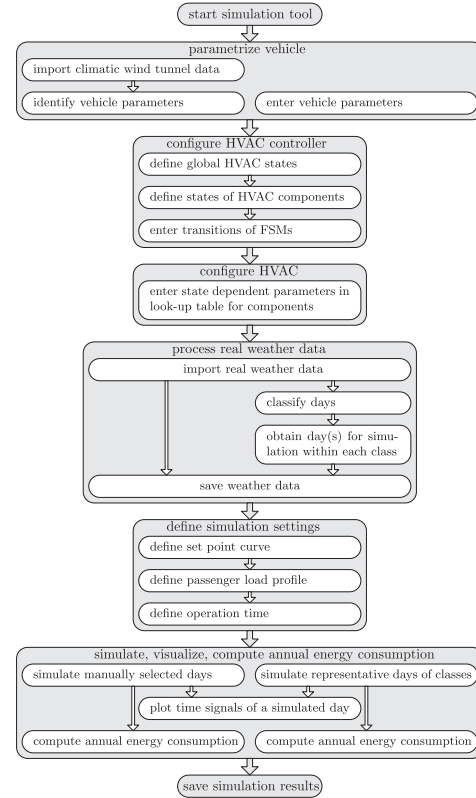


Fig. 6. Work flow of the simulation tool.

- cloud cover $\varepsilon_{\text{shad}}$

In order to obtain a fast estimate of the annual energy consumption (of the HVAC system), the simulation tool provides the possibility to perform the calculation based on only a few representative days of a year. The method to obtain these representative days is described in the following.

Utilizing an upper and a lower threshold on the maximum measured temperature, a day d is classified as summer, winter or autumn/spring day, respectively. Then each of those three classes c_s (defining a season s) is divided into three subclasses by applying an upper and a lower threshold φ_{sunny} and $\varphi_{\text{overcast}}$, respectively:

$$d \in \begin{cases} c_{s,\text{sunny}} & \varphi_{sd} \geq \varphi_{\text{sunny}} \\ c_{s,\text{cloudy}} & \varphi_{\text{overcast}} \leq \varphi_{sd} \leq \varphi_{\text{sunny}}, \quad \forall d \in c_s \\ c_{s,\text{overcast}} & \varphi_{sd} \leq \varphi_{\text{overcast}} \end{cases} \quad (44)$$

with

$$\varphi_{sd} = \frac{\sum_k |\dot{q}_{\text{rad},sd}(k)|}{\sum_k (\max_d |\dot{q}_{\text{rad},sd}(k)|)}, \quad (45)$$

where $|\dot{q}_{\text{rad},sd}(k)|$ is the magnitude of the sun radiation vector at time step k of day d in the class c_s defined by the maximum temperature.

The representative day(s) within each class are obtained as follows: Utilizing weights the user has the possibility to define the relative importance of stochastic parameters – mean and variance of the time signals temperature, radiation and humidity, respectively – on the energy consumption of the HVAC system. Each day of the investigated class is then represented by a point in an up to 6-dimensional hyperspace. The clustering algorithm K-Means (see Ref. [24]) with squared Euclidean distance measure is used to obtain the centroid of that point cloud. Then the day which is closest to that centroid in terms of the squared Euclidean distance is chosen as simulation day for that class.

By also taking the variance of a signal into account it is guaranteed that the selected day's variance is close to average variance of the days in the class. Due to the switching behavior of the HVAC system (alternating heating and cooling periods) the variance of the temperature is expected to have a major impact on the energy consumption.

4.5. Defining the simulation settings

4.5.1. Outdoor air temperature dependent set point temperature

The simulation tool enables to specify the set point temperature of the indoor air temperature as a piecewise linear function of the outdoor air temperature, i.e. during simulation the set point temperature of the indoor air at time step k is given by

$$\vartheta_{\text{set}} = \vartheta_{\text{set}}(\vartheta_{\text{ODA}}(kT_s)). \tag{46}$$

4.5.2. Passenger load profile and operation time

The passenger load profile as a function of time $n_p(kT_s)$ can be defined in the simulation tool or loaded from an Excel file. In case of a real measurement signal of the passenger volume available the simulation tool can be easily adapted to incorporate this information. The time of operation defines which part of a day is to be simulated.

5. Simulation, visualization and computation of the annual energy consumption

After all settings are defined an arbitrary number of manually selected days or the representative days of the classified days (see Section 4.4) can be simulated. Fig. 7 shows the GUI used for simulation, visualization, and computation of the annual energy consumption.

The simulation procedure and its results (fast sampled time signals) is described in Sections 5.1 and 5.2, respectively. Section 5.3 deals with the computation of the annual energy consumption of one HVAC unit.

5.1. Simulation

Depending on the “current state” of an HVAC component its parameters are selected from the corresponding look-up table (LUT) (taking into account the “global state” of the HVAC system). Together with the dynamically calculated variables describing the state of the indoor air ($\vartheta_{\text{IDA}}(k)$, $x_{\text{H}_2\text{O,IDA}}(k)$, $c_{\text{IDA}}(k)$) (of the thermal vehicle model) and the variables describing the state of the outdoor air ($\vartheta_{\text{ODA}}(k)$, $x_{\text{H}_2\text{O,ODA}}(k)$, $c_{\text{ODA}}(k)$) at time step k the parameters of these LUTs are utilized for evaluating the HVAC model at time step k . Then the thermal vehicle model is updated. Applying the variables describing the state of the supply air (SUP) ($\vartheta_{\text{SUP}}(k)$, $m_{\text{SUP}}(k)$, $x_{\text{H}_2\text{O,SUP}}(k)$, $c_{\text{SUP}}(k)$) as inputs to the state-space model of the vehicle and considering the disturbances (see Fig. 1) at time step k the state vector at time step $k + 1$

$$\mathbf{x}(k + 1) = \begin{bmatrix} \vartheta_{\text{IDA}}(k + 1) \\ \vartheta_{\text{VEH}}(k + 1) \\ c_{\text{IDA}}(k + 1) \\ x_{\text{H}_2\text{O,IDA}}(k + 1) \end{bmatrix} \tag{47}$$

is computed. Then the calculation is repeated for the next time step $k + 1$. Note that no numerical integration is carried out, as all model parts are discrete-time.

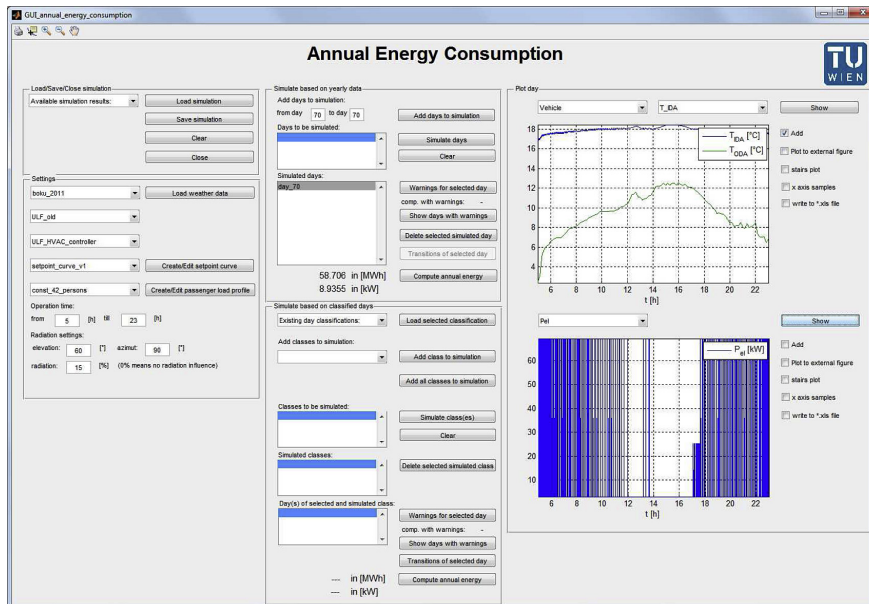


Fig. 7. GUI used for simulation, visualization, and computation of the annual energy consumption.

The power consumption $P_i(k)$ of an HVAC component i at time step k is also obtained from the corresponding look-up table (LUT). The look-up table for the supply air fan (SAF) (of the HVAC system implemented in the ULF trams of Vienna), which is independent of the “global state” is exemplarily shown in Table 1.

5.2. Visualization

After the simulation stopped the tool enables an easy visualization of the computed discrete time signals by selecting them in a pop-up menu. For each simulated day the following signals are available for visualization:

- state of the indoor air ($\vartheta_{IDA}(k)$, $c_{IDA}(k)$, $x_{H_2O,IDA}(k)$) and fictitious temperature $\vartheta_{VEH}(k)$
- set point temperature ($\vartheta_{set}(k)$)
- mass flow and state of the supply air ($\dot{m}_{SUP}(k)$, $h_{SUP}(k)$, $\vartheta_{SUP}(k)$, $c_{SUP}(k)$, $x_{H_2O,SUP}(k)$)
- electrical power consumption of each HVAC component i ($P_i(k)$)
- overall electrical power consumption of the HVAC system(s) ($P(k)$)
- overall electrical energy consumption of the HVAC system(s) up to time step k ($E(k)$)
- “global state” of the HVAC System and states of HVAC components

5.3. Computation of the annual energy consumption of one HVAC unit

For a given day d , the energy consumed by the HVAC system up to the time kT_s is computed by

$$E_d(kT_s) = \sum_{n=0}^{k-1} \left(\sum_i P_i(nT_s) \right) \cdot T_s, \quad (48)$$

where $P_i(nT_s)$ is the power consumption of the HVAC component i at time instance n ($T_s = 10$ s is the sampling time).

The annual energy consumption based on manually selected days is obtained by

$$E_y = 365 \cdot \frac{1}{n_d} \sum_{d=1}^{n_d} E_d, \quad (49)$$

where E_d is the energy consumption of the simulated day d and n_d is the number of simulated days.

The possibility to simulate an arbitrary number of manually selected days enables the user to compute the annual energy consumption by simulating all 365 days of a year. However, this is time consuming (i.e. about 12 h on an up to date standard laptop).

The approach of simulating only the representative days of the classified days (see Section 4.4) is well suited to obtain quick results (for the annual energy consumption) for different case scenarios. The annual energy consumption based on classified days is computed by

Table 1
Look-up table of the supply air fan (SAF) (HVAC system of ULF trams).

State of FSM for SAF	P_{SAF} in W	\dot{m}_{SUP} in kg/s
S 1	570	0.283
S 2	1050	0.383
S 3	1380	0.517
Init	0	0

$$E_y = \frac{365}{\sum_{c=1}^{n=9} H_c} \sum_{c=1}^{n=9} \left(H_c \cdot \frac{1}{n_c} \sum_{d=1}^{n_c} E_{dc} \right), \quad (50)$$

where E_{dc} is the energy consumption of the simulated day d in class c , n_c is the number of simulated days in class c and H_c is the number of days in class c (and $n = 9$ is the number of classes).

6. Measurements and validation

In Section 6.1 the specific experiment in a climatic wind tunnel required for the parametrization of the thermal vehicle model (see Section 2.2) is described. In Section 6.2 the measurement campaign used for validation of the simulation tool is presented. A validation based on a specific day is shown in Section 6.3.

6.1. Climatic wind tunnel experiments

The experiment performed in the climatic wind tunnel utilized for the gray-box identification of the vehicle parameters is described in the following (see also Fig. 3). The temperature in the climatic wind tunnel (i.e. ϑ_{ODA}) is set to 5 °C and all doors of the vehicle are opened. Then it is waited until a steady state is reached, i.e. until all temperature measuring points, measuring air temperatures (mean value is assigned to ϑ_{IDA}) or surface temperatures inside the vehicle (within a particular tolerance) measure 5 °C. Then all doors are closed and utilizing heaters and fans the electric power $P_{hf} = 15$ kW ($\dot{Q}_{hf} = P_{hf}$) is introduced to the passenger cabin for six hours, and ϑ_{IDA} is continuously measured.

6.2. Validation measurements

Within the framework of the research project “EcoTram” an Ultra Low Floor tram was equipped with measuring equipment. The so-equipped tram was subjected to various tests in the climatic wind tunnel (see Fig. 8). Then this vehicle was put into passenger service from 01.09.2010 till 31.08.2011 gathering information about weather conditions around the vehicle (temperature, relative humidity, sun radiation), power consumption of the HVAC components, state of the indoor air (temperature, relative humidity, CO₂ concentration), and a variety of other signals, with a temporal resolution of only 10 s.

These extensive real data sets were used for validation of the presented simulation tool.



Fig. 8. Viennese Ultra Low Floor tram in the climatic wind tunnel, courtesy of “RTA Rail Tec Arsenal Fahrzeugversuchsanlage GmbH”.

626

C. Dullinger et al. / Applied Thermal Engineering 78 (2015) 616–629

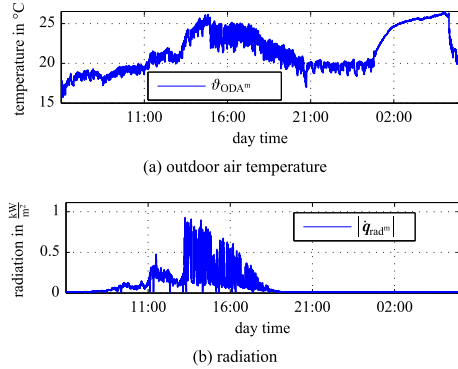


Fig. 9. Measured weather data of one day used for validation.

6.3. Validation based on the ULF tram

In the following the simulation tool is validated based on measurements obtained by an ULF tram (see Fig. 8) in Vienna.

6.3.1. Validation of fast dynamic phenomena against measurement data from in-service operation

Fig. 9a and b shows the weather data of a specific test day used for validation in terms of the measured outdoor air temperature $\vartheta_{ODA^m}(kT_s)$ and the measured magnitude of the radiation vector $|\mathbf{q}_{rad^m}(kT_s)|$, respectively.

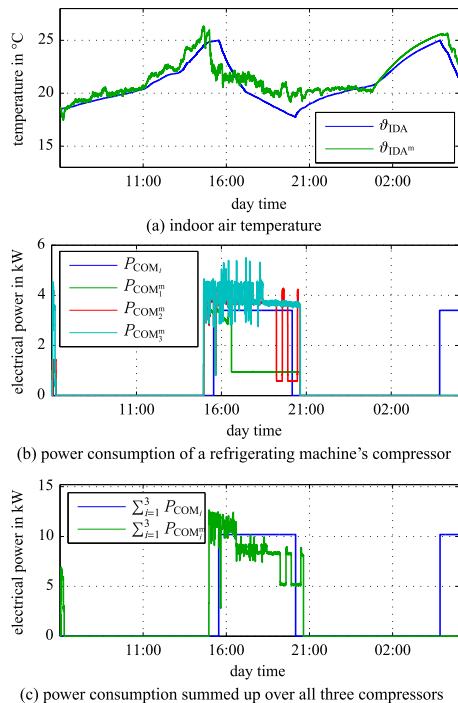


Fig. 10. Simulated and measured time signals.

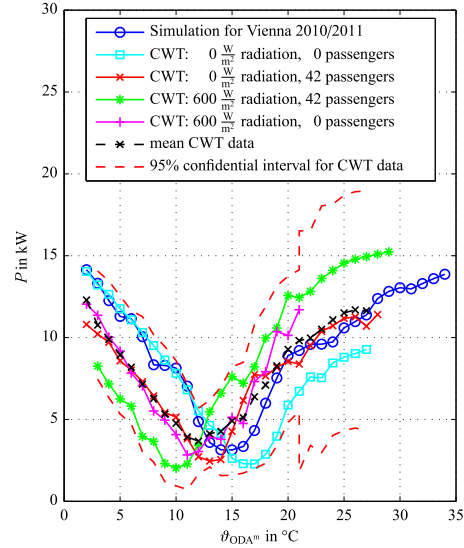


Fig. 11. Average power consumption for HVAC of the ULF tram in dependency of the outdoor air temperature (class width 1 °C). Comparison between simulation based on weather data 2010/2011 Vienna and measurements obtained by specific experiments in the climatic wind tunnel (CWT) (see Ref. [25]).

Fig. 10a compares the simulated indoor air temperature $\vartheta_{IDA}(kT_s)$ with the measured indoor air temperature $\vartheta_{IDA^m}(kT_s)$. For the two curves a root-mean-square error (RMSE) of 1.02 °C is obtained. The simulated power consumption of the compressor P_{COM_i} of the i -th HVAC unit (for $i = 1, \dots, 3$) and the measured power consumption of the compressors $P_{COM_i^m}$ (for $i = 1, \dots, 3$) of the three independent HVAC units are depicted in Fig. 10b. As evident from Fig. 10a and b at around 15:00 in the simulation and in reality the compressors of the refrigerating machines are turned on causing the indoor air temperature to decrease until the compressors are turned off again at around 20:40. As evident from Fig. 10b the three compressors do not act synchronously. The reason for this is that each of the three HVAC units of the ULF tram is controlled by a dedicated controller utilizing its respective sensors signals. Fig. 10c compares the simulated and the measured power consumption summed up over all three compressors. Fig. 10c reveals that on average the overall power demand of the compressors in the simulation (8.28 kW) and in reality (8.81 kW) is similar for the time interval from 14:57 till 20:39. Furthermore, investing a similar amount of electrical energy causes the average indoor air temperature in simulation to closely resemble the actual measured temperature, see Fig. 10a. Whereas in the simulation the electrical power demand of the three compressors stays constant, in reality the sum power demand of the three compressors decreases, causing the measured indoor air temperature to decrease with a smaller gradient and at a higher temperature level than in the simulation. Possible explanations for these different behaviors of the compressors in reality and in the simulation are: (i) the non-uniform distribution of the indoor air temperature in reality, (ii) (different) offsets of the temperature sensors, (iii) slightly different switching conditions of the three HVAC control units.

6.3.2. Validation of the average power consumption against data from climatic wind tunnel (CWT) experiments

The average power consumption for HVAC of the ULF tram in dependency of the outdoor air temperature ϑ_{ODA^m} (ϑ_{ODA^m} classified

with class width 1 °C) is depicted in Fig. 11. The figure compares the simulation based on weather data from Vienna (01.09.2010 till 31.08.2011) with measurement data obtained by specific experiments (with/without passengers and with/without radiation introduced by solar panels) in the climatic wind tunnel (CWT) of Vienna. Note, that the variation of the measurement data obtained from climatic wind tunnel experiments is significant. As evident from Fig. 11 (assuming that the operating states are Gaussian distributed) the curve of the simulation results lies within the 95% confidential interval (CI) of the curves obtained by the CWT experiments.

6.3.3. Validation of the average power consumption against data from in-service operation

Fig. 12 compares the simulation results based on weather data from Vienna with measurement data obtained in-service operation (from 01.09.2010 till 31.08.2011) in terms of the average power consumption in dependency of the outdoor air temperature ϑ_{ODA^m} . At low and high outdoor air temperatures, where a significant amount of heating power respectively cooling power is required in order to comply with the set-point temperature both curves match well. However, at temperatures around 20 °C a significant deviation occurs and the minimum of the curves is shifted by 2 °C.

Possible explanations for this deviations are: (i) offsets in the temperate measurements (1–2 °C have been identified during in-service operation), (ii) breakdown of one of three HVAC units in-service operation occurred at least once for more than three weeks, (iii) slightly different switching transitions, (iv) unknown passenger volume in-service operation (the simulation was performed with a constant passenger volume of 42 persons), (v) non-uniform shading distribution along the vehicle length during in-service operation.

The large amount of in-service data together with documented and undocumented faults in-service operation poses a challenge for correct reconciliation of data. Nevertheless, also the curves based on measurement data obtained from CWT experiments (see Fig. 11) exhibit a shoulder at temperatures around 20 °C. Furthermore, it should be pointed out that at temperatures around 20 °C the curve obtained from measurement data during in-service operation in Fig. 12 lies below all curves based on measurement data obtained from CWT experiments (compare Fig. 11). Consequently the measurement data obtained during in-service operation cannot be trusted in this region around 20 °C. Therefore the deviations in Fig. 12 are not only due to the prediction error of the model. The documented and undocumented faults in-service operation mentioned above are considered to severely contribute to these deviations.

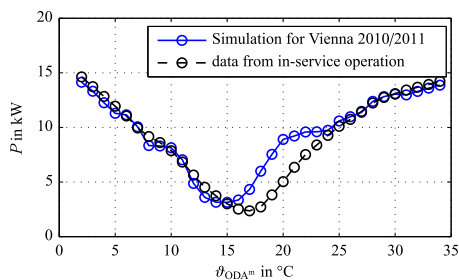


Fig. 12. Average power consumption for HVAC of the ULF tram in dependency of the outdoor air temperature (class width 1 °C). Comparison between simulation based on weather data 2010/2011 Vienna and measurement data obtained from 01.09.2010 till 31.08.2011 in-service operation.

In Table 2 the mean error (ME) between the simulated and measured curves of Figs. 11 and 12, respectively, is evaluated for three different sectors defined by the outdoor air temperature ϑ_{ODA^m} .

The deviation in the average power consumption for HVAC of the ULF tram in dependency of the outdoor air temperature between in-service operation and the different climatic wind tunnel experiments raises the problem of which data to utilize for model calibration. Because within the framework of the project “EcoTram” it was not possible to measure passenger volume during in-service operation and the fact that for a specific experiment the environmental conditions in the CWT are well-defined, the data obtained from these CWT experiments was utilized for model calibration.

7. Extrapolation of the annual energy consumption based on classified days

In the following a simulation result for the annual energy consumption needed for heating, ventilation and air conditioning of the ULF tram is presented. The result for the annual energy consumption is obtained by extrapolating the energy consumption of nine simulated days (see Section 5.3, Equation (50)) each representing a weather class. The result is based on historical weather for 2011 in Vienna.

Fig. 13 visualizes the selection of the simulation day for the class “summer sunny”.

In Fig. 13a all days of this class and the selected day for simulation are depicted. Fig. 13b shows the days in terms of their weighted stochastic parameters. The selected, representative day of the class, which is closest to the point cloud's centroid obtained by K-means is highlighted.

For the simulated days (each representing a weather class) Fig. 14 shows the component-by-component electric energy consumption of one HVAC unit. In Fig. 14 $E_{\text{HB},dc}$, $E_{\text{COM},dc}$, and $E_{\text{SAF},dc}$ are the energy consumptions of the simulated day d (here $n_c = 1$) in weather class c of the heater battery, the compressor, and the supply air fan, respectively.

Fig. 15 shows the simulated energy consumption of one HVAC unit extrapolated for all weather classes.

The energy consumption for class c is obtained by

$$E_{\text{HVAC},c} = H_c \cdot \frac{1}{n_c} \sum_{d=1}^{n_c} E_{dc} \quad (51)$$

with $n_c = 1$ and

$$E_{dc} = E_{\text{HB},dc} + E_{\text{COM},dc} + E_{\text{SAF},dc}. \quad (52)$$

Fig. 16 depicts the annual energy consumption of one HVAC unit's components obtained by extrapolation.

The annual energy consumption for component i is obtained by

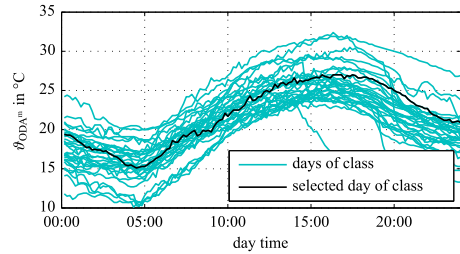
Table 2

Mean error (ME) of average power consumption for HVAC of the ULF tram in dependency of the outdoor air temperature ϑ_{ODA^m} (ϑ_{ODA^m} classified with class width 1 °C). Comparison between simulation results and measurement data obtained by experiments in the CWT (see Fig. 11) and during in-service operation (see Fig. 12), respectively.

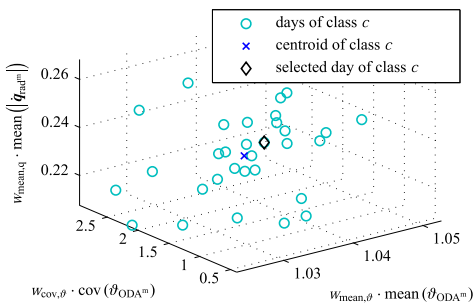
Sector	Mean error between simulation &	
	Mean CWT data	Operational data
$2\text{ °C} \leq \vartheta_{\text{ODA}^m} \leq 14\text{ °C}$	2.001 kW	−0.374 kW
$15\text{ °C} \leq \vartheta_{\text{ODA}^m} \leq 23\text{ °C}$	−1.080 kW	2.214 kW
$24\text{ °C} \leq \vartheta_{\text{ODA}^m} \leq 27\text{ °C}$	−0.810 kW	0.278 kW

628

C. Dullinger et al. / Applied Thermal Engineering 78 (2015) 616–629



(a) outdoor air temperature of days in class: "summer sunny"



(b) weighted stochastic parameters of the days in class "summer sunny"

Fig. 13. Selection of the (representative) simulation day for the class "summer sunny" by applying the clustering algorithm K-Means on its days weighted stochastic parameters.

$$E_{y,i} = \frac{365}{\sum_{c=1}^{n=9} H_c} \sum_{c=1}^{n=9} \left(H_c \cdot \frac{1}{n_c} \sum_{d=1}^{n_c} E_{i,d,c} \right) \quad (53)$$

where $E_{i,d,c}$ is the energy consumption of the component i of the simulated representative day d of class c .

The extrapolated annual energy consumption is given by $E_y = n_{HVAC} \cdot \sum_i E_{y,i}$, where $n_{HVAC} = 3$ is the number of HVAC units of

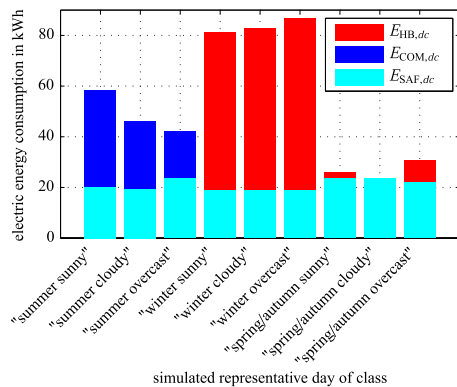


Fig. 14. Simulated component-by-component electric energy consumption of one HVAC unit for the simulated days d each representing a weather class c (one simulated day per class, i.e. $n_c = 1$). $E_{HB,d,c}$, $E_{COM,d,c}$, and $E_{SAF,d,c}$ are the energy consumptions of the heater battery, the compressor, and the supply air fan, respectively.

the ULF tram. A numerical value of 54.68 MWh is obtained which corresponds to an average power consumption of 8.32 kW.

8. Conclusion

A simulation tool embedded in a user friendly graphical user interface for computing the annual energy consumption of the HVAC system of a light rail vehicle is presented. It comprises a dynamic thermal vehicle model and a modular structured HVAC model. Using the GUI the model parameters can be identified respectively adjusted to fit a given or fictitious rail vehicle or HVAC system, respectively. The simulation tool was validated using real data obtained by a tram equipped with measuring equipment operated in Vienna for one year. Validation showed a good correspondence between reality and simulation for fast sampled ($T_s = 10$ s) time domain signals (like indoor air temperature, supply air temperature, etc.).

Care has to be taken to calibrate the model on measured data, as results from the climatic wind tunnel and in-service operation show significant variations within measured data. It will be a topic of further research how to efficiently calibrate such a thermal model from existing data.

The presented simulation tool is capable to provide realistic insight in the energy use for heating, ventilation and air-conditioning in light rail as a function of ambient weather conditions, operational conditions and passenger volume. Furthermore, the compliance with thermal comfort limits (in terms of temperature, humidity, CO₂ concentration) can be monitored and reasons for violations can be identified.

In the design phase the simulation tool can help HVAC manufacturers with the dimensioning of the HVAC components (for a given vehicle, climate, desired indoor air temperature, etc.) by testing different scenarios of the cooling capacity of the compressor, heat output of the heater battery, etc. by entering the component's essential parameters in the respective numerical look-up table, as well as testing of different control concepts.

Furthermore, the tool enables to test novel ideas in air-conditioning technology of rail vehicles, like adding a heat pump or a CO₂ dependent fresh air control strategy. Rail vehicle manufacturers can use the tool in the offer phase to decide which HVAC system to choose for a given climatic region. By utilizing the simulation tool operators are able study the effects of different set point curves on energy consumption and thermal comfort without

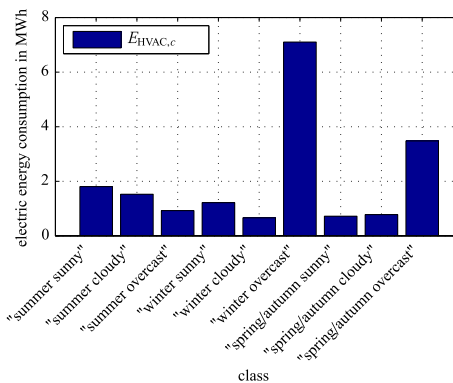


Fig. 15. Simulated energy consumption of one HVAC unit extrapolated for the weather classes (of one year).

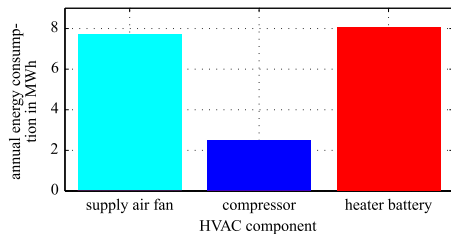


Fig. 16. Annual energy consumption of one HVAC unit's components obtained by extrapolation.

the requirement of time-consuming and expensive reprogramming and experiments, respectively.

Ultimately, the presented simulation tool can significantly contribute to reduce energy consumption for heating, ventilation and air-conditioning in light rail.

Acknowledgement

The authors wish to thank Mr. Raphael Hofstädter for his contribution to the simulation tool.

This work was supported by the Klima-Und Energiefond Project "EcoTram" (FFG, No. 825443) in cooperation with RTA Rail Tec Arsenal Fahrzeugversuchsanlage GmbH, Schieneninfrastruktur-Dienstleistungsgesellschaft m.b.H, Siemens AG Österreich, Vossloh Kiepe Ges.m.b.H, and Wiener Linien GmbH & Co KG.

References

- [1] W. Struckl, Green Line: Environmental Related Product Development Strategies for Railway Vehicles Based on the Life Cycle Assessment of a Metro in Oslo (in German), Vienna University of Technology, Vienna, Austria, 2007.
- [2] B. Beusen, B. Degraeuwe, P. Debeuf, Energy savings in light rail through the optimization of heating and ventilation, *Transp. Res. Part D Transp. Environ.* 23 (2013) 50–54. <http://dx.doi.org/10.1016/j.trd.2013.03.005>.
- [3] J. Powell, A. González-Gil, R. Palacin, Experimental assessment of the energy consumption of urban rail vehicles during stabling hours: influence of ambient temperature, *Appl. Therm. Eng.* 66 (2) (2014) 541–547. <http://dx.doi.org/10.1016/j.applthermaleng.2014.02.057>.
- [4] D. Marcos, F.J. Pino, C. Bordons, J.J. Guerra, The development and validation of a thermal model for the cabin of a vehicle, *Appl. Therm. Eng.* 66 (2) (2014) 646–656. <http://dx.doi.org/10.1016/j.applthermaleng.2014.02.054>.
- [5] J. Marachlian, R. Benelmir, A.E. Bakkali, G. Olivier, Exergy based simulation model for vehicle HVAC operation, *Appl. Therm. Eng.* 31 (5) (2011) 696–700. MNF 2009 Special Issue, <http://dx.doi.org/10.1016/j.applthermaleng.2010.10.001>.
- [6] B. Torregrosa-Jaime, F. Bjurling, J.M. Corberán, F.D. Sciullo, J. Payá, Transient thermal model of a vehicle's cabin validated under variable ambient conditions, *Appl. Therm. Eng.* 75 (2015) 45–53.
- [7] J.S. Brown, S.F. Yana-Motta, P.A. Domanski, Comparative analysis of an automotive air conditioning systems operating with CO₂ and R134a, *Int. J. Refrig.* 25 (1) (2002) 19–32. [http://dx.doi.org/10.1016/S0140-7007\(01\)00011-1](http://dx.doi.org/10.1016/S0140-7007(01)00011-1).
- [8] A. Afram, F. Janabi-Sharifi, Review of modeling methods for HVAC systems, *Appl. Therm. Eng.* 67 (2) (2014) 507–519. <http://dx.doi.org/10.1016/j.applthermaleng.2014.03.055>.
- [9] J.S. Brown, P.A. Domanski, Review of alternative cooling technologies, *Appl. Therm. Eng.* 64 (2) (2014) 252–262. <http://dx.doi.org/10.1016/j.applthermaleng.2013.12.014>.
- [10] MAGNA, Kuli: Thermal Management Simulation Software KULI, 06 2014. www.kuli.at.
- [11] J. Rugh, K. Bennion, A. Brooker, J. Langewisch, K. Smith, J. Meyer, PHEV/EV integrated vehicle thermal management - development of a KULI model to assess combined cooling loops, in: *Vehicle Thermal Management Systems Conference and Exhibition (VTMS10)*, Woodhead Publishing, 2011, pp. 649–660. <http://dx.doi.org/10.1533/9780857095053.8.649>.
- [12] W. Liu, Q. Deng, W. Huang, R. Liu, Variation in cooling load of a moving air-conditioned train compartment under the effects of ambient conditions and body thermal storage, *Appl. Therm. Eng.* 31 (7) (2011) 1150–1162. <http://dx.doi.org/10.1016/j.applthermaleng.2010.12.010>.
- [13] Z. Zhang, S. Liu, L. Tian, Thermodynamic analysis of air cycle refrigeration system for Chinese train air conditioning, *Syst. Eng. Procedia* 1 (2011) 16–22. *Engineering and Risk Management*, <http://dx.doi.org/10.1016/j.sepro.2011.08.004>.
- [14] W. Li, J. Sun, Numerical simulation and analysis of transport air conditioning system integrated with passenger compartment, *Appl. Therm. Eng.* 50 (1) (2013) 37–45. <http://dx.doi.org/10.1016/j.applthermaleng.2012.05.030>.
- [15] H. Amri, R. Hofstädter, M. Kozek, Energy efficient design and simulation of a demand controlled heating and ventilation unit in a metro vehicle, in: *2011 IEEE Forum on Integrated and Sustainable Transportation System (FISTS)*, 2011, pp. 7–12. <http://dx.doi.org/10.1109/FISTS.2011.5973605>.
- [16] R. Hofstädter, M. Kozek, Holistic thermal simulation model of a tram, in: *In Proceedings of 2nd International Conference on Computer Modelling and Simulation (CSSim2011)*, Brno, Czech Republic, 2011.
- [17] Deutsches Institut für Normung, Railway Applications – Air Conditioning for Urban and Suburban Rolling Stock – Part 1: Comfort Parameters, German version EN 14750-1:2006, Tech. rep., DIN Deutsches Institut für Normung e.V., Berlin, Germany, 2006.
- [18] L. Ljung, *System Identification: Theory for the User*, Pearson Education, New Jersey, USA, 1998.
- [19] L. Ljung, Prediction error estimation methods, *Circuits Syst. Signal Process.* 21 (1) (2002) 11–21. <http://dx.doi.org/10.1007/BF01211648>.
- [20] F. Wagner, R. Schmuki, T. Wagner, P. Wolstenholme, *Modeling Software with Finite State Machines: a Practical Approach*, Taylor & Francis, Boca Raton, USA, 2006.
- [21] A. Kumar, *Fundamentals of Digital Circuits*, PHI Learning, New Delhi, India, 2009.
- [22] J. Davis, J. Davis, R. Reese, *Finite State Machine Datapath Design, Optimization, and Implementation, Synthesis Lectures on Digital Circuits and Systems*, Morgan & Claypool, California, USA, 2008.
- [23] ZAMG, Central Institute for Meteorology and Geodynamics, (in German), www.zamg.ac.at, 10.2014.
- [24] O. Nelles, *Nonlinear System Identification: from Classical Approaches to Neural Networks and Fuzzy Models*, Engineering online library, Springer, Berlin, Germany, 2001.
- [25] G. Richter, How Much Energy Is Used by the HVAC Unit of a Tram? Investigations in the Climatic Wind Tunnel and in Operation, *Railvolution* 6/10, 2010, p. 4.

2.2 Publication B

Christian Dullinger, Walter Struckl, and Martin Kozek.

Simulation-based multi-objective system optimization of train traction systems.

Simulation Modelling Practice and Theory, Volume 72, 2017, Pages 104-117.

DOI: 10.1016/j.simpat.2016.12.008

Own contribution

Problem analysis, selection of methods, execution of the solution, development and programming of algorithms, consideration of implementation aspects, performing simulations studies, and structuring, writing, and editing of the manuscript was done by the applicant. Problem statement and discussion was done by the second author. Problem statement, discussion and editing was done by the third author.



Contents lists available at ScienceDirect

Simulation Modelling Practice and Theory

journal homepage: www.elsevier.com/locate/simpat

Simulation-based multi-objective system optimization of train traction systems

Christian Dullinger^{a,*}, Walter Struckl^b, Martin Kozek^a^a Institute of Mechanics and Mechatronics Division of Control and Process Automation Getreidemarkt, 9/325-A5 A-1060 Vienna, Austria^b Siemens AG Österreich, Austria

ARTICLE INFO

Article history:

Received 16 February 2016

Revised 1 September 2016

Accepted 8 December 2016

Keywords:

Rail vehicle model

Multi-objective configuration optimization

Train trajectory optimization

Energy simulation

Pareto front

ABSTRACT

A holistic framework for multi-objective optimization of the traction system configuration of trains with mixed-integer decision variables is presented. Rail vehicles have to be energy-efficient and must be operated on a tight schedule. Furthermore, the number of decision variables to fulfill these objectives is large, and some components (like motors and gears) can only be chosen from a small set of discrete elements. In this work, the overall optimization is achieved by a two level approach: The Pareto front of optimal system configurations is obtained by a multi-objective mixed-integer elitist genetic algorithm (GA) on the upper-level. To capture the influence of a specific system configuration on travel time and energy consumption, a suitable train trajectory optimizer is developed and employed in the lower-level. The train trajectory optimization is solved by sequential quadratic programming (SQP) and considers the power losses of the different components. A case study is presented which highlights the benefits of the holistic multi-objective optimization.

© 2016 Elsevier B.V. All rights reserved.

1. Introduction

Rail vehicles have to fulfill multiple conflicting objectives. They have to be cost-effective, but at the same time energy-efficient and must be operated on a tight schedule. Furthermore, the number of decision variables in the design phase to fulfill these objectives is large and some components like motors and gears can only be chosen from a small set of discrete elements, whereas others like the input chokes can be produced with arbitrary parameters.

Up to now much effort has been put into time table and speed profile optimization for given rail vehicles, and there exists a variety of long and well tried software products. Particularly the speed profile optimization problem has a long history with many different solution approaches. Li and Gao [1] introduced a model that can well describe the dynamic behavior of the train movement under the moving block condition. But, finding the best system configuration with respect to the multiple conflicting objectives by simulating each system configuration's performance with individually optimized speed profile has not been applied yet. However, simulation-based system optimization has already been successfully applied to many different engineering problems. Figueira and Almada-Lobo [2] provide a taxonomy that aims at giving an overview of the full spectrum of current simulation-optimization approaches. The purpose of the study is to guide researchers who want to use one of the existing methods and create a standard for a better communication in the scientific community.

* Corresponding author.

E-mail addresses: christian.dullinger@tuwien.ac.at (C. Dullinger), walter.struckl@siemens.com (W. Struckl), martin.kozek@tuwien.ac.at (M. Kozek).<http://dx.doi.org/10.1016/j.simpat.2016.12.008>

1569-190X/© 2016 Elsevier B.V. All rights reserved.

For multiple conflicting objectives multi-objective evolutionary algorithms (MOEAs) are well suited because due to their population-based approach they can find a number of trade-off solutions in one iteration. Deb et al. [3] introduced the famous non-dominated sorting-based MOEA, called NSGA-II which has found many applications. A variant of NSGA-II is implemented in MATLAB™.

In [4] a numerical model is developed by evolving an efficiency prediction code for the pre-design of radial turbines. The efficiency prediction code includes the mean-line calculations associated with an optimizer based on the NSGA-II version of MATLAB™. In [5], an optimization analysis of the thermally regenerative electrochemical cycle system is conducted for different heat source inlet temperatures with maximum power output and exergy efficiency as the objective functions. The problem is solved by the NSGA-II version of MATLAB™. Also Kamjoo et al. [6] use the NSGA-II algorithm in the design of a standalone hybrid renewable energy system comprising wind turbine, photovoltaic panel and battery bank. The aforementioned works have in common that integer constraints are not treated. In this work the algorithm has been adapted to handle mixed-integer variables as well.

Chen et al. [7] introduce a wind farm layout optimization method. A multi-objective genetic algorithm with mixed discrete real integer string is used to represent the wind turbines' positions, types and the hub heights simultaneously. The presented work utilizes mixed-integer decision variables to represent the traction system's component respectively parameter configuration. In [8] a constrained, multi-objective problem (solved by NSGA-II), with mixed-integer variables, from the building design domain is presented. However, unlike in the presented work, a two level optimization with an optimized input trajectory applied to a dynamic simulation model in the lower-level is not performed.

In [9] a framework coupling EnergyPLAN (an analytical simulation model for energy systems) with a MOEA is presented. The framework of this work couples an analytical energy simulation model for the rail vehicle's electrical drive energy to a multi-objective optimization for the component configuration. Thereby optimized input trajectories are applied to the energy simulation model.

In [10] the so-called configuration problem is addressed using simulation associated with a distributed evolutionary algorithm, and it is illustrated through an example from the area of manufacturing system design. The authors conclude that the limitations of this approach are in the development of simulation models, which have to provide the capability of switching from one option to another. In this work, the developed dynamic rail vehicle model utilized by the train trajectory optimizer (lower-level optimizer) fulfills this necessary specification.

For tandem cold rolling in [11] a multi-objective optimization problem is formulated to optimize energy efficiency and damage simultaneously. The authors claim that the obtained Pareto front enables the mill operators to select the most appropriate optimized schedule. Analogous to these objectives, with the presented multi-objective framework Pareto fronts can be obtained and utilized to select the most appropriate traction system configuration according to energy efficiency and traction power (i.e. travel time). This is enabled by the train trajectory optimizer (applied in the lower-level), which is capable of providing the values of these two objectives for each system configuration.

Multi-objective optimization is also applied to optimize the design and operating strategy of electric vehicles. In [12] a multi-objective optimization methodology is applied on hybrid electric vehicles in order to define the optimal powertrain configurations of the vehicle, estimate the cost of the powertrain equipment and show the environmental impact of the technical choices on the lifecycle perspective of the vehicle. Also in the performed case studies of this work (Section 5.3) investment costs (of the traction system) and energy consumption are chosen as objectives. Therefore, here too the obtained optimal trade-off solutions can be utilized as a sound foundation for computing realistic life cycle costs. For a subway vehicle in [13] NSGA-II is utilized to perform a multi-objective optimization of its gradual energy-absorbing structure. Only continuous decision variables are defined. In [14] an applied methodology for multi-objective optimum sizing of hybrid electric vehicle (car) components is developed. However, unlike in the presented work, a true multi-objective optimization is not performed. Instead a weighted sum method is applied. In [15] an optimal driving strategy for electric vehicles powered by batteries is proposed. Energy consumption, acceleration duration, and jerk are considered as objectives. Pareto-optimal fronts are obtained using NSGA-II. However, the effects of (Pareto) optimal system configurations on the aforementioned objectives are not investigated.

In this work the optimal train trajectory (speed profile) is obtained in the lower-level. For electric trains recent works started to consider the electrical net energy required for traction and the influence of regenerative braking on the optimal train trajectory. Martinis and Gallo [16] proposed models and methods to optimize speed profiles in suburban areas with and one without energy recovery systems. Albrecht et al. [17,18] discuss the problem of finding an energy-efficient driving strategy for an undulating track with steep grades subject to a maximum prescribed journey time. The aforementioned works have in common that they do not consider the operating point dependent power losses of the traction system components in the optimization. Furthermore, a multi-objective optimization was not performed.

Domínguez et al. [19] develop a detailed simulator of the train motion and use it for design of optimal Automatic Train Operation (ATO) speed commands for the ATO equipment implemented on line 3 of the Madrid Underground. A variable efficiency model of the traction system as a function of the train speed and the ratio between the required and the maximum force is included. Domínguez et al. [20] use the aforementioned model to design optimal ATO speed profiles taking into account the regenerative energy and the total net energy consumption in substations. A network model for calculating the total energy recovered as well as a model of a train with an on-board energy storage device is presented to calculate a realistic network receptivity. The authors analyze several realistic case studies for the Madrid Underground to assess the achievable energy savings due to possible investments and optimal design of ATO speed profiles. Because the updated

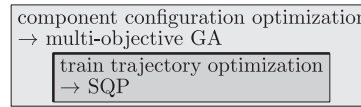


Fig. 1. Two level optimization: multi-objective mixed-integer component configuration optimization (upper-level) solved by mixed-integer multi-objective genetic algorithm (GA) & train trajectory optimization (lower-level) solved by sequential quadratic programming (SQP).

signaling technology implemented in the Madrid Underground allows for a finer discretization of the ATO speed commands resulting in an exponential growth of the solution space, [21] uses the detailed simulator presented in [19] in combination with a proposed Multi Objective Particle Swarm Optimization (MOPSO) to obtain the Pareto curve of the new possible speed profiles. It is shown that the developed MOPSO outperforms the NSGA-II algorithm with respect to the diversity of the solutions and proximity to the real Pareto front. Fernández-Rodríguez et al. [22] consider the main uncertainties in train operation (i.e. train load and delays) to obtain robust Pareto fronts of efficient ATO speed commands utilizing the MOPSO proposed in [21]. A robust optimization technique and an alternative method ensuring pattern-robustness (i.e. sequence of driving modes) of the optimal ATO commands with respect to mass variations are compared. The subset of four speed profiles of the robust Pareto front to be programmed in the targeted ATO equipment of the Madrid Underground is selected based on a stochastic optimization considering the probability distribution of target running times.

In this work, the robustness approach of [22] handling uncertainties in the target running time on the optimal ATO speed commands is adapted to obtain a robust Pareto front of optimal traction system configurations with respect to varying target running times and passenger loads. A case study presents the robust Pareto front for a whole line with different track characteristics.

The novel contribution of this paper is the holistic multi-objective optimization of the traction system configuration consisting of electrical and mechanical parts (upper-level optimization) together with the train trajectory (lower-level optimization), see Fig. 1. None of the aforementioned references utilizes such a framework. The specially developed and validated subordinated train trajectory optimizer is capable of considering the effects of regenerative braking on the optimal train trajectory by simulation. Speed limits, technological constraints (motor characteristics, maximum braking force, etc.), and constraints ensuring passenger comfort (i.e. acceleration and jerk) are observed. Furthermore, a unique feature of the trajectory optimizer is that it also considers the operating point dependent power losses of the traction components given by validated static lookup tables. An iterative adaptive track discretization algorithm is utilized to ensure an automatic and track specific generation of adequate position samples for the trajectory optimization. With the presented holistic multi-objective optimization framework it is possible for the first time to optimize the essential conflicting design objectives simultaneously and visualize the different optimal trade-off solutions. The shape of the approximated Pareto front can reveal valuable information for the decision-maker to what extent a compromise between the conflicting objectives is worthwhile. If the shape of the Pareto front does not lead directly to an unambiguous solution, higher-level information, which is often non-technical, qualitative and experience-driven, can be used to decide on a concrete optimal system configuration.

The remainder of this paper is structured as follows: In Section 2 the simulation model used by the train trajectory optimizer is derived. In Section 3 the train trajectory optimization problem is formulated and its workflow is presented. In Section 4 the multi-objective mixed-integer component configuration optimization problem is formulated and its workflow is described. Section 5 is devoted to simulation results and case studies. A conclusion and an outlook is given in Section 6.

2. Simulation model for train trajectory optimization

The system model consists of two main parts. The dynamic part of the model is derived in Section 2.1 and the part dealing with the electrical net energy computation is presented in Section 2.2.

2.1. Dynamic simulation model for trajectory optimization

2.1.1. Equation of motion for the train movement

In the standard work on train control [23] it is shown that the motion of a train with distributed mass can be reduced to the motion of a point-mass train. By applying the center-of-mass theorem to a point mass train the equation of motion is obtained as

$$m_t \ddot{s} = F_t(s) - F_b(s) - F_r(v) - mg \sin \alpha(s). \quad (1)$$

In (1) s denotes the track position, $F_t \geq 0$ is the traction force, $F_b \geq 0$ is the braking force, g is the gravitational acceleration, α is the gradient angle of the track, and $F_r(v) \geq 0$ is the resistance force as a function of the velocity v given by the quadratic formula

$$F_r(v) = c_1 + c_2 \cdot v + c_3 \cdot v^2. \quad (2)$$

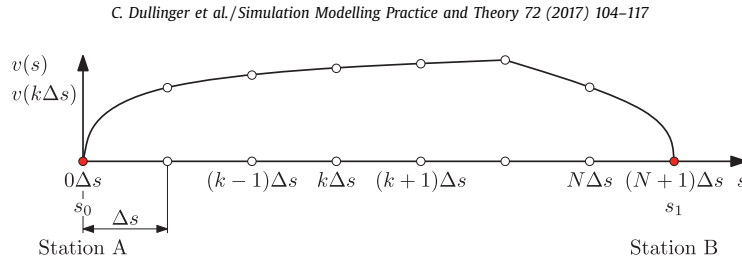


Fig. 2. Schematic track discretization .

The coefficients c_1 , c_2 and c_3 in (2) can be computed from the parameters of the well known Davis formula for train resistance, see [23,24]. In (1) m_t is the total mass to be accelerated given by

$$m_t = m_{\text{empty}} + m_{\text{cargo}} + \Delta m_{\text{rot}} = m + \Delta m_{\text{rot}} \quad (3)$$

where m_{empty} is the mass of the empty train, m_{cargo} is the mass of the cargo load (m is the mass of the train), and Δm_{rot} is the additional mass which considers the rotatory energy.

In a time-free formulation the acceleration can be expressed as

$$a = \ddot{s} = \frac{dv}{dt} = \frac{dv}{ds} \frac{ds}{dt} = v' v. \quad (4)$$

Inserting (4) in (1) and rearranging leads to

$$v' = \frac{1}{m_t} \frac{1}{v(s)} (F_t(s) - F_b(s) - F_r(v(s)) - mg \sin \alpha(s)). \quad (5)$$

Eq. (5) constitutes a nonlinear time-free equation of motion for the train movement.

2.1.2. Travel time computation

In the time-free description the travel time T from s_0 to s_1 can be computed by integrating $t' = dt/ds = v^{-1}(s)$ along the track from station “A” at the position s_0 to station “B” at position s_1 :

$$T = t(s_1) - t(s_0) = \int_{s_0=0}^{s_1} t' ds \quad (6)$$

2.1.3. Nonlinear position-varying state space model

By choosing the state vector $\mathbf{x}^T(s) = [x_1(s) \quad x_2(s)] = [t(s) \quad v(s)]$ and defining the input $u(s) = F(s) = F_t(s) - F_b(s)$, the nonlinear differential Eq. (5) can be represented by the nonlinear position-varying state space model

$$\underbrace{\begin{bmatrix} x_1'(s) \\ x_2'(s) \end{bmatrix}}_{\mathbf{x}'(s)} = \underbrace{\begin{bmatrix} \frac{1}{x_2(s)} \\ \frac{1}{m_t x_2(s)} (u(s) - F_r(x_2(s)) - mg \sin \alpha(s)) \end{bmatrix}}_{f(s, \mathbf{x}(s), u(s))}. \quad (7)$$

2.1.4. Discretized nonlinear position-varying state space model

Fig. 2 shows a schematic equidistant track discretization with Δs . The train travels from station “A”, where $\mathbf{x}(k=0) = \mathbf{0}$, to station “B”, where the train stops and $v(k=N+1) = x_2(k=N+1) = 0$.

Let

$$\frac{dx_i(s)}{ds} = x_i'(s) = f_i(s, \mathbf{x}(s), u(s)) \quad (8)$$

be the state equation of the i -th state of the continuous nonlinear position-varying state space model (7). Using Euler's method the first derivative of the i -th state with respect to the position s can be approximated by

$$x_i'(s) = x_i'(k\Delta s) \approx \frac{x_i((k+1)\Delta s) - x_i(k\Delta s)}{\Delta s}. \quad (9)$$

Reformulating (9) and inserting (8) leads to

$$x_i(k+1) \approx x_i(k) + f_i(k, \mathbf{x}(k), u(k)) \cdot \Delta s. \quad (10)$$

Eq. (10) is a finite-difference equation, and solving this equation (i.e. applying the explicit Euler method) gives an approximate solution to the differential equation of the i -th state. By this means the discretized nonlinear position-varying state space model is obtained as

$$\underbrace{\begin{bmatrix} x_1(k+1) \\ x_2(k+1) \end{bmatrix}}_{\mathbf{x}(k+1)} = \underbrace{\begin{bmatrix} x_1(k) \\ x_2(k) \end{bmatrix}}_{\mathbf{x}(k)} + \underbrace{\begin{bmatrix} \frac{1}{x_2(k)} \\ \frac{1}{m_t x_2(k)} (u(k) - F_r(x_2(k)) - mg \sin \alpha(k)) \end{bmatrix}}_{f(k, \mathbf{x}(k), u(k))} \cdot \Delta s. \quad (11)$$

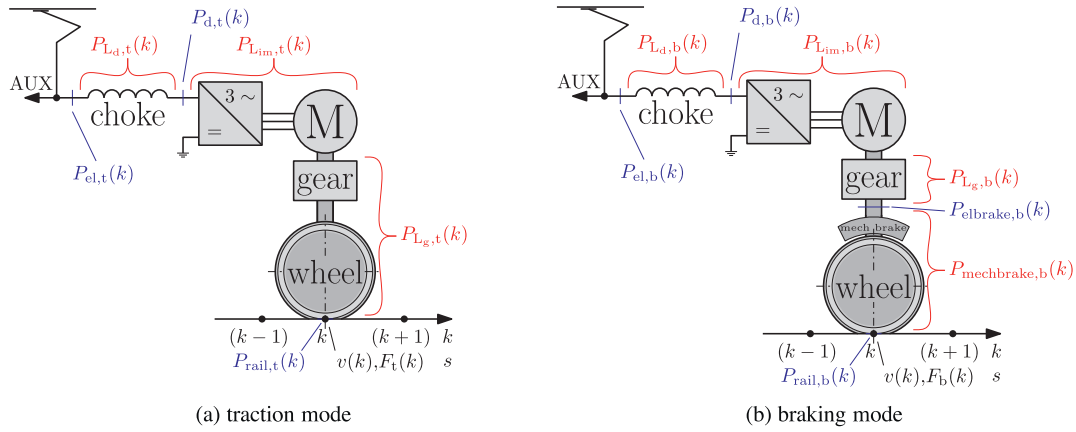


Fig. 3. Sketch: mechanical and electrical powers and power losses at sampling instance k .

Remark: Assuming that the train does not move backwards (i.e. $x_2(k) = v(k) \geq 0$), (11) can only be applied if $x_2(k) = v(k) > 0$ holds. Moreover, the problem is numerically ill conditioned if $x_2(k)$ is close to zero.

2.2. Electrical net energy computation

In this section it is shown how the electrical energy required respectively provided by the components of the traction system is computed, utilizing the characteristics of the components. The characteristics are obtained from validated static lookup tables. Fig. 3a and b depict the mechanical and electrical powers and power losses at sampling instance k if the train is currently operated in traction and braking mode, respectively. The traction system of a state of the art traction vehicle operating on a DC net basically consists of input chokes, the three-phase pulse width modulated power inverters, three-phase motors, gears, the mechanical braking system, and wheels.

2.2.1. Traction mode

The effective (mechanical) traction power $P_{\text{rail,t}}(k) = v(k) \cdot F_t(k)$ in Fig. 3a is the product of velocity $v(k)$ and traction force

$$F_t(k) = \begin{cases} F(k) & \text{for } F(k) \geq 0 \\ 0 & \text{for } F(k) < 0 \end{cases} \quad (12)$$

In traction mode the power losses of the gears are modeled by

$$P_{L_g,t}(k) = \frac{F_t(k) \cdot v(k)}{\eta_{\text{gF}_t,t}(F_t(k))} - \underbrace{F_t(k) \cdot v(k)}_{P_{\text{rail,t}}(k)} \quad (13)$$

where $\eta_{\text{gF}_t,t}(F_t(k))$ is the efficiency of a gear in traction mode. In Figure 3a $P_{L_{\text{im,t}}}(k)$ are the power losses of all three-phase pulse width modulated power inverters and three-phase motors given by the static mapping

$$P_{L_{\text{im,t}}}(k) = P_{L_{\text{im,t}}}(F_t(k), v(k)). \quad (14)$$

In traction mode the power losses of the input choke in Fig. 3a are obtained by the characteristic curve

$$P_{L_d,t}(k) = P_{L_d,t}(P_{d,t}(k)) \quad (15)$$

where $P_{d,t}(k) = P_{\text{rail,t}}(k) + P_{L_g,t}(k) + P_{L_{\text{im,t}}}(k)$ is the electrical power between the choke and the power inverters. With the power losses given in (13)–(15) the electrical power at sampling instance k required for traction is computed by

$$P_{\text{el,t}}(k) = P_{\text{rail,t}}(k) + P_{L_g,t}(k) + P_{L_{\text{im,t}}}(k) + P_{L_d,t}(k). \quad (16)$$

2.2.2. Braking mode

The total braking power $P_{\text{rail,b}}(k) = v(k) \cdot F_b(k)$ in Fig. 3b is the product of velocity $v(k)$ and total braking force

$$F_b(k) = \begin{cases} 0 & \text{for } F(k) \geq 0 \\ -F(k) & \text{for } F(k) < 0 \end{cases} \quad (17)$$

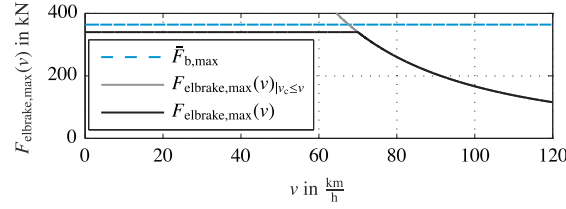


Fig. 4. Maximum total braking force $\bar{F}_{b,\max}$ and maximum electrical braking force $F_{\text{elbrake,max}}(v)$ of a specific train.

Fig. 4 shows an example of the maximum total braking force and the maximum electrical braking force for a specific train. The maximum total braking force is considered constant with $\bar{F}_{b,\max} = 364$ kN. From 0 km/h till $v_c = 70$ km/h the maximum electrical braking force $F_{\text{elbrake,max}}(v)$ is constant and has its maximum value of 340 kN. For velocities higher than $v_c = 70$ km/h the force $F_{\text{elbrake,max}}(v)$ is modeled by the hyperbola $F_{\text{elbrake,max}}(v)|_{v_c \leq v} = F_{\text{elbrake,max}}(v_c) \cdot v_c^2 / v^2$. If at sampling instance k the applied total braking force $F_b(k)$ is higher than $F_{\text{elbrake,max}}(k)$, the force difference has to be compensated by the mechanical brake with the mechanical braking force given by

$$F_{\text{mechbrake}}(k) = F_b(k) - F_{\text{elbrake,max}}(v(k)), \quad (18)$$

otherwise the mechanical braking force is zero. The dissipated power due to mechanical braking is obtained by

$$P_{\text{mechbrake,b}}(k) = F_{\text{mechbrake}}(k) \cdot v(k) \quad (19)$$

and the electrical braking power is computed by

$$P_{\text{elbrake,b}}(k) = P_{\text{rail,b}}(k) - P_{\text{mechbrake,b}}(k). \quad (20)$$

In case of electrical braking the power losses of the gears are modeled by

$$P_{L_g,b}(k) = (1 - \eta_{gF_{\text{elbrake,b}}}(F_{\text{elbrake}}(k))) \cdot P_{\text{elbrake,b}}(k) \quad (21)$$

where $\eta_{gF_{\text{elbrake,b}}}(F_{\text{elbrake}}(k))$ is the efficiency of a gear in braking mode.

For electrical braking the power losses of all inverters and three-phase motors are given by the static mapping

$$P_{L_{\text{im,b}}}(k) = P_{L_{\text{im,b}}}(F_{\text{elbrake}}(k), v(k)). \quad (22)$$

The power losses of the input choke in Fig. 3b are obtained by the static mapping

$$P_{L_{\text{d,b}}}(k) = P_{L_{\text{d,b}}}(P_{\text{d,b}}(k)), \quad (23)$$

where $P_{\text{d,b}}(k) = P_{\text{elbrake,b}}(k) - P_{L_g,b}(k) - P_{L_{\text{im,b}}}(k)$ is the provided electrical power between the choke and the power inverters. With the power losses given in (21)–(23) the electrical power at sampling instance k provided by electrical braking is computed by

$$P_{\text{el,b}}(k) = P_{\text{elbrake,b}}(k) - P_{L_g,b}(k) - P_{L_{\text{im,b}}}(k) - P_{L_{\text{d,b}}}(k). \quad (24)$$

3. Train trajectory optimization (lower-level optimization)

In this chapter the train trajectory optimization problem (see Fig. 1) for minimizing the travel time and for minimizing the electrical net energy required by the traction system are formulated, respectively.

3.1. Decision vector

The decision vector $\mathbf{u} = [u(0), \dots, u(k), \dots, u(N)]^T$ of the trajectory optimization problem is the input sequence $u(k)$ for $k = 0, \dots, N$ to the discretized nonlinear position-varying state space model (11), where $u(k) = F(k) = F_t(k) - F_b(k)$ is the external force acting on the wheels of the train in the direction of movement of the train (see Section 2).

3.2. Constraints

3.2.1. Linear inequality constraints (box constraints)

The box constraints on $u(k)$ are given by

$$-\bar{F}_{b,\max} \leq u(k) \leq \bar{F}_{t,\max} \quad \text{for } k = 0, \dots, N. \quad (25)$$

In (25) the negative lower bound $\bar{F}_{b,\max}$ is the magnitude of the maximum braking force. The upper bound $\bar{F}_{t,\max}$ is the maximum traction force at $v = 0$ m/s.

3.2.2. Nonlinear equality constraints

To stop at station “B” requires the nonlinear terminal constraint for the velocity at sampling instance $k = N + 1$:

$$x_2(N + 1) = 0. \quad (26)$$

3.2.3. Nonlinear inequality constraints

To prevent the train from driving backwards can be secured as follows: The constraints in (27) demand that the velocity is larger than zero at all sampling instances different from 0 and $N + 1$:

$$-x_2(k) < 0 \text{ for } k = 1, \dots, N \quad (27)$$

The constraints in (28) enforce that time has to be monotonically increasing during the journey:

$$-(x_1(k + 1) - x_1(k)) \leq 0 \text{ for } k = 0, \dots, N \quad (28)$$

The constraints in (29) require that time is larger than zero at all sampling instances different from 0. At station “A” the journey starts at $t = 0$ s (i.e. $x_1(0) = 0$):

$$-x_1(k) < 0 \text{ for } k = 1, \dots, N + 1 \quad (29)$$

The maximum velocity constraints read

$$x_2(k) - v_{\max}(k) \leq 0 \text{ for } k = 1, \dots, N + 1. \quad (30)$$

With $a_{\min} < 0$ and $a_{\max} > 0$ for the acceleration $a(k)$ the inequalities

$$a_{\min} - a(k) \leq 0 \text{ for } k = 0, \dots, N \quad \text{and} \quad a(k) - a_{\max} \leq 0 \text{ for } k = 0, \dots, N \quad (31)$$

must hold. Utilizing the states of the dynamic system (11) the acceleration $a(k)$ in (31) is approximated using the first order forward difference quotient

$$a(k) \approx \frac{x_2(k + 1) - x_2(k)}{x_1(k + 1) - x_1(k)}. \quad (32)$$

With $j_{\min} < 0$ and $j_{\max} > 0$ for the jerk $j(k)$ the inequalities

$$j_{\min} - j(k) \leq 0 \text{ for } k = 0, \dots, N + 1 \quad \text{and} \quad j(k) - j_{\max} \leq 0 \text{ for } k = 0, \dots, N + 1 \quad (33)$$

must hold. The jerk $j(k)$ in (33) is approximated by

$$j(k) \approx \frac{4(\Delta t(k - 1)\Delta v(k) - \Delta t(k)\Delta v(k - 1))}{(\Delta t^2(k) + \Delta t^2(k - 1))(\Delta t(k) + \Delta t(k - 1))}, \quad (34)$$

where $\Delta t(k) = x_1(k + 1) - x_1(k)$ and $\Delta v(k) = x_2(k + 1) - x_2(k)$. In (34) a non-equidistant (in time) central difference quotient is utilized.

The maximum traction force of a train $F_{t, \max}(v)$ is a function of the velocity v . A typical model for the maximum traction force of a train with an induction motor powered by a frequency-inverter is given by

$$F_{t, \max}(v) = \begin{cases} \bar{F}_{t, \max} = \text{const.} & 0 \leq v < v_a \\ \bar{F}_{t, \max} \cdot \frac{v_a}{v} & v_a \leq v < v_b \\ F_{t, \max}(v_b) \cdot \frac{v_b^2}{v^2} & v_b \leq v \end{cases} \quad (35)$$

With $F_{t, \max}(x_2(k))$ obtained by (35) the constraints

$$u(k) - F_{t, \max}(x_2(k)) \leq 0 \text{ for } k = 0, \dots, N, \quad (36)$$

have to hold.

3.3. Penalty functions and constraint scaling

In order to improve the convergence speed penalty functions and constraint scaling (see [25]) turned out to be successful measures. An additional exterior penalty function term is added to the cost function given by

$$P(\mathbf{u}) = \sum_i^m p_{h_i} \cdot (\max(0, h_i(\mathbf{u})))^2 + \sum_j^m p_{g_j} \cdot (g_j(\mathbf{u}))^2. \quad (37)$$

In (37) $h_i(\mathbf{u})$ and $g_j(\mathbf{u})$ are the i -th inequality and j -th equality constraint, respectively. The quantities p_{h_i} and p_{g_j} are appropriately chosen weighting factors.

3.4. Travel time criterion

To compute the minimum possible travel time T_{\min} from station “A” to station “B” under all constraints given in Section 3.2 the minimum of the cost function

$$J_T(\mathbf{u}) = x_1(N+1) \quad (38)$$

with respect to the decision vector \mathbf{u} is searched for (i.e. $T_{\min} = \min_{\mathbf{u}} J_T(\mathbf{u})$).

3.5. Electrical net energy criterion

In order to minimize the electrical net energy required by the traction system for a travel from station “A” to station “B” under all constraints given in Section 3.2 the minimum of the cost function

$$J_E(\mathbf{u}) = \sum_{k=0}^N \{Q_{te}(k)P_{el,t}(k) - Q_{be}(k)P_{el,b}(k)r(k)\} \Delta t(k) \quad (39)$$

with respect to the decision vector \mathbf{u} is searched for, where $\Delta t(k) = x_1(k+1) - x_1(k)$, and the optimal solution to (39) (i.e. $E_{\min} = \min_{\mathbf{u}} J_E(\mathbf{u})$) has to fulfill the additional constraint

$$x_1(N+1) - T_{\max} \leq 0. \quad (40)$$

In (40) T_{\max} is the maximum travel time allowed. With T_{\min} being the optimal objective value of the constraint problem (38), $T_{\max} \geq T_{\min}$ must hold in order to render the problem feasible.

In (39) the quantity $r(k)$ ($0 \leq r(k) \leq 1$) is the degree of regeneration at the position of sampling instance k . It specifies to which extent the electrical energy provided by electrical braking can be re-utilized. For a given track and time it can be taken from operating statistics. The quantities $Q_{te}(k)$ and $Q_{be}(k)$ (for $k = 0, \dots, N$) in (39) can be used for problem specific weighting of the energy contributions $P_{el,t}(k) \cdot \Delta t(k)$ and $P_{el,b}(k) \cdot \Delta t(k)$.

3.6. Iterative adaptive track discretization

To relieve the user of the tedious definition of adequate position samples for a given track (with specific speed limits, gradient angles, rolling resistance, etc.) an automatic adaptive track discretization is included in the trajectory optimizer. The starting point of the adaptive track discretization is a rough initial track discretization (iteration counter $i = 0$).

In iteration i of the adaptive track discretization the constraint optimal solution \mathbf{u}_{i-1}^* to (38) of iteration $i-1$ is utilized to generate new position samples for the optimization performed in iteration i . Based on dynamic simulation, these samples are placed at positions where the relative and/or absolute change in position, speed and/or acceleration are larger than given thresholds. Furthermore, \mathbf{u}_{i-1}^* is interpolated at these new position samples to obtain an adequate initial decision vector for the minimization of (38) performed in iteration i .

3.7. Flowchart of the train trajectory optimization

In Fig. 5a the flowchart of the train trajectory optimization is depicted. The trajectory optimization is solved by a sequential quadratic programming (SQP) algorithm (see [26,27]). Because both minimum travel time T_{\min} (see Section 3.4) and minimum electrical net energy E_{\min} for a given (maximum) travel time T_{\max} (see Section 3.5) are important goals a separate minimization is performed for each of these criteria.

First general settings (e.g. optimization work flow, track and train characteristics, comfort constraints, etc.), the initial track discretization, and the initial decision vector are defined. Then the travel time minimization (see Section 3.4) is performed and the dynamic system is simulated with the optimized inputs. For the electrical net energy minimization (see Section 3.5) the set of constraints is augmented by adding the additional constraint (40) on the travel time. Furthermore, the optimal decision vector of the travel time minimization is utilized as a good initial decision vector. A fast overall convergence of the electrical net energy minimization is achieved by neglecting the power losses of the components in the first place.

Remark: Advanced Communications-based train control (CBTC) systems (e.g. SIEMENS Trainguard MT) utilize a train trajectory optimizer like the presented optimizer to compute the target speed online based on the timetable, the current delay, safety restrictions, and possibly energy saving goals. The train trajectory optimizer of this work (lower-level optimizer) however is only used offline to compute commonly occurring trajectories in order to be able to perform the component optimization (upper-level optimization) in the best possible way.

4. Multi-objective mixed-integer system configuration optimization (upper-level optimization)

4.1. Problem formulation

With the vector of objectives $\mathbf{F}(\boldsymbol{\theta}) = [F_1(\boldsymbol{\theta}), \dots, F_j(\boldsymbol{\theta}), \dots, F_n(\boldsymbol{\theta})]^T$ and the parameter vector (decision vector) representing the system configuration $\boldsymbol{\theta} = [\theta_1, \dots, \theta_i, \dots, \theta_n]^T$ the multi-objective mixed-integer system configuration optimization

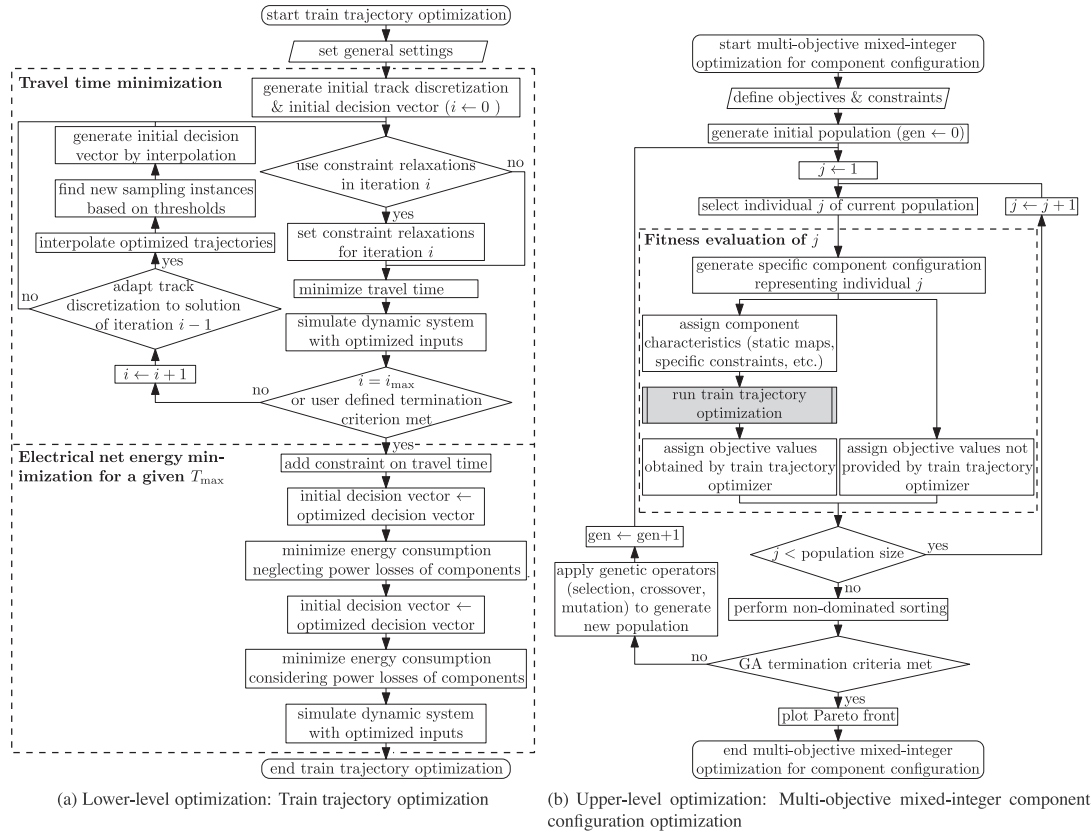


Fig. 5. Flowcharts of the two different optimization levels.

problem (upper-level optimization problem) is given by

$$\min_{\theta} \mathbf{F}(\theta) \quad \text{subject to: } \theta_L \leq \theta \leq \theta_U, \quad \theta_i \in \mathbb{Z}, \forall i \in I, \quad \text{and } \theta_i \in \mathbb{R}, \forall i \notin I \quad (41)$$

In (41) θ_L and θ_U are the (vectorized) lower and upper bounds, respectively, on the decision vector θ and $I \subseteq \{1, \dots, n\}$ is the index set of integer variables. The constraints in (41) constitute the mixed-integer decision space.

Beside investment costs, maintenance costs, required installation space, etc., the minimum travel time T_{\min} (see Section 3.4) and the minimum electrical net energy E_{\min} for a fixed maximum travel time (see Section 3.5) can be included in the vector of objectives $\mathbf{F}(\theta)$. For a specific system configuration $\theta = \theta_s$ the objective values $T_{\min} = T_{\min}(\theta_s)$ and $E_{\min} = E_{\min}(\theta_s)$ are obtained by the train trajectory optimizer (lower-level optimization problem) specially developed for that purpose.

4.2. Flowchart of the mixed-integer component configuration optimization

In Fig. 5b the flowchart of the multi-objective mixed-integer component configuration optimization is depicted.

First general settings have to be made and the optimization problem stated in Section 4.1 has to be defined. In accordance to the constraints in (41) a random initial population ($\text{gen} = 0$) is generated.

The specific traction system component configuration representing the individual j is generated. The train trajectory optimization of Fig. 5a is run with its specific characteristics. For individual j the objective values are assigned. Thereby, important objective values provided by the trajectory optimizer are T_{\min} and E_{\min} (see Sections 3.4 and 3.5). The objective values constitute the fitness of the individual j .

The fitness evaluation continues until the fitness of all individuals of the current population has been evaluated. Then the controlled elitist genetic algorithm (GA) (a variant of NSGA-II, see [28]) performs the non-domination sorting and applies the genetic operators (selection, crossover, and mutation) to generate a new generation. The generation counter is increased by one and the algorithm starts evaluating the individuals of the new population. The multi-objective GA stops if the spread,

a measure of the movement of the Pareto front, is smaller than a threshold or the maximum number of generations is reached.

5. Simulation results

First a simulation run of the iterative adaptive track discretization is shown and the train trajectory optimizer is validated. Then two case studies for optimizing the traction system configuration of a metro vehicle are carried out.

5.1. Adaptive track discretization run

In Fig. 6 the adaption of the track discretization in iteration $i = 1$ to the optimal solution of iteration $i - 1 = 0$ (with initial track discretization) is visualized in terms of velocity and force. In iteration $i = 1$ the admissible maximum distance of the samples and the applied thresholds for the absolute and/or the relative change of velocity, force, and acceleration were $\Delta s_{\max,i} = 100$ m, $\Delta v_{\max,i} = 3$ m/s, $\delta v_{\max,i} = 100\%$, $\Delta F_{\max,i} = 60$ kN, and $\Delta a_{\max,i} = 0.2$ m/s².

5.2. Validation of the train trajectory optimization

In this subsection the developed train trajectory optimization framework is validated using the results obtained from a proprietary SIEMENS train trajectory optimizer (TTO). Due to its long and well-tried record, high acceptance, and validation based on measurement data the optimization results obtained by the SIEMENS train trajectory optimizer can be considered as an accurate reference solution. In Fig. 7a and b the results of the two trajectory optimizers are compared in terms of time $t(s)$ and velocity $v(s)$, respectively. The obtained trajectories match very well. The difference in travel time between the SIEMENS TTO and the presented TTO is 0.334 s (-0.51%). For the two velocity curves a root-mean-square error (RMSE) of 0.0752 m/s is obtained.

5.3. Case studies: optimal traction system configuration of a metro

In this section two case studies for optimizing the traction system configuration of a metro are presented. First the problem setup is stated. Then the case studies are carried out. To demonstrate the main ideas and make a Brute-Force-Method applicable the first case study considers only a journey between two stations, and only one target running time. The Brute-Force-Method is utilized to validate the obtained Pareto front. In the second case study a robust Pareto front with respect to varying track characteristics, target running times, and train load variations is derived.

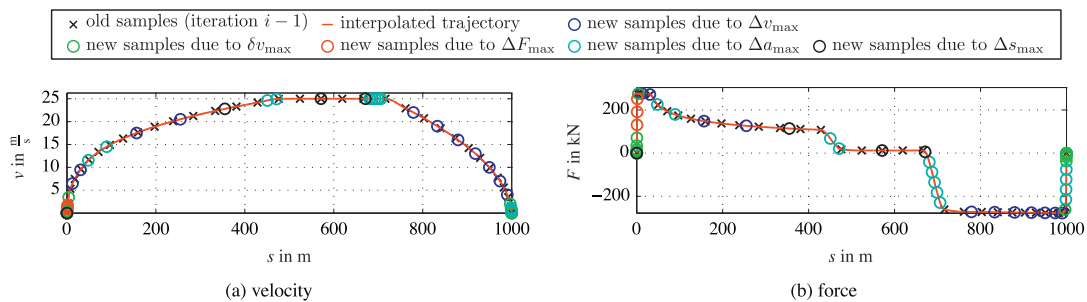


Fig. 6. Iterative adaptive track discretization. Optimal solution of iteration $i - 1$, interpolated trajectories based on optimal solution and discretization of iteration $i - 1$ (query points), and adapted track discretization (i.e. new samples) for optimization in iteration i .

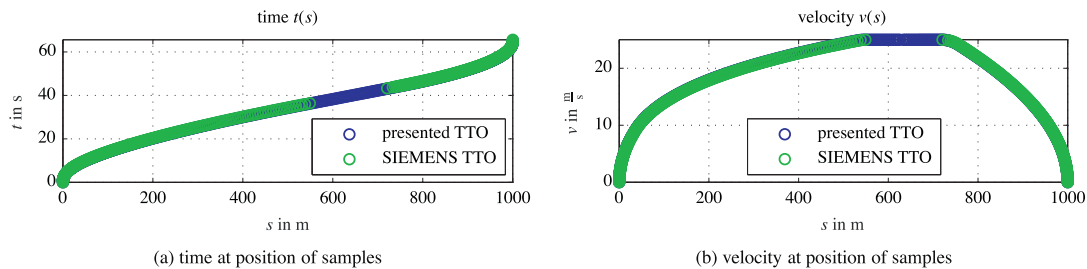
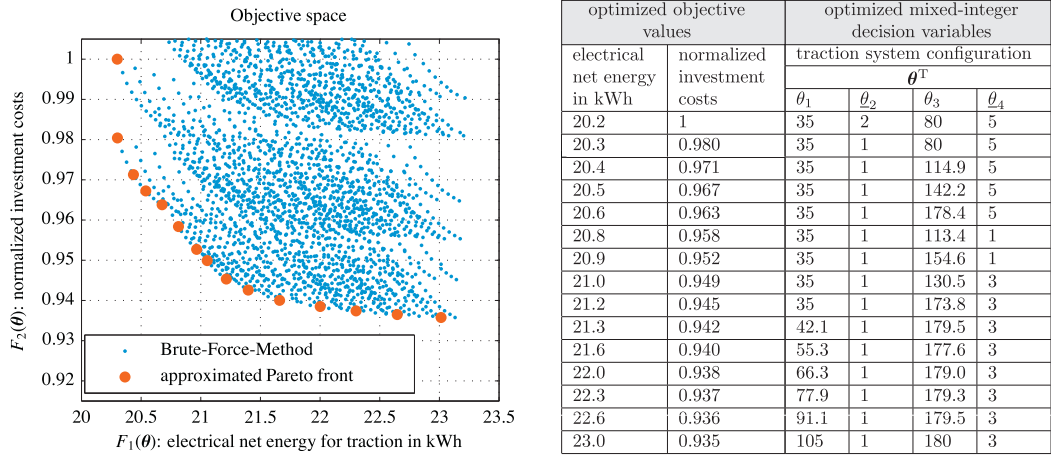


Fig. 7. Validation of the travel time minimization problem.



(a) approximate Pareto front for optimal traction system configurations (b) optimized objective values and corresponding mixed-integer decision variables

Fig. 8. Results case study 1: overall investment costs for the traction system vs electrical net energy for a fixed maximum travel time $T_{\max} = 65$ s.

5.3.1. Problem setup

In the following two case studies a traction system configuration is represented by the mixed-integer decision vector $\theta^T = [\theta_1 \ \theta_2 \ \theta_3 \ \theta_4]$. The index set of integer variables is $I = \{2, 4\}$. The continuous decision variables θ_1 ($35 \text{ m}\Omega \leq \theta_1 \leq 105 \text{ m}\Omega$) and θ_3 ($80^\circ\text{C} \leq \theta_3 \leq 180^\circ\text{C}$) represent the ohmic resistance of the input chokes and the stator temperature of the three-phase motors, respectively. The variables θ_1 and θ_3 have a negative relationship on a component's mass contribution. For a concrete value the respective component's static map of the power losses (see Section 2.2) is obtained by interpolation, utilizing validated static maps obtained from electrical simulations. The integer decision variables $\theta_2 \in \{1, \dots, 6\}$ and $\theta_4 \in \{1, \dots, 6\}$ represent the chosen inverter/motor kit variant and the chosen gear variant, respectively, each with its associated mass contribution, technical characteristics, and power losses given by its static mappings, see Section 2.2.

The economical impact of a specific component is either explicitly entered by the user or computed by a user defined law.

5.3.2. Case study 1: Pareto front for simple example (one track section with only one target running time) validated by a Brute-Force-method

In the first case study the chosen objectives to be minimized are the electrical net energy for a fixed maximum travel time $T_{\max} = 65$ s ($F_1(\theta)$) and the overall investment costs for the traction system ($F_2(\theta)$). The resulting approximated Pareto front is shown in Fig. 8a. Its optimized objective values and the corresponding mixed-integer decision variables are listed in Fig. 8b. For validation of the obtained approximated Pareto front also the objective values obtained by a Brute-Force-Method are depicted in Fig. 8a. To apply the Brute-Force-Method the continuous decision variables θ_1 and θ_3 where discretized in 13 and 11, respectively, equidistant steps. On a standard laptop the Brute-Force-Method took more than 5 days to compute, whereas the approximated Pareto front was obtained in less than 12 h.

As evident from Fig. 8b the optimized decision variable θ_2 is either one or two. The other inverter/motor kit variants do not lead to Pareto optimal solutions. The most energy efficient trade-off solution is obtained for $\theta_2 = 2$. However, it is also the most expensive trade-off solution and the achieved additional energy saving is small compared to the second most energy efficient trade-off solution (where $\theta_2 = 1$).

5.3.3. Case study 2: robust Pareto front considering varying track characteristics, target running times, and train loads

In this case study a robust Pareto front of optimal component configurations with respect to varying target running times and passenger loads is obtained. A whole line with four track sections with quite different track characteristics and speed limits is considered. The first track section is a straight section with a high speed limit. The second section is a curved track section with low speed limits. The third has a steep uphill and the fourth a steep downhill part.

Robustness of the Pareto optimal component configurations with respect to the considered variations and track characteristics is obtained as follows: The energy objective $F_1(\theta)$ (for an individual θ) is now obtained by weighting the energy $F_{1,i,j_i,k_i}(\theta, L_{j_i}, T_{\max,k_i})$ of each case (combination of considered passenger load L_{j_i} and target running time T_{\max,k_i} for a given track section i) with its discrete probability of occurrence p_{i,j_i,k_i} and summing up over all possible cases ($n_{j_i} \cdot n_{k_i}$) and track

Table 1
Passenger loads (L_{j_i}) and target running times ($T_{\max k_i}$) and their discrete probabilities of occurrence ($p_{L_{j_i}}$ and $p_{T_{\max k_i}}$, respectively) for track section $i = 1$.

Section 1	L_{j_i} :	100%	60%	30%	10%
	$p_{L_{j_i}}$:	0.05	0.40	0.35	0.20
	$T_{\max k_i}$:	92 s	104 s	117 s	129 s
	$p_{T_{\max k_i}}$:	0.20	0.50	0.20	0.10

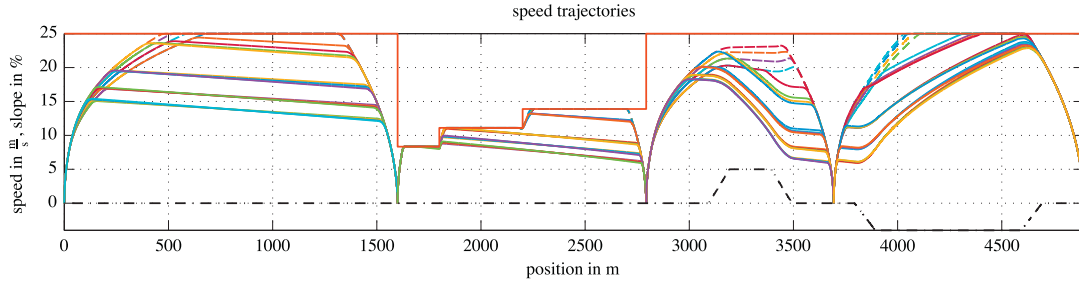


Fig. 9. Optimal speed trajectories (whole line with four track sections) for the individual $\theta^T = [70 \text{ m}\Omega \quad 1 \quad 150 \text{ }^\circ\text{C} \quad 1]$ (solid lines: energy optimal speed trajectories for target travel times; dashed lines: time optimal speed trajectories due to passenger load variations; dotted-dashed line: slope).

sections ($i = 1, \dots, n$).

$$F_1(\theta) = \sum_i^n \sum_{j_i}^{n_{j_i}} \sum_{k_i}^{n_{k_i}} p_{i,j_i,k_i} \cdot F_{1,i,j_i,k_i}(\theta, L_{j_i}, T_{\max k_i}) \quad (42)$$

For target running time variations a similar robustness approach was performed in [22]. However, the goal was to obtain Pareto optimal driving parameters required by a specific ATO equipment. In this work the interest lies in Pareto optimal traction system configurations.

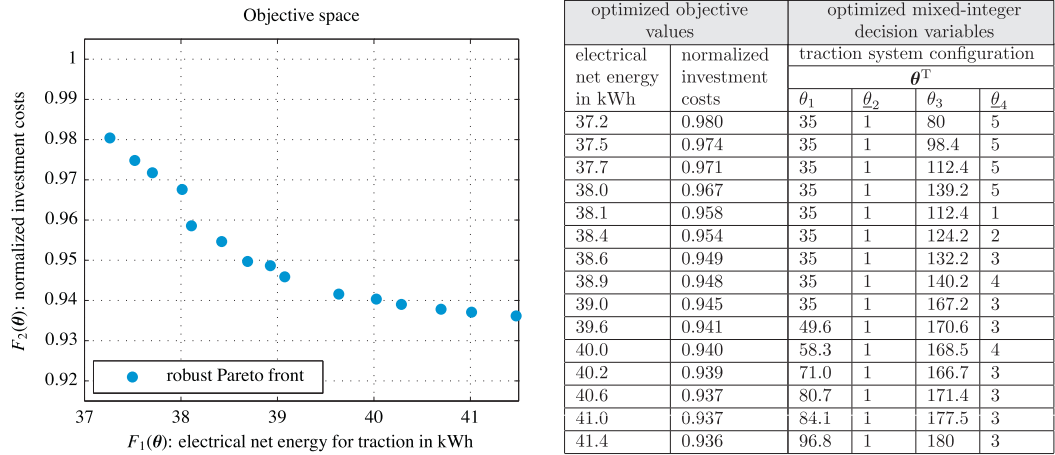
For the first track section ($i = 1$) the considered passenger load (L_{j_1} with $j_1 = 1, \dots, 4$) and target running time variations ($T_{\max k_1}$ with $k_1 = 1, \dots, 4$) and their discrete probabilities of occurrence ($p_{L_{j_1}}$ and $p_{T_{\max k_1}}$, respectively) are given in Table 1. Without limiting the performed method, the discrete joint probability distribution p_{i,j_i,k_i} utilized in (42) is obtained by considering statistical independence i.e. $p_{i,j_i,k_i} = p_{L_{j_i}} \cdot p_{T_{\max k_i}}$. For a specific track section the discrete probabilities can be obtained from operating statistics by interval discretization or from an expert estimate.

For convenience for each track section four target running time variations and four passenger load variations were considered (i.e. 16 cases per section). For the specific individual $\theta^T = [70 \text{ m}\Omega \quad 1 \quad 150 \text{ }^\circ\text{C} \quad 1]$ all 64 obtained energy optimal speed trajectories utilized to determine $F_1(\theta)$ (applying (42)) are depicted in Fig. 9 (solid lines). Additionally Fig. 9 shows all 16 time optimal speed trajectories due to the considered passenger load variations (dashed lines) and the slope of the track (dotted-dashed line).

With the new energy objective $F_1(\theta)$ given by (42) the robust Pareto front of optimal component configurations is shown in Fig. 10a. The optimized objective values and the corresponding mixed-integer decision variables are listed in Fig. 10b. As evident from Fig. 10a the obtained robust Pareto front is similar in shape to the Pareto front of the simple example in Section 5.3.2 (compare Fig. 8a). Also the optimized mixed-integer decision variables (see Fig. 10b) are similar to those obtained in Section 5.3.2 (compare Fig. 8b). This indicates that even the simple example of the first case study (one track section with only one target running time) can be used for a quick pre-design. However, the optimized integer variable $\theta_2 = 2$ (θ_2 represents the inverter/motor kit variant) does not lead to a robust Pareto optimal solution. Fortunately, the low-priced inverter/motor kit variant $\theta_2 = 1$ leads to robust Pareto optimal solutions.

6. Conclusion & outlook

A holistic framework for optimizing the traction system configuration of trains with respect to the multiple conflicting objectives is proposed. The overall multiobjective optimization is achieved by a two level approach. To capture the influence of a specific traction system configuration on travel time and energy a subordinated train trajectory optimizer (lower-level optimizer) is developed, validated, and utilized as centerpiece. The train trajectory optimizer considers the power losses of the components given as validated static look up tables. Speed limits, technological constraints, and constraints ensuring passenger comfort are observed. Furthermore, the effects of regenerative braking on the optimal train trajectory are considered.



(a) Robust Pareto front of optimal traction system configurations with respect to varying track characteristics, target running times, and train load variations (b) robust optimized objective values and corresponding mixed-integer decision variables

Fig. 10. Results case study 2: overall investment costs for the traction system vs electrical net energy.

If for a specific application a specific ATO system/equipment exists and severely limits the possible train trajectories, then the methods presented in [19–22] must be used to capture the influence of the variability of the speed trajectories on the optimal traction system configuration. Nevertheless, the robustness approach presented in Section 5.3.3 can be used to obtain a robust Pareto front of optimal component configurations with respect to train speed profile variations.

Because some components are chosen from a finite set of few elements, whereas other components can easily be produced with arbitrary parameters, mixed-integer decision variables were defined. The component configuration optimization problem (upper-level optimization) is solved by using a multi-objective mixed-integer elitist genetic algorithm. Thus, it is possible for the first time to optimize the essential conflicting design objectives simultaneously and visualize the different Pareto-optimal trade-off solutions.

In case of a huge set of possible system configurations the presented optimization framework is a valuable tool. However, also in case of only a small closed set with a few eligible discrete variants for each component the presented holistic optimization can provide valuable assistance in finding the possibly unique global optimum. If the investment costs and energy consumption are chosen as objectives of the holistic optimization, the obtained optimal trade-off solutions can be utilized as a sound foundation for the computation of realistic life cycle costs.

The proposed holistic simulation-based optimization approach has the potential to yield better, customer-specific traction systems and can contribute to the reduction of energy consumption for traction. It is planned to augment the presented method by considering also the auxiliaries and the heating, ventilation and air conditioning (HVAC) units in the holistic optimization, based on the results of [29], where a dynamic thermal vehicle model of a tram and a modular structured and easy to parameterize HVAC model has been presented. Reuse of regenerative braking energy for HAVC and/or the auxiliaries is expected to have effects on the obtained optimal train trajectory.

Acknowledgment

This work was supported by the project “EnerCom” (FFG, No. 846041) in cooperation with Siemens AG Österreich.

References

- [1] K. Li, Z. Gao, An improved equation model for the train movement, *Simul. Modell. Pract. Theory* 15 (9) (2007) 1156–1162, doi:10.1016/j.simpat.2007.07.006.
- [2] G. Figueira, B. Almada-Lobo, Hybrid simulation-optimization methods: a taxonomy and discussion, *Simul. Modell. Pract. Theory* 46 (2014) 118–134, doi:10.1016/j.simpat.2014.03.007. *Simulation-Optimization of Complex Systems: Methods and Applications*
- [3] K. Deb, A. Pratap, S. Agarwal, T. Meyarivan, A fast and elitist multiobjective genetic algorithm: NSGA-II, *Evol. Comput. IEEE Trans.* 6 (2) (2002) 182–197, doi:10.1109/4235.996017.
- [4] M. Erbas, A. Biyikoglu, Design and multi-objective optimization of organic rankine turbine, *Int. J. Hydrogen Energy* 40 (44) (2015) 15343–15351, doi:10.1016/j.ijhydene.2015.04.143. The 4th International Conference on Nuclear and Renewable Energy Resources (NURER2014), 26–29 October 2014, Antalya, Turkey.
- [5] R. Long, B. Li, Z. Liu, W. Liu, Multi-objective optimization of a continuous thermally regenerative electrochemical cycle for waste heat recovery, *Energy* 93 (Part 1) (2015) 1022–1029, doi:10.1016/j.energy.2015.09.098.

- [6] A. Kamjoo, A. Maheri, A.M. Dizqah, G.A. Putrus, Multi-objective design under uncertainties of hybrid renewable energy system using NSGA-II and chance constrained programming, *Int. J. Electr. Power Energy Syst.* 74 (2016) 187–194, doi:10.1016/j.ijepes.2015.07.007.
- [7] Y. Chen, H. Li, B. He, P. Wang, K. Jin, Multi-objective genetic algorithm based innovative wind farm layout optimization method, *Energy Convers. Manage.* 105 (2015) 1318–1327, doi:10.1016/j.enconman.2015.09.011.
- [8] A.E. Brownlee, J.A. Wright, Constrained, mixed-integer and multi-objective optimisation of building designs by NSGA-II with fitness approximation, *Appl. Soft Comput.* 33 (2015) 114–126, doi:10.1016/j.asoc.2015.04.010.
- [9] M.S. Mahbuba, M. Cozzini, P.A. Ostergaard, F. Albertia, Combining multi-objective evolutionary algorithms and descriptive analytical modelling in energy scenario design, *Appl. Energy* 164 (2016) 140–151, doi:10.1016/j.apenergy.2015.11.042.
- [10] H. Pierrelval, J.L. Paris, From “simulation optimization” to “simulation configuration” of systems, *Simul. Modell. Pract. Theory* 11 (1) (2003) 5–19, doi:10.1016/S1569-190X(02)00096-5. *Modelling and Simulation: Analysis, Design and Optimisation of Industrial Systems.*
- [11] M. Poursina, N.T. Dehkordi, A. Fattahi, H. Mirmohammadi, Application of genetic algorithms to optimization of rolling schedules based on damage mechanics, *Simul. Modell. Pract. Theory* 22 (2012) 61–73, doi:10.1016/j.simpat.2011.11.005.
- [12] Z. Dimitrova, F. Maréchal, Techno-economic design of hybrid electric vehicles and possibilities of the multi-objective optimization structure, *Appl. Energy* 161 (2016) 746–759, doi:10.1016/j.apenergy.2015.09.071.
- [13] P. Xu, C. Yang, Y. Peng, S. Yao, D. Zhang, B. Li, Crash performance and multi-objective optimization of a gradual energy-absorbing structure for subway vehicles, *Int. J. Mech. Sci.* (2016), doi:10.1016/j.ijmecsci.2016.01.001.
- [14] Y. Eren, H. Gorgun, An applied methodology for multi-objective optimum sizing of hybrid electric vehicle components, *Int. J. Hydrogen Energy* 40 (5) (2015) 2312–2319, doi:10.1016/j.ijhydene.2014.12.024.
- [15] A.K. Nandi, D. Chakraborty, W. Vaz, Design of a comfortable optimal driving strategy for electric vehicles using multi-objective optimization, *J. Power Sources* 283 (2015) 1–18, doi:10.1016/j.jpowsour.2015.02.109.
- [16] V.D. Martinis, M. Gallo, Models and methods to optimise train speed profiles with and without energy recovery systems: a suburban test case, *Procedia* 87 (2013) 222–233, doi:10.1016/j.sbspro.2013.10.606. *SIDT Scientific Seminar 2012.*
- [17] A. Albrecht, P. Howlett, P. Pudney, X. Vu, P. Zhou, The key principles of optimal train control-Part 1: formulation of the model, strategies of optimal type, evolutionary lines, location of optimal switching points, *Transp. Res. B* (2015), doi:10.1016/j.trb.2015.07.023.
- [18] A. Albrecht, P. Howlett, P. Pudney, X. Vu, P. Zhou, The key principles of optimal train control-Part 2: existence of an optimal strategy, the local energy minimization principle, uniqueness, computational techniques, *Transp. Res. B* (2015), doi:10.1016/j.trb.2015.07.024.
- [19] M. Domínguez, A. Fernández, A.P. Cucala, P. Lukaszewicz, Optimal design of metro automatic train operation speed profiles for reducing energy consumption, *Proc. Inst. Mech. Eng. F* 225 (5) (2011) 463–474, doi:10.1177/09544097JRR1420.
- [20] M. Domínguez, A. Fernández, A.P. Cucala, R.R. Pecharroman, Energy savings in metropolitan railway substations through regenerative energy recovery and optimal design of ATO speed profiles, *Automat. Sci. Eng. IEEE Trans.* 9 (3) (2012) 496–504, doi:10.1109/TASE.2012.2201148.
- [21] M. Domínguez, A. Fernández-Cardador, A.P. Cucala, T. Gonsalves, A. Fernández, Multi objective particle swarm optimization algorithm for the design of efficient ATO speed profiles in metro lines, *Eng. Appl. Artif. Intell.* 29 (2014) 43–53, doi:10.1016/j.engappai.2013.12.015.
- [22] A. Fernández-Rodríguez, A. Fernández-Cardador, A.P. Cucala, M. Domínguez, T. Gonsalves, Design of robust and energy-efficient ATO speed profiles of metropolitan lines considering train load variations and delays, *IEEE Trans. Intell. Transp. Syst.* 16 (4) (2015) 2061–2071, doi:10.1109/TITS.2015.2391831.
- [23] P. Howlett, P. Pudney, *Energy-Efficient Train Control, Advances in Industrial Control, Springer London, 2012.*
- [24] W. Hay, *Railroad engineering, A Wiley-Interscience publication, Wiley, 1982.*
- [25] O. Nelles, *Nonlinear System Identification: From Classical Approaches to Neural Networks and Fuzzy Models, Engineering online library, Springer, Berlin, Germany, 2001.*
- [26] J. Nocedal, S. Wright, *Numerical Optimization, Springer Series in Operations Research and Financial Engineering, Springer New York, 2006.*
- [27] J. Bonnans, J. Gilbert, C. Lemaréchal, C. Sagastizábal, *Numerical Optimization: Theoretical and Practical Aspects, Universitext, Springer Berlin Heidelberg, 2013.*
- [28] K. Deb, *Multi-Objective Optimization Using Evolutionary Algorithms, Wiley Interscience Series in Systems and Optimization, Wiley, 2001.*
- [29] C. Dullinger, W. Struckl, M. Kozek, A modular thermal simulation tool for computing energy consumption of HVAC units in rail vehicles, *Appl. Therm. Eng.* 78 (2015) 616–629, doi:10.1016/j.applthermaleng.2014.11.065.

2.3 Publication C

Christian Dullinger, Walter Struckl, and Martin Kozek.

A general approach for mixed-integer predictive control of HVAC systems using MILP.

Applied Thermal Engineering, Volume 128, 2018, Pages 1646-1659.

DOI: 10.1016/j.applthermaleng.2017.09.104

Own contribution

Problem analysis, selection of methods, execution of the solution, development and programming of algorithms, consideration of implementation aspects, performing simulations studies, and structuring, writing, and editing of the manuscript was done by the applicant. Problem statement and discussion was done by the second author. Problem statement, discussion and editing was done by the third author.

Applied Thermal Engineering 128 (2018) 1646–1659



Contents lists available at ScienceDirect

Applied Thermal Engineering

journal homepage: www.elsevier.com/locate/apthermeng

Research Paper

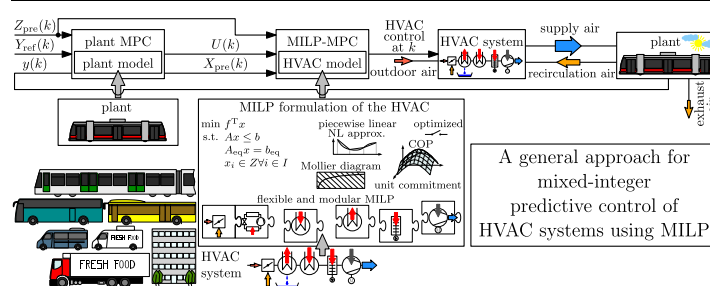
A general approach for mixed-integer predictive control of HVAC systems using MILP

Christian Dullinger^{a,*}, Walter Struckl^b, Martin Kozek^a^a Institute of Mechanics and Mechatronics, Division of Control and Process Automation, Getreidemarkt 9/325-A5, A-1060 Vienna, Austria^b Siemens AG Österreich, Austria

HIGHLIGHTS

- Optimized HVAC operation highly versatile in terms of energy, comfort, and wear.
- Modular and flexible MILP model of HVACs to achieve (near) global optimum.
- Hierarchical MIMO model predictive control (MPC) framework for HVAC operation.
- Adjustable piecewise-linear approximation of nonlinear component characteristics.
- Optimal switching decision for components with dwell times.

GRAPHICAL ABSTRACT



ARTICLE INFO

Article history:
 Received 5 May 2017
 Revised 3 September 2017
 Accepted 21 September 2017
 Available online 22 September 2017

ABSTRACT

The topic of the paper is optimal control of heating, ventilation, and air conditioning (HVAC) systems. Using mixed-integer linear programming (MILP) the main contribution is a flexible and modular MILP model of HVACs. It is the centerpiece of the proposed hierarchical multi-input multi-output (MIMO) model predictive control (MPC) framework for energy, comfort, and wear optimization. On the upper-level a plant MPC takes care of the slow dynamics of a plant. On the lower-level a MILP-MPC based on a MILP optimization model of an HVAC system optimizes the HVAC operation. The MILP-MPC considers the first few samples of the control trajectory of the plant MPC as its reference trajectory. It minimizes power consumption and switching of the HVAC. Thereby it has to obey constraints, consider component characteristics by nonlinearity approximation, and solve a unit commitment problem. The fact that the plant MPC can be based on an almost arbitrary plant model and the MILP model of the MILP-MPC can represent a variety of different HVAC systems unifies HVAC control. Features and results are presented in case studies: The first case study shows that state of the art HVAC operation is outperformed even if the predictive capability is not used. The second case study demonstrates that temperature, CO₂ level, and humidity can be controlled simultaneously in a decoupled fashion. The third case study reveals that if also the lower-level MILP-MPC oversees the latency periods of HVAC components optimal switching is achieved.

© 2017 Elsevier Ltd. All rights reserved.

Abbreviations: AC, air condition; CHP, combined heat and power; COP, coefficient of performance; DOF, degrees of freedom; FSM, finite state machine; HB, heater battery; HEN, heat exchanger network; HP, heat pump; HVAC, heating, ventilation, and air conditioning; IDA, indoor air; LP, linear programming; MILP, mixed-integer linear programming; MIMO, multi-input multi-output; MINLP, mixed-integer nonlinear programming; MPC, model predictive control; NLP, nonlinear programming; ODA, outdoor air; PID, proportional integral derivative; PWM, pulse width modulation; QP, quadratic program; RBF, radial basis function; RCA, recirculation air; RM, refrigeration machine; SAF, supply air fan; SOS-2, special ordered set of type 2; SUP, supply air; TES, thermal energy storage; ULF, Ultra Low Floor; VCP, vapor compression plant.

* Corresponding author.

E-mail addresses: christian.dullinger@tuwien.ac.at (C. Dullinger), walter.struckl@siemens.com (W. Struckl), martin.kozek@tuwien.ac.at (M. Kozek).

<https://doi.org/10.1016/j.applthermaleng.2017.09.104>
 1359-4311/© 2017 Elsevier Ltd. All rights reserved.

Nomenclature	
b_{AC}	by-pass valve state refrigeration machine •
c_A	volume fraction CO ₂ air mass/mass flow A
$c_{p,a}/c_{p,v}$	specific heat capacity dry air/water vapor
$\bullet_{\max}/\bullet_{\min}$	maximal/minimal value of quantity •
\bullet^*	optimal value of quantity •
\bullet	parameter provided to the MILP
\hat{h}_A	specific enthalpy wet air mass/mass flow A
$H_{H_2O,COND}$	enthalpy flow of condensed water
$h_{H_2O,COND}$	specific enthalpy of condensed water
i	time instance of a prediction
$I_{\bullet,ON/OFF}$	switching component • on indicator
J_{\bullet}	MILP cost function term of •
$J(k)$	overall MILP cost function at time step k
$J_P(k)$	MILP cost function term electrical power
$J_{p,\bullet,change}$	MILP cost function term penalizing state changes of component •
$J_{p,\bullet,ON/OFF}$	MILP cost function term penalizing switching component • on
$J_{p,u_1,\vartheta_{SUP}}$	MILP cost function term supply air temperature ϑ_{SUP} violations
$J_{p,u_j}(k)$	MILP cost function term penalizing deviations from desired plant input j
k	current time step
\dot{m}_A	wet air mass flow A
$\dot{m}_{H_2O,COND}$	water mass flow of condensed water
\underline{m}_{\bullet}	lower bound utilized in big-M formulation
\overline{M}_{\bullet}	upper bound utilized in big-M formulation
n	largest index number (i.e. $j = 1, \dots, n$)
N_c	control horizon plant MPC
$N_{c,MILP}$	control horizon MILP-MPC
N_p	prediction horizon plant MPC
$N_{p,MILP}$	prediction horizon MILP-MPC
$P(k+i)$	power consumption HVAC at $k+i$
P_{\bullet}	electrical power consumption of component •
$Q(k+i)$	plant MPC weighting matrix reference tracking
$\hat{Q}_{AC\ast xb}$	reduced cooling power refrigeration machine (first type; version •) due to by-pass
$\hat{Q}_{HP\ast xb}$	reduced heating power heat pump (first type; version •) due to by-pass
$\hat{Q}_C(k+i)$	total cooling power of the HVAC at $k+i$
\hat{Q}_{\bullet}	cooling/heating power of component •
$\hat{Q}_H(k+i)$	total heating power of the HVAC at $k+i$
$R(k+i)$	plant MPC weighting matrix control
r_0	enthalpy of evaporation
$S(k+i)$	plant MPC weighting matrix control increments
$T_{\bullet,ON}$	min. consecutive on time component •
$T_{\bullet,OFF}$	min. consecutive off time component •
$T_{s,L}(k+i)$	plant MPC weighting matrix lower slack variables
$T_{s,U}(k+i)$	plant MPC weighting matrix upper slack variables
$U(k)$	plant MPC optimized control trajectories
$u(k+i)$	plant MPC optimized control at $k+i$
u_j	input j plant MPC plant model
$u_{j,MILP}$	plant input j computed by MILP
$U_{\max}(k)$	time-variant upper bound on $U(k)$
$u_{\max}(k+i)$	upper bound on control $u(k+i)$ plant MPC
$U_{\min}(k)$	time-variant lower bound on $U(k)$
$u_{\min}(k+i)$	lower bound on control $u(k+i)$ plant MPC
v_{\bullet}	valve position of RM/HP (second type) •
$W_{t,SAF}$	power introduced by the supply air fan
$W_{\bullet}(k+i)$	weight sequence for MILP objective •
$x_{H_2O,A}$	water content wet air mass/mass flow A
$X_{pre}(k)$	predicted state trajectories at k
$x_{pre}(k+i k)$	plant MPC state predictions for $k+i$ at k
$y(k)$	plant output (state of the indoor air)
$Y(k)$	predicted plant output trajectories at k
$y(k+i k)$	predicted plant output for $k+i$ at k
$Y_{\max}(k)$	time variant upper limit on $Y(k)$
$Y_{\min}(k)$	time variant lower limit on $Y(k)$
$Y_{ref}(k)$	predicted reference trajectories for y at k
$y_{ref}(k+i k)$	reference trajectories for $k+i$ at k
$Y_{ref,MILP}(k)$	reference trajectories for MILP-MPC at k
$Y_{s,L}(k)$	slack variables subtracted from $Y_{\min}(k)$
$Y_{s,U}(k)$	slack variables added to $Y_{\max}(k)$
$Z_{pre}(k)$	predicted disturbance trajectories at k
$z_{pre}(k+i k)$	disturbance predictions for $k+i$ at k
Greek letters	
α	fresh air ratio
$\delta_{\bullet,j}$	j -th binary variable for modeling •
$\delta_{\bullet,ON/OFF}$	binary indicating if component • is switched on
ϑ_A	temperature of air mass/mass flow A
ϑ_{AC}	temperature of the evaporator heat exchanger (RM of type & version •)
$\lambda_{\bullet,j}$	SOS-2 variable for approximating nonlinearities of component •
ω	rotational speed of compressor
Δ_{\bullet}	variable for penalizing deviations/violations of •
Subscripts	
ACD	RM (first type) with discrete compressor power P_{ACD}
ACS	RM (first type) with semi-continuous compressor power P_{ACS}
ACV	RM (second type) with semi-continuous (electronic expansion/by-pass) valve
c	multiplicity counter of components with same MILP formulation
C	cooling
COND	condensed water
H	heating
HB	heater battery
HP	heat pump
HPD	HP (first type) with discrete compressor power P_{ACD}
HPS	HP (first type) with semi-continuous compressor power P_{ACS}
HPV	HP (second type) with semi-continuous (electronic expansion/by-pass) valve
IDA	indoor air
j	index counter (e.g. $j = 1, \dots, n$)
ODA	outdoor air
RCA	recirculation air
SAF	supply air fan
SUP	supply air

1. Introduction

Heating, ventilation, and air conditioning (HVAC) systems have to provide the required heating/cooling power for a plant and ensure the quality of the indoor air in terms of temperature, CO₂ level, and humidity with growing expectations of occupants. In

doing so, they should be operated as energy efficient as possible. Furthermore, life expectancy of the HVAC components should be maximized. With many HVAC subsystems and consequently degrees of freedom (DOF) this becomes a challenging task. Continuous, discrete, and switched components render the overall system hybrid. Both technical and comfort-related criteria impose needs

1648

C. Dullinger et al./Applied Thermal Engineering 128 (2018) 1646–1659

and restrictions on the HVAC operation. Dwell times of certain components (e.g. compressors) have to be observed, evaporator icing must be prevented, the temperature of the supply air has to lie within a comfort zone, and many more restrictions apply.

The task is often accomplished by a rule based control strategy with well-defined switching transitions between constant operating modes. However, with several different or multiple HVAC components the number of distinct operating modes increases rapidly. Because the number of required rules grows exponentially with the number of components, the task quickly becomes impossible to solve. Furthermore, unexpected operating conditions and unsuitable switching transitions can yield trapped operating modes.

In this work a highly versatile and numerically tractable hierarchical MIMO MPC framework is proposed to meet the aforementioned requirements (see Fig. 1). On the upper-level a computationally inexpensive plant MPC enables large horizons to take care of the slow dynamics of a plant. It can effectively incorporate available disturbance forecasts if available. The plant MPC can be based on an almost arbitrary plant model. On the lower-level a MILP-MPC based on a flexible and modular MILP model which can represent a variety of different HVAC systems optimizes the HVAC operation. The MILP-MPC considers the control trajectory of the plant MPC as its reference trajectory. It minimizes power consumption and switching. Thereby it obeys the technological limitations and solves a unit commitment problem. Because the control variables of the MILP-MPC are those mixed-integer decision variables of the MILP model defining the continuous and discrete states of the HVAC components no heuristics have to be applied to account for discrete or switching HVAC components. Due to its prediction horizon the MILP-MPC can oversee the dwell times of HVAC components achieving optimized switching times. The mixed-integer linear formulation of the HVAC ensures a (near) global optimality and reduces the computational burden. Nonlinear component characteristics and the Mollier diagram are piecewise linear approximated to balance modeling accuracy with computation time.

A standard approach to solve the HVAC operation task is to apply a hierarchical control scheme. Often the continuous-valued control signal of a proportional integral derivative (PID) controller on the upper level is followed by heuristics or pulse width modulation (PWM) to account for discrete states of HVAC components on the lower level. In [1] a novel optimization algorithm based on epsilon constraint radial basis function (RBF) neural network for a self tuning PID controller of a decoupled HVAC system is presented. However, the system model of the HVAC does not contain integer or discrete variables. In [2] a fuzzy self-tuning PID controller is designed for temperature control of a vehicle climate chamber. Heuristics are applied in the lower level to account for switching HVAC equipment but yield suboptimal energy consumption. Furthermore, frequent switching increases wear and tear.

Increasing availability of accurate disturbance forecasts (like ambient temperature, occupancy, driving speed, etc.) motivates the usage of predictive controllers in the upper-level which can attain extra performance by utilizing this information.

In [3] a hierarchical control structure, including model predictive controllers (MPCs), is applied on a transport refrigeration system with a thermal energy storage (TES) unit parallel to the evaporator. The predictive controller on the upper level solves a

charge scheduling problem for the TES, regarding a predicted driving profile of the delivery truck. In the lower level an MPC optimizes the compressor speed. With the proposed hierarchical optimal control approach, capturing the traffic pattern, performance is improved. However, integer or discrete decision variables are again not addressed.

The authors in [4] design a discrete MPC for an automotive air-conditioning system with a three-speed compressor. Three continuous MPCs are solved simultaneously, each associated to one compressor speed with two continuous inputs (evaporator and condenser fan frequency). The three cost values of the MPCs are compared. The three inputs corresponding to that MPC with the lowest cost value are applied. For a system with only one discrete component and only with a few discrete states this method is appropriate. However, for a whole HVAC with many switching and discrete states the computational burden of this method will increase in an exponential way. Furthermore, [4] did not yet include a power consumption model (e.g. via the COP map) in the objective function. Instead only control efforts were weighted. In this work the MILP-MPC (controlling the HVAC operation) considers static nonlinear power consumption models of all HVAC components (refrigeration machines, heat pumps, supply air fan, etc.) via piecewise linear approximation.

From existing literature a hierarchical control scheme seems advantageous to achieve computational tractability, especially if predictive controllers with large prediction horizons are applied in the upper level. However, in the lower level mixed-integer optimization should be applied. The benefit of mixed-integer optimization is that the mixed-integer nature of the decision variables (defining the HVAC operation mode) is optimally addressed, and the subsequent application of heuristics or PWM is not required. In this work the MILP-MPC of the MPC + MILP-MPC framework is based on a flexible and modular mixed-integer linear programming (MILP) model of an HVAC. Early works on mixed-integer predictive control of a hybrid system (with continuous and integer decision variables) using MILP are given by [5,6].

MILP models have been successfully applied to many thermal optimization problems. In [7] a MILP model of a distributed energy supply network integrated with electricity and hot water interchanges is presented. Ref. [8] proposes a stochastic model for steam and power system design composed of both system configuration and operating scheduling. The system model is formulated as MILP. In [9] a mathematical programming formulation for the design of water and heat exchanger networks (HENs) based on a two-step methodology is presented. In the first step, an MILP formulation is used to solve the water and energy allocation problem. In [10] a MILP optimization model for the retrofit of large scale HENs with intensified heat transfer techniques is presented. In [11] a MILP model for sizing a combined heat and power (CHP) system to be installed within a micro-grid is proposed. The objectives are minimizing the total operational cost of the micro-grid and finding the optimal size of the CHP.

All the afore-mentioned MILP models consider flows of hot/cold water, steam, and electricity, respectively. In the presented work the MILP model of the HVAC considers the required net enthalpy flows of humid air, net mass flows of CO₂, and net mass flows of water for the plant. Thereby it minimizes power consumption and wear of the HVAC.

In [12] a power grid simulation model for long term operation planning is presented. The work utilizes a MILP formulation and additionally addresses the unit commitment problem, which limits the on/off states of units. Because the MILP-model of the presented framework utilizes a prediction horizon it is capable to consider future demand in its decision upon the optimal on/off states of switched HVAC components with dwell times.



Fig. 1. Basic control architecture MPC + MILP-MPC framework.

The idea to split a complex nonlinear optimization problem into a sequential approach is computationally beneficial. In [13] a sequential approach for the synthesis of multi-period HENs is presented. An approach was proposed to solve the problem, in three sequential steps, represented by LP, MILP and NLP models. In this work also a sequential approach is chosen to solve the HVAC operation problem. First, for the plant MPC a constrained quadratic program (QP), and then for the MILP-MPC a MILP model of the HVAC is solved.

In contrast to nonlinear programming (NLP) and mixed-integer nonlinear programming (MINLP) (e.g. [14]), MILP offers the clear advantage that exact algorithms of MILP obtain the global optimum or in case of early stopping a statement with respect to optimality of the found solution [15]. The authors in [16] present a shortcut model for energy efficient water network synthesis with single contaminant. To solve the model efficiently and guarantee the solution to be the global optimum the model is formulated as a MILP. The drawback compared to NLP and MINLP is that a close approximation of nonlinearities often requires the introduction of many binary variables. In this work nonlinear component characteristics (e.g. characteristic diagram of a refrigerating machine) and the Mollier diagram are approximated as piecewise linear (with adjustable precision) to balance modeling accuracy with computation time. The MILP formulation of the HVAC ensures a (near) global optimality.

The remainder of this paper is structured as follows: In Section 2 the hierarchical MPC + MILP-MPC structure and its connection to the HVAC and plant is explained. In Section 3 the HVAC model is stated. Section 4 gives insights into the plant MPC. In Sections 5 and 6 the flexible and modular MILP optimization model of the MILP-MPC is presented. Section 7 is devoted to case studies. Section 8 gives a conclusion.

2. Hierarchical MPC + MILP-MPC structure

Fig. 2 shows the control concept of the hierarchical MPC + MILP-MPC structure.

The dynamics of the plant are slow. To optimally take available disturbance predictions into account large prediction horizons are favored. With large prediction horizons mixed-integer MIMO predictive control optimization becomes a numerically expensive problem. Therefore, the optimization problem is separated into two different controllers:

The plant MPC incorporates a dynamic model of the plant. At time sample k it obtains disturbance predictions $\mathbf{Z}_{pre}(k) = [\mathbf{z}_{pre}^T(k+1|k), \dots, \mathbf{z}_{pre}^T(k+N_p|k)]^T$, reference trajectories $\mathbf{Y}_{ref}(k) = [\mathbf{y}_{ref}^T(k+1|k), \dots, \mathbf{y}_{ref}^T(k+N_p|k)]^T$, the vectors $\mathbf{U}_{min}(k) = [\mathbf{u}_{min}^T(k), \dots, \mathbf{u}_{min}^T(k+N_c-1)]^T$ & $\mathbf{U}_{max}(k) = [\mathbf{u}_{max}^T(k), \dots,$

$\mathbf{u}_{max}^T(k+N_c-1)]^T$ being the time-variant bounds on its optimized control trajectory (required net enthalpy and mass flows) $\mathbf{U}(k) = [\mathbf{u}^T(k), \dots, \mathbf{u}^T(k+N_c-1)]^T$, and the output $\mathbf{y}(k)$ of the plant (state of the indoor air). The outputs of the plant MPC are the optimized control trajectory $\mathbf{U}(k)$ and the state predictions of its plant model $\mathbf{X}_{pre}(k) = [\mathbf{x}_{pre}^T(k+1|k), \dots, \mathbf{x}_{pre}^T(k+N_p|k)]^T$. Its control horizon N_c and prediction horizon N_p ($N_c \leq N_p$) are chosen large enough to capture the slow thermal dynamics of the plant. The plant MPC is computationally inexpensive.

The constraint computation for the plant MPC considers the HVAC configuration (e.g. maximum refrigerating/heating capacity). It combines $\mathbf{y}(k)$ with the time shifted predictions $\mathbf{X}_{pre}(k)$, gets the disturbance predictions $\mathbf{Z}_{pre}(k)$, and combines this information to compute $\mathbf{U}_{min}(k)$ and $\mathbf{U}_{max}(k)$ due to technological limitations. Thereby it considers minimum consecutive ON/OFF constraints of certain HVAC components imposed by past control action of the MILP-MPC.

The MILP-MPC is based on a flexible and modular MILP optimization model of the HVAC. It obtains the disturbance predictions $\mathbf{Z}_{pre}(k)$, the optimized control trajectory $\mathbf{U}(k)$ of the plant MPC and its state predictions $\mathbf{X}_{pre}(k)$. At each time step k the MILP-MPC solves a MILP problem. It considers the first $N_{p,MILP}$ samples ($N_{p,MILP} \leq N_c$) of the future control trajectory $\mathbf{U}(k)$ of the plant MPC as its reference trajectory (i.e. $\mathbf{Y}_{ref,MILP}(k) = [\mathbf{u}^T(k), \dots, \mathbf{u}^T(k+N_{p,MILP}-1)]^T$). The control variables of the MILP-MPC are those mixed-integer decision variables of the MILP model defining the continuous and discrete states of the HVAC components over the control horizon of the MILP-MPC $N_{c,MILP}$. Only the first sample $k+i$ of this sequence $k+i$ (for $i=0, \dots, N_{c,MILP}-1$) is sent to the HVAC.

Beside tracking the reference $\mathbf{Y}_{ref,MILP}(k)$ the objective of the MILP-MPC is to minimize power consumption and switching of the HVAC. Thereby it has to obey a variety of constraints and solve a unit commitment problem.

3. HVAC model

A modular structured HVAC model is proposed. This approach enables a quick adaption of the HVAC model to fit the structure of different HVAC system by adding or removing components. Fig. 3 shows a schematic illustration of the assumed HVAC system. Multiplicities of components are depicted aggregated.

In the mixing chamber the fresh outdoor air (ODA) mass flow \dot{m}_{ODA} is isobarically mixed with the recirculation air (RCA) mass flow \dot{m}_{RCA} from the plant interior. In Fig. 3 the quantities h_{ODA}/h_{IDA} , $x_{H_2O,ODA}/x_{H_2O,IDA}$, and c_{ODA}/c_{IDA} are the specific enthalpy, the water content, and the volume fraction of CO₂ in air (in ppmv) of the wet outdoor air (ODA)/ indoor air (IDA).

In the refrigerating machines the total heat flow \dot{Q}_C is isobarically withdrawn from the wet air mass flow. If due to cooling the temperature falls below the dew point temperature the condensate is removed. In this case the leaving air is saturated air.

In heat pumps and heater batteries the total heat flows \dot{Q}_{HP} and \dot{Q}_{HB} , respectively, are isobarically introduced to the wet air mass flow. The total heating power is \dot{Q}_H .

The supply air fan delivers the conditioned wet air mass flow \dot{m}_{SUP} to the plant. Thereby it introduces the power \dot{W}_{LSAF} to the air mass flow. The supply air (SUP) has the specific enthalpy h_{SUP} , water content $x_{H_2O,SUP}$, and volume fraction of CO₂ in air c_{SUP} . A typical HVAC model was derived and validated in [17].

For the HVAC system depicted in Fig. 3 the system equations of the HVAC model, derived from stationary mass and energy balances, read:

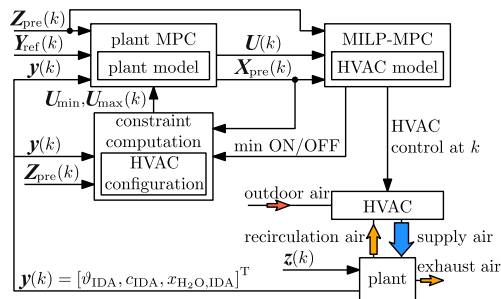


Fig. 2. Conceptual architecture of the plant MPC, the MILP-MPC, the HVAC, and the plant.

1650

C. Dullinger et al./Applied Thermal Engineering 128 (2018) 1646–1659

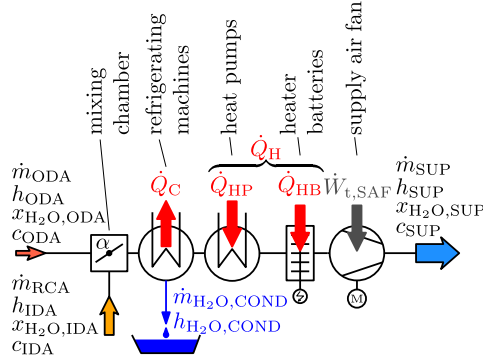


Fig. 3. Conceptual HVAC system.

$$\dot{m}_{\text{SUP}}(h_{\text{SUP}} - h_{\text{IDA}}) = \alpha \dot{m}_{\text{SUP}}(h_{\text{ODA}} - h_{\text{IDA}}) - \dot{Q}_C + \dot{Q}_H + \dot{W}_{\text{t,SAF}} - \dot{m}_{\text{H}_2\text{O,COND}} h_{\text{H}_2\text{O,COND}} \quad (1)$$

$$\dot{m}_{\text{SUP}}(c_{\text{SUP}} - c_{\text{IDA}}) = \alpha \dot{m}_{\text{SUP}}(c_{\text{ODA}} - c_{\text{IDA}}) \quad (2)$$

$$\dot{m}_{\text{SUP}}(x_{\text{H}_2\text{O,SUP}} - x_{\text{H}_2\text{O,IDA}}) = \alpha \dot{m}_{\text{SUP}}(x_{\text{H}_2\text{O,ODA}} - x_{\text{H}_2\text{O,IDA}}) - \dot{m}_{\text{H}_2\text{O,COND}} \quad (3)$$

In (1)–(3) the quantity $\alpha = \dot{m}_{\text{ODA}}/\dot{m}_{\text{SUP}} \leq 1$ is the fresh air ratio. It defines the state of the mixing chamber.

The HVAC model (1)–(3) is a static model. The behavior of the vapor compression plants (VCPs) is described by their coefficient of performance (COP). The COPs are given via characteristic diagrams specified by static lookup tables. A detailed description of modeling and control of VCPs can be found in [18].

4. Plant MPC

In this Section first the input to the plant model and the optimization criterion of the plant MPC are stated. Then the time-variant input constraints of the plant MPC, imposed by the hierarchical MPC + MILP-MPC structure, are derived.

4.1. MPC plant model

The output of the plant model is the temperature ϑ_{IDA} , the water content $x_{\text{H}_2\text{O,IDA}}$ and volume fraction of CO_2 in air c_{IDA} of its indoor air (IDA). The plant model considers the disturbances acting on the plant imposed by its environment (radiation, ambient temperature, etc.).

The input to the plant model (provided by the HVAC) reads

$$\mathbf{u}(k) = \begin{bmatrix} u_1 \\ u_2 \\ u_3 \end{bmatrix} = \begin{bmatrix} \dot{m}_{\text{SUP}}(h_{\text{SUP}} - h_{\text{IDA}}) \\ \dot{m}_{\text{SUP}}(c_{\text{SUP}} - c_{\text{IDA}}) \\ \dot{m}_{\text{SUP}}(x_{\text{H}_2\text{O,SUP}} - x_{\text{H}_2\text{O,IDA}}) \end{bmatrix}. \quad (4)$$

In (4) it is implicitly assumed that the exhaust air mass flow blown into the environment (see Fig. 2) equals the fresh air mass flow \dot{m}_{ODA} sucked in by the HVAC system. The exhaust air has the state of the indoor air.

Note that in (4) the right hand sides of the equations (1)–(3) are being stacked. This defines the interrelation between the decision variables of the plant MPC and those of the MILP-MPC for the HVAC operation.

A general time-variant continuous state space representation of the plant model reads

$$\dot{\mathbf{x}} = \mathbf{f}(\mathbf{x}, \mathbf{u}, \mathbf{z}, t); \mathbf{x}(t_0) = \mathbf{x}_0 \quad (5)$$

$$\mathbf{y} = \mathbf{g}(\mathbf{x}, \mathbf{u}, \mathbf{z}, t). \quad (6)$$

The time-variant vector functions \mathbf{f} and \mathbf{g} map the current state $\mathbf{x}(t)$, the input $\mathbf{u}(t)$, and the disturbances $\mathbf{z}(t)$ onto the state-derivative $\dot{\mathbf{x}}$ and the output \mathbf{y} , respectively. In (5) \mathbf{x}_0 denotes the initial state vector at the initial time t_0 . The plant MPC is based on the zero-order hold (see [19,20]) discretized plant model.

Remark: A suitable plant model for a rail vehicle was derived and validated in [17]. Estimation of some of its parameters (i.e. heat capacity and heat transfer coefficient) based on measurements is discussed in [21]. Predictions of speed, position, and orientation of the rail vehicle can be obtained by a speed profile optimizer like the one presented in [22].

4.2. Plant MPC optimization criterion

The plant MPC optimizes the criterion

$$\begin{aligned} \min_{\mathbf{u}, \mathbf{Y}_{\text{s,l}}, \mathbf{Y}_{\text{s,u}}} J(k) &= (\mathbf{Y}_{\text{ref}} - \mathbf{Y})^T \mathbf{Q}(k) (\mathbf{Y}_{\text{ref}} - \mathbf{Y}) \\ &+ \mathbf{U}^T \mathbf{R}(k) \mathbf{U} + \Delta \mathbf{U}^T \mathbf{S}(k) \Delta \mathbf{U} \\ &+ \mathbf{Y}_{\text{s,l}}^T \mathbf{T}_{\text{s,l}}(k) \mathbf{Y}_{\text{s,l}} \\ &+ \mathbf{Y}_{\text{s,u}}^T \mathbf{T}_{\text{s,u}}(k) \mathbf{Y}_{\text{s,u}} \end{aligned} \quad (7)$$

$$\text{s.t. } \mathbf{U}_{\text{min}}(k) \leq \mathbf{U}(k) \leq \mathbf{U}_{\text{max}}(k) \quad (8)$$

$$\mathbf{Y}_{\text{min}}(k) - \mathbf{Y}_{\text{s,l}}(k) \leq \mathbf{Y}(k) \quad (9)$$

$$\mathbf{Y}(k) \leq \mathbf{Y}_{\text{max}}(k) + \mathbf{Y}_{\text{s,u}}(k) \quad (10)$$

$$\mathbf{0} \leq \mathbf{Y}_{\text{s,l}}(k) \quad (11)$$

$$\mathbf{0} \leq \mathbf{Y}_{\text{s,u}}(k) \quad (12)$$

where \mathbf{Q} , \mathbf{R} , \mathbf{S} , $\mathbf{T}_{\text{s,l}}$, and $\mathbf{T}_{\text{s,u}}$ are positive semi-definite weighting matrices, which are used for tuning. The optimal control vector $\mathbf{U}(k)$ contains the current and future control $\mathbf{u}(k+i)$ (for $i = 0, \dots, N_c - 1$). The vector $\Delta \mathbf{U}(k)$ contains the control increments $\Delta \mathbf{u}(k+i) = \mathbf{u}(k+i) - \mathbf{u}(k+i-1)$. The vector $\mathbf{Y}_{\text{ref}}(k)$ contains the future reference trajectory $\mathbf{y}_{\text{ref}}(k+i|k)$ (for $i = 1, \dots, N_p$) at time step k . In the vector $\mathbf{Y}(k)$ the predictions of the output vector signal $\mathbf{y}(k+i|k)$ (for $i = 1, \dots, N_p$) at time step k are being stacked, see [23]. In the vectors $\mathbf{U}_{\text{min}}(k)$ and $\mathbf{U}_{\text{max}}(k)$ the time-variant constraints on the input vector $\mathbf{u}(k+i)$ are being stacked. The optimal parameter vectors $\mathbf{Y}_{\text{s,l}}(k)$ and $\mathbf{Y}_{\text{s,u}}(k)$ contain positive real slack variables subtracted from, respectively added to, the vectors $\mathbf{Y}_{\text{min}}(k)$ and $\mathbf{Y}_{\text{max}}(k)$ containing the lower respectively upper limit on the predicted output $\mathbf{y}(k+i|k)$ (i.e. (9)–(12) represent “soft” constraints on $\mathbf{y}(k+i|k)$).

4.3. Plant MPC time-variant input constraints

In this section the time-variant bounds $\mathbf{u}_{\text{min}}(k+i)$ and $\mathbf{u}_{\text{max}}(k+i)$ (for $i = 0, \dots, N_c - 1$) on the control input of the plant MPC (4) are derived. The bounds depend on the current and (for $i > 1$) the future state of the outdoor/indoor air, the HVAC configuration, supply air temperature constraints, and in case of minimum consecutive on/off constraints explicitly on past control action of the MILP-MPC for the HVAC.

4.3.1. Constraints imposed on u_1 due to restricted heating/cooling power

The minimum constraint on u_1 (see (4) and (1)) with respect to the enthalpy of the outdoor/indoor air $h_{\text{ODA}}/h_{\text{IDA}}$, the fresh air ratio α , the supply air mass flow \dot{m}_{SUP} , the power introduced to the air mass flow by the supply air fan $\dot{W}_{\text{t,SAF}}$, and the heating/cooling powers of the HVAC \dot{Q}_H/\dot{Q}_C reads (i.e. (1) evaluated at extremes):

$$u_{1,\min}(k+i) = \alpha_{\min} \cdot \dot{m}_{\text{SUP},\min} \cdot (h_{\text{ODA}}(k+i) - h_{\text{IDA}}(k+i)) - \dot{Q}_{\text{C,max}}(k+i) + \dot{Q}_{\text{H,min}}(k+i) + \dot{W}_{\text{t,SAF}}(\dot{m}_{\text{SUP},\min}) \quad (13)$$

$$\forall i \in \{0, \dots, N_c - 1\} | h_{\text{ODA}}(k+i) \geq h_{\text{IDA}}(k+i)$$

$$u_{1,\min}(k+i) = \alpha_{\max} \dot{m}_{\text{SUP}}^*(k+i) (h_{\text{ODA}}(k+i) - h_{\text{IDA}}(k+i)) - \dot{Q}_{\text{C,max}}(k+i) + \dot{Q}_{\text{H,min}}(k+i) + \dot{W}_{\text{t,SAF}}(\dot{m}_{\text{SUP}}^*(k+i)) \quad (14)$$

$$\forall i \in \{0, \dots, N_c - 1\} | h_{\text{ODA}}(k+i) < h_{\text{IDA}}(k+i)$$

where $\dot{m}_{\text{SUP}}^*(k+i)$ is given by

$$\dot{m}_{\text{SUP}}^*(k+i) = \arg \min_{\dot{m}_{\text{SUP}}} (\dot{m}_{\text{SUP}}, k, i) \quad (15)$$

$$J_{u_{\min}}(\dot{m}_{\text{SUP}}, k, i) = \alpha_{\max} \dot{m}_{\text{SUP}} (h_{\text{ODA}}(k+i) - h_{\text{IDA}}(k+i)) + \dot{W}_{\text{t,SAF}}(\dot{m}_{\text{SUP}}) \quad (16)$$

$$\dot{m}_{\text{SUP}} \in \{\dot{m}_{\text{SUP},\min}, \dots, \dot{m}_{\text{SUP},\max}\} \quad (17)$$

The maximum constraints on u_1 reads:

$$u_{1,\max}(k+i) = \alpha_{\max} \cdot \dot{m}_{\text{SUP},\max} \cdot (h_{\text{ODA}}(k+i) - h_{\text{IDA}}(k+i)) - \dot{Q}_{\text{C,min}}(k+i) + \dot{Q}_{\text{H,max}}(k+i) + \dot{W}_{\text{t,SAF}}(\dot{m}_{\text{SUP},\max}) \quad (18)$$

$$\forall i \in \{0, \dots, N_c - 1\} | h_{\text{ODA}}(k+i) \geq h_{\text{IDA}}(k+i)$$

$$u_{1,\max}(k+i) = \alpha_{\min} \dot{m}_{\text{SUP}}^*(k+i) (h_{\text{ODA}}(k+i) - h_{\text{IDA}}(k+i)) - \dot{Q}_{\text{C,min}}(k+i) + \dot{Q}_{\text{H,max}}(k+i) + \dot{W}_{\text{t,SAF}}(\dot{m}_{\text{SUP}}^*(k+i)) \quad (19)$$

$$\forall i \in \{0, \dots, N_c - 1\} | h_{\text{ODA}}(k+i) < h_{\text{IDA}}(k+i)$$

where $\dot{m}_{\text{SUP}}^*(k+i)$ in this case is given by

$$\dot{m}_{\text{SUP}}^*(k+i) = \arg \max_{\dot{m}_{\text{SUP}}} (\dot{m}_{\text{SUP}}, k, i) \quad (20)$$

$$J_{u_{\max}}(\dot{m}_{\text{SUP}}, k, i) = \alpha_{\min} \dot{m}_{\text{SUP}} (h_{\text{ODA}}(k+i) - h_{\text{IDA}}(k+i)) + \dot{W}_{\text{t,SAF}}(\dot{m}_{\text{SUP}}) \quad (21)$$

$$\dot{m}_{\text{SUP}} \in \{\dot{m}_{\text{SUP},\min}, \dots, \dot{m}_{\text{SUP},\max}\} \quad (22)$$

It is assumed that the function $\dot{m}_{\text{SUP}} = \dot{m}_{\text{SUP}}(P_{\text{SAF}})$ is monotonically increasing and the electric consumption of the supply air fan (SAF) adds completely to the heat input, i.e. $\dot{W}_{\text{t,SAF}} = P_{\text{SAF}}$.

In case of minimum consecutive on and off constraints on a refrigeration machine's compressor the refrigeration machines minimum and maximum cooling power, respectively, can be affected. In case a refrigeration machine has to stay on at some time step $k+i$ its provided minimum cooling power is different from zero. Whereas in case it can not be turned on its maximum cooling power is zero.

4.3.2. Constraints imposed on u_1 due to supply air temperature constraints

The supply air temperature ϑ_{SUP} has to lie between an upper $\vartheta_{\text{SUP},\max}$ and a lower bound $\vartheta_{\text{SUP},\min}$ to fulfill comfort or quality requirements. The bounds on u_1 due to this constraints are derived in the following.

From (3) the water content of the supply air is

$$x_{\text{H}_2\text{O},\text{SUP}} = \alpha x_{\text{H}_2\text{O},\text{ODA}} + (1 - \alpha) x_{\text{H}_2\text{O},\text{IDA}} - \frac{\dot{m}_{\text{H}_2\text{O},\text{COND}}}{\dot{m}_{\text{SUP}}} \quad (23)$$

Neglecting the water mass flow of condensed water (i.e. $\dot{m}_{\text{H}_2\text{O},\text{COND}} \approx 0$) removed in the refrigeration machines for the moment, $x_{\text{H}_2\text{O},\text{SUP}}$ with minimum and maximum fresh air ratio α is given by:

$$x_{\text{H}_2\text{O},\text{SUP},\min}^* = \alpha_{\min} x_{\text{H}_2\text{O},\text{ODA}} + (1 - \alpha_{\min}) x_{\text{H}_2\text{O},\text{IDA}} \quad (24)$$

$$x_{\text{H}_2\text{O},\text{SUP},\max}^* = \alpha_{\max} x_{\text{H}_2\text{O},\text{ODA}} + (1 - \alpha_{\max}) x_{\text{H}_2\text{O},\text{IDA}} \quad (25)$$

The minimum and maximum water content of the supply air is then given by:

$$x_{\text{H}_2\text{O},\text{SUP},\min}^* = \min(\{x_{\text{H}_2\text{O},\text{SUP},\min}^*, x_{\text{H}_2\text{O},\text{SUP},\max}^*\}) \quad (26)$$

$$x_{\text{H}_2\text{O},\text{SUP},\max}^* = \max(\{x_{\text{H}_2\text{O},\text{SUP},\min}^*, x_{\text{H}_2\text{O},\text{SUP},\max}^*\}) \quad (27)$$

If $x_{\text{H}_2\text{O},\text{SUP},\min}^* > x_{\text{H}_2\text{O},\text{SUP},s}(\vartheta_{\text{SUP},\min})$, with $x_{\text{H}_2\text{O},\text{SUP},s}$ being the saturation water content of air for $\vartheta_{\text{SUP},\min}$ (for a given air pressure), water is condensed in the refrigeration machines and the condensed water is removed. Thus the maximum water content of the supply air with temperature $\vartheta_{\text{SUP},\min}$ is given by

$$x_{\text{H}_2\text{O},\text{SUP},\min} = \min(\{x_{\text{H}_2\text{O},\text{SUP},\min}^*, x_{\text{H}_2\text{O},\text{SUP},s}(\vartheta_{\text{SUP},\min})\}) \quad (28)$$

and $\dot{m}_{\text{H}_2\text{O},\text{COND}}/\dot{m}_{\text{SUP}} = x_{\text{H}_2\text{O},\text{SUP},\min}^* - x_{\text{H}_2\text{O},\text{SUP},\min}$. Thus the minimum and maximum enthalpy of the supply air are:

$$h_{\text{SUP},\min} = c_{p,a} \vartheta_{\text{SUP},\min} + x_{\text{H}_2\text{O},\text{SUP},\min} (c_{p,v} \vartheta_{\text{SUP},\min} + r_0) \quad (29)$$

$$h_{\text{SUP},\max} = c_{p,a} \vartheta_{\text{SUP},\max} + x_{\text{H}_2\text{O},\text{SUP},\max} (c_{p,v} \vartheta_{\text{SUP},\max} + r_0) \quad (30)$$

The enthalpy of evaporation r_0 , the specific heat capacities of dry air $c_{p,a}$ and water vapor $c_{p,v}$ are considered constant. The lower and upper bound on $u_1(k+i)$ due to supply air temperature constraints read:

$$u_{1,\min}(k+i) = \dot{m}_{\text{SUP},\max} (h_{\text{SUP},\min}(k+i) - h_{\text{IDA}}(k+i)) \quad (31)$$

$$u_{1,\max}(k+i) = \dot{m}_{\text{SUP},\max} (h_{\text{SUP},\max}(k+i) - h_{\text{IDA}}(k+i)) \quad (32)$$

In (31) and (32) it is assumed that $h_{\text{SUP},\min}(k+i) \leq h_{\text{IDA}}(k+i) \leq h_{\text{SUP},\max}(k+i)$ holds.

The current plant output and the state predictions of the previous time step $k-1$ are utilized to formulate the constraints at the current time step k over the prediction horizon $k+i$ (for $i = 0, \dots, N_c - 1$).

4.3.3. Constraints imposed on u_2

The minimum constraint on u_2 (see (4) and (2)) reads:

$$u_{2,\min}(k+i) = \alpha_{\min} \dot{m}_{\text{SUP},\min} (c_{\text{ODA}} - c_{\text{IDA}}) \quad (33)$$

$$\forall i \in \{0, \dots, N_c - 1\} | c_{\text{ODA}}(k+i) \geq c_{\text{IDA}}(k+i)$$

$$u_{2,\min}(k+i) = \alpha_{\max} \dot{m}_{\text{SUP},\max} (c_{\text{ODA}} - c_{\text{IDA}}) \quad (34)$$

$$\forall i \in \{0, \dots, N_c - 1\} | c_{\text{ODA}}(k+i) < c_{\text{IDA}}(k+i)$$

Maximum constraints on u_2 are not imposed since the introduction of CO_2 to the plant is not an objective.

4.3.4. Constraints imposed on u_3

The minimum constraint on u_3 (see (4) and (3)) reads:

$$u_{3,\min}(k+i) = \dot{m}_{\text{SUP},\min} (x_{\text{H}_2\text{O},\text{SUP},\min} - x_{\text{H}_2\text{O},\text{IDA}}) \quad (35)$$

$$\forall i \in \{0, \dots, N_c - 1\} | x_{\text{H}_2\text{O},\text{SUP},\min}(k+i) \geq x_{\text{H}_2\text{O},\text{IDA}}(k+i)$$

$$u_{3,\min}(k+i) = \dot{m}_{\text{SUP},\max} (x_{\text{H}_2\text{O},\text{SUP},\min} - x_{\text{H}_2\text{O},\text{IDA}}) \quad (36)$$

$$\forall i \in \{0, \dots, N_c - 1\} | x_{\text{H}_2\text{O},\text{SUP},\min}(k+i) < x_{\text{H}_2\text{O},\text{IDA}}(k+i)$$

with $x_{\text{H}_2\text{O},\text{SUP},\min}$ from (28). Eq. (35) and (36) assume that the cooling power of the HVAC is large enough to achieve $\vartheta_{\text{SUP},\min}$ independent of the enthalpy of the outdoor/indoor air and \dot{m}_{SUP} .

The maximum constraint on u_3 reads:

$$u_{3,\max}(k+i) = \alpha_{\max} \dot{m}_{\text{SUP},\max} (x_{\text{H}_2\text{O},\text{ODA}} - x_{\text{H}_2\text{O},\text{IDA}}) \quad (37)$$

$$\forall i \in \{0, \dots, N_c - 1\} | x_{\text{H}_2\text{O},\text{ODA}}(k+i) \geq x_{\text{H}_2\text{O},\text{IDA}}(k+i)$$

1652

C. Dullinger et al./Applied Thermal Engineering 128 (2018) 1646–1659

$$u_{3,\max}(k+i) = \alpha_{\min} \dot{m}_{\text{SUP},\min}(x_{\text{H}_2\text{O,ODA}} - x_{\text{H}_2\text{O,IDA}}) \quad (38)$$

$$\forall i \in \{0, \dots, N_c - 1\} | x_{\text{H}_2\text{O,ODA}}(k+i) < x_{\text{H}_2\text{O,IDA}}(k+i)$$

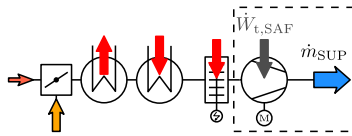
5. MILP optimization model of the HVAC: MILP formulation of the HVAC components

In this section the modular MILP formulation for the HVAC components is presented; it can handle a multiplicity of components. Beside the mixed-integer decision variables defining the state of the HVAC components the MILP model contains additional auxiliary decision variables. These continuous or binary variables are utilized for modeling product terms of decision variables, identifying switching, and piecewise linear approximation of nonlinear mappings (e.g COP maps, the Mollier diagram, etc.).

5.1. Notation of the MILP optimization model

To simplify notation the time instance $k+i$ is omitted whenever possible, i.e. when the terms do not contain mixed time instances like $k+i$ and $k+j$ with $i \neq j$. Numerical values provided to the MILP optimizer are marked by an underline, i.e. \underline{z}_{\min} , \underline{z}_j , \underline{z}_{\max} are numeric values the decision variable α of the MILP model can take. Specific quantities like the enthalpy of the indoor air $\underline{h}_{\text{IDA}}(k+i)$ are computed based on the state predictions of the plant MPC and are constants to the MILP model, updated at each time step k . The subscript “c” is utilized to count multiplicity of components modeled by the same MILP formulation.

5.2. Supply air fan (SAF)



If the HVAC is in operation the supply air fan is on. I.e. the supply air mass flow \dot{m}_{SUP} , the electrical power consumption of the SAF P_{SAF} , and the power $\dot{W}_{t,\text{SAF}}$ introduced to the air mass flow are larger than zero.

Variable speed SAF: The power consumption of the SAF P_{SAF} is modeled as a continuous decision variable with $\underline{P}_{\text{SAF},\min} \leq P_{\text{SAF}} \leq \underline{P}_{\text{SAF},\max}$. The nonlinear relationship between \dot{m}_{SUP} and P_{SAF} is approximated by introducing n_{SAF} special ordered set of type 2 (SOS-2) variables $\lambda_{\text{SAF},j}$ (see [24]). By claiming that at most two $\lambda_{\text{SAF},j}$ are non-zero and smaller 1, the non-zero variables are consecutive in their ordering, and $\sum \lambda_{\text{SAF},j} = 1$ holds, they enable a piecewise linear approximation.

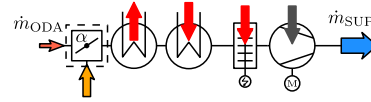
Discrete speed SAF: The power consumption of the SAF P_{SAF} is modeled as a discrete decision variable i.e. $P_{\text{SAF}} \in \{\underline{P}_{\text{SAF},\min}, \dots, \underline{P}_{\text{SAF},j}, \dots, \underline{P}_{\text{SAF},\max}\}$ and $\dot{m}_{\text{SUP}} \in \{\underline{\dot{m}}_{\text{SUP},\min}, \dots, \underline{\dot{m}}_{\text{SUP},j}, \dots, \underline{\dot{m}}_{\text{SUP},\max}\}$. The quantities P_{SAF} and \dot{m}_{SUP} are modeled by

$$\sum_j \delta_{\text{SAF},j} = 1 \quad \delta_{\text{SAF},j} \in \{0, 1\} \forall j \quad (39)$$

$$P_{\text{SAF}} = \sum_j \underline{P}_{\text{SAF},j} \cdot \delta_{\text{SAF},j}$$

$$\dot{m}_{\text{SUP}} = \sum_j \underline{\dot{m}}_{\text{SUP},j} \cdot \delta_{\text{SAF},j}$$

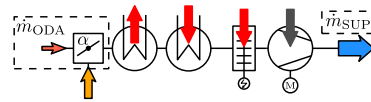
5.3. Fresh air ratio α



The discrete decision variable $\alpha = \dot{m}_{\text{ODA}}/\dot{m}_{\text{SUP}} \in \{\underline{z}_{\min}, \dots, \underline{z}_j, \dots, \underline{z}_{\max}\}$ (with $\underline{z}_{\min} \geq 0$ and $\underline{z}_{\max} \leq 1$) defines the flap/rotary slide position in the mixing chamber and is modeled as follows:

$$\alpha = \sum_j \underline{z}_j \cdot \delta_{\alpha,j} \quad \delta_{\alpha,j} \in \{0, 1\} \forall j \quad \sum_j \delta_{\alpha,j} = 1 \quad (40)$$

5.4. Fresh air mass flow \dot{m}_{ODA} as auxiliary decision variable



The modeling of the product term $\dot{m}_{\text{SUP}} \cdot \alpha$ in (1)–(3) is achieved by introducing the fresh air mass flow $\dot{m}_{\text{ODA}} = \dot{m}_{\text{SUP}} \cdot \alpha$ as auxiliary decision variable. For \dot{m}_{ODA} the following box constraint has to hold:

$$\underline{\dot{m}}_{\text{SUP},\min} \underline{z}_{\min} \leq \dot{m}_{\text{ODA}} \leq \underline{\dot{m}}_{\text{SUP},\max} \underline{z}_{\max} \quad (41)$$

The auxiliary variable \dot{m}_{ODA} (continuous variable) is connected to the fresh air mass flow \dot{m}_{SUP} (continuous variable) and the fresh air ratio α (discrete variable) by the following two inequality constraints:

$$m_{\alpha_j} \leq \dot{m}_{\text{ODA}} - \dot{m}_{\text{SUP}} \cdot \underline{z}_j \leq M_{\alpha_j} \quad (42)$$

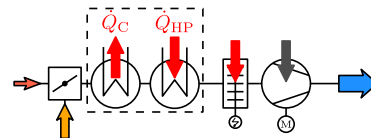
with

$$m_{\alpha_j} = (\underline{\dot{m}}_{\text{SUP},\min} \underline{z}_{\min} - \underline{\dot{m}}_{\text{SUP},\max} \underline{z}_j) \cdot (1 - \delta_{\alpha,j}) \quad (43)$$

$$M_{\alpha_j} = (\underline{\dot{m}}_{\text{SUP},\max} \underline{z}_{\max} - \underline{\dot{m}}_{\text{SUP},\min} \underline{z}_j) \cdot (1 - \delta_{\alpha,j}) \quad (44)$$

Note that if $\delta_{\alpha,j} = 1$ the decision variable $\alpha = \underline{z}_j$.

5.5. Refrigeration machines and heat pumps



Only the modeling of the refrigeration machines (“AC”) is presented in this section since heat pumps (“HP”) are modeled identically. The presented MILP model can distinguish between two main refrigeration machine model types.

The first type is presented in Section 5.5.1. For this type the cooling power \dot{Q}_{AC} is modeled as a function of the compressor power P_{AC} . It can be subdivided into two versions. The first version “ACS” considers P_{AC} to be a semi-continuous decision variable (either zero or real valued), denoted by P_{ACS} . The “S” stands for semi-continuous. The second version “ACD” of the first type considers P_{AC} to be a discrete decision variable, denoted by P_{ACD} . The “D” stands for discrete. For both versions (“ACS” & “ACD”) of the

first type a by-pass valve can be added. The modeling of the by-pass valve is explained in the last paragraph of Section 5.5.1.

The second type (“ACV”) is presented in Section 5.5.2. For the second type the cooling power \dot{Q}_{ACV} and the electrical power P_{ACV} are modeled both as a function of the discrete compressor speed and the semi-continuous (electronic expansion/by-pass) valve position.

5.5.1. Cooling power as a function of the electrical compressor power and by-pass valve state

Variable speed compressors: The compressor power $P_{ACS,c}$ is modeled as a semi-continuous decision variable i.e. $P_{ACS,c} = 0 \vee \underline{P}_{ACS,c,\min} \leq P_{ACS,c} \leq \underline{P}_{ACS,c,\max}$. With the binary $\delta_{ACS,ON,c}$ which is 1 if the compressor is ON (otherwise 0) this is modeled by

$$\underline{P}_{ACS,c,\min} \delta_{ACS,ON,c} \leq P_{ACS,c} \leq \underline{P}_{ACS,c,\max} \delta_{ACS,ON,c} \quad (45)$$

The nonlinear relationship between the cooling power $\dot{Q}_{ACS,c}$ and $P_{ACS,c}$ is approximated by introducing $n_{ACS,c}$ SOS-2 variables $\lambda_{ACS,c,j}$:

$$P_{ACS,c} = \sum_j^{n_{ACS,c}} \underline{P}_{ACS,c,j} \cdot \lambda_{ACS,c,j} \quad (46)$$

$$\dot{Q}_{ACS,c} = \sum_j^{n_{ACS,c}} \underline{\dot{Q}}_{ACS,c,j} \cdot \lambda_{ACS,c,j} \quad (47)$$

with $\underline{P}_{ACS,c,1} = 0$, $\underline{P}_{ACS,c,2} = \underline{P}_{ACS,c,\min}$, $\underline{P}_{ACS,c,n_{ACS,c}} = \underline{P}_{ACS,c,\max}$ and $\underline{\dot{Q}}_{ACS,c,j}(k+i) = \underline{\dot{Q}}_{ACS,c,j}(\vartheta_{ODA}(k+i), \vartheta_{ACS,c}(k+i))$. The quantities $\underline{P}_{ACS,c,j}$ and $\underline{\dot{Q}}_{ACS,c,j}$ denote the supporting points of the piecewise linear approximation. To fulfill the order relation their numerical values are sorted in ascending order of $\underline{P}_{ACS,c,j}$. The quantities $\vartheta_{ODA}(k+i)$ and $\vartheta_{ACS,c}(k+i)$ are the outdoor air temperature and the temperature of the evaporator heat exchanger. For $\vartheta_{ACS,c}(k+i)$ assumptions have to be made, whereas for $\vartheta_{ODA}(k+i)$ the disturbance predictions are utilized. With $n_{ACS,c} - 1$ auxiliary binaries $\delta_{ACS,c,j}$ the following constraints have to hold (see [15]):

$$\sum_j^{n_{ACS,c}-1} \delta_{ACS,c,j} = 1; \text{ with } \delta_{ACS,c,j} \in \{0, 1\} \forall j \quad (48)$$

$$\sum_j^{n_{ACS,c}} \lambda_{ACS,c,j} = 1; \text{ with } \lambda_{ACS,c,j} \in [0, 1] \forall j \quad (49)$$

$$\lambda_{ACS,c,1} \leq \delta_{ACS,c,1} \quad (50)$$

$$\lambda_{ACS,c,j} \leq \delta_{ACS,c,j-1} + \delta_{ACS,c,j}; \quad j = 2, \dots, n_{ACS,c} - 1 \quad (51)$$

$$\lambda_{ACS,c,n_{ACS,c}} \leq \delta_{ACS,c,n_{ACS,c}-1} \quad (52)$$

Discrete speed compressors: The compressor power $P_{ACD,c}$ is modeled as a discrete decision variable i.e. $P_{ACD,c} \in \{0, \dots, \underline{P}_{ACD,c,j}, \dots, \underline{P}_{ACD,c,\max}\}$. With the binary $\delta_{ACD,c,j}$ which is 1 if $P_{ACD,c} = \underline{P}_{ACD,c,j}$ (otherwise 0) $P_{ACD,c}$ and $\dot{Q}_{ACD,c}$ are modeled by

$$P_{ACD,c} = \sum_j^{n_{ACD,c}} \underline{P}_{ACD,c,j} \cdot \delta_{ACD,c,j} \quad (53)$$

$$\dot{Q}_{ACD,c} = \sum_j^{n_{ACD,c}} \underline{\dot{Q}}_{ACD,c,j} \cdot \delta_{ACD,c,j} \quad (54)$$

$$\sum_j^{n_{ACD,c}} \delta_{ACD,c,j} = 1; \text{ with } \delta_{ACD,c,j} \in \{0, 1\} \forall j \quad (55)$$

with $\underline{\dot{Q}}_{ACD,c,j}(k+i) = \underline{\dot{Q}}_{ACD,c,j}(\vartheta_{ODA}(k+i), \vartheta_{ACD,c}(k+i))$. Where (again) $\vartheta_{ACD,c}(k+i)$ is the assumed temperature of the evaporator heat exchanger.

Refrigeration machine with by-pass valve: The cooling power of a refrigeration machine (“ACS” and “ACD” type) with a by-pass valve is computed by

$$\dot{Q}_{ACxb,c} = \dot{Q}_{AC,c} \cdot b_{AC,c} \quad (56)$$

In (56) the subscripts “S” and “D” of “ACS” and “ACD” were neglected. Both versions are modeled as follows.

The by-pass valve state is considered a discrete decision variable $b_{AC,c} \in \{\underline{b}_{AC,c,\min}, \dots, \underline{b}_{AC,c,j}, \dots, \underline{b}_{AC,c,\max}\}$ (with $\underline{b}_{AC,c,\min} > 0$ and $\underline{b}_{AC,c,\max} = 1$). It is modeled by:

$$b_{AC,c} = \sum_j \underline{b}_{AC,c,j} \cdot \delta_{b_{AC,c,j}} \quad (57)$$

$$\sum_j \delta_{b_{AC,c,j}} = 1; \text{ with } \delta_{b_{AC,c,j}} \in \{0, 1\} \forall j \quad (58)$$

If $b_{AC,c} = \underline{b}_{AC,c,\max} = 1$ the by-pass valve is not used. If $b_{AC,c} < 1$ the by-pass valve is used and the cooling power of its associated refrigeration machine is reduced by $b_{AC,c}$, see (56). Modeling of the product term in (56) requires the introduction of the auxiliary decision variable $\dot{Q}_{ACxb,c}$ and connecting it to $\dot{Q}_{AC,c}$ and $b_{AC,c}$. This is done as outlined in the following.

The reduced cooling power $\dot{Q}_{ACxb,c}$ has to fulfill

$$\underline{\dot{Q}}_{AC,c,\min} \underline{b}_{AC,c,\min} \leq \dot{Q}_{ACxb,c} \leq \underline{\dot{Q}}_{AC,c,\max} \underline{b}_{AC,c,\max} \quad (59)$$

The auxiliary variable $\dot{Q}_{ACxb,c}$ (semi-continuous or discrete variable) is connected to $\dot{Q}_{AC,c}$ and $b_{AC,c}$ by:

$$\underline{m}_{b_{AC,c,j}}(1 - \delta_{b_{AC,c,j}}) \leq \dot{Q}_{ACxb,c} - \dot{Q}_{AC,c} \underline{b}_{AC,c,j} \quad (60)$$

$$\dot{Q}_{ACxb,c} - \dot{Q}_{AC,c} \underline{b}_{AC,c,j} \leq \underline{M}_{b_{AC,c,j}}(1 - \delta_{b_{AC,c,j}}) \quad (61)$$

with

$$\underline{m}_{b_{AC,c,j}} = (\underline{\dot{Q}}_{AC,c,\min} \underline{b}_{AC,c,\min} - \underline{\dot{Q}}_{AC,c,\max} \underline{b}_{AC,c,j}) \quad (62)$$

$$\underline{M}_{b_{AC,c,j}} = (\underline{\dot{Q}}_{AC,c,\max} \underline{b}_{AC,c,\max} - \underline{\dot{Q}}_{AC,c,\min} \underline{b}_{AC,c,j}) \quad (63)$$

5.5.2. Cooling power and electrical power as a function of compressor speed and valve position

The rotational speed of the compressor $\omega_{ACV,c}$ is a discrete decision variable i.e. $\omega_{ACV,c} \in \{0, \dots, \underline{\omega}_{ACV,c,m}, \dots, \underline{\omega}_{ACV,c,\max}\}$. With the binary $\delta_{ACV,c,m}$ which is 1 if $\omega_{ACV,c} = \underline{\omega}_{ACV,c,m}$ (otherwise 0) this is modeled by

$$\omega_{ACV,c} = \sum_m^{n_{ACV,c}} \underline{\omega}_{ACV,c,m} \cdot \delta_{ACV,c,m} \quad (64)$$

$$\sum_m^{n_{ACV,c}} \delta_{ACV,c,m} = 1; \text{ with } \delta_{ACV,c,m} \in \{0, 1\} \forall m \quad (65)$$

The position of the (electronic/by-pass) valve $v_{ACV,c}$ is considered to be a semi-continuous variable i.e. $v_{ACV,c} = 0 \vee \underline{v}_{ACV,c,\min} \leq v_{ACV,c} \leq \underline{v}_{ACV,c,\max}$. The nonlinear mappings $P_{ACV,c} = P_{ACV,c}(v_{ACV,c}, \omega_{ACV,c})$ and $\dot{Q}_{ACV,c} = \dot{Q}_{ACV,c}(v_{ACV,c}, \omega_{ACV,c}, \vartheta_{ODA}, \vartheta_{ACV,c})$ are modeled by piecewise linear approximation as follows:

$$\lambda_{ACV,c,m,j} \in [0, 1] \forall j \forall m; \quad \delta_{ACV,c,m,j} \in \{0, 1\} \forall j \forall m \quad (66)$$

$$\sum_j^{n_{ACV,c,m}-1} \delta_{ACV,c,m,j} = \delta_{ACV,c,m} \forall m \quad (67)$$

$$\sum_j^{n_{ACV,c,m}} \lambda_{ACV,c,m,j} = \delta_{ACV,c,m} \forall m \quad (68)$$

$$\lambda_{ACV,c,m,1} \leq \delta_{ACV,c,m,1} \quad (69)$$

$$\lambda_{ACV,c,m,j} \leq \delta_{ACV,c,m,j-1} + \delta_{ACV,c,m,j}; \quad j = 2, \dots, n_{ACV,c,m} - 1 \quad (70)$$

$$\lambda_{ACV,c,m,n_{ACV,c,m}} \leq \delta_{ACV,c,m,n_{ACV,c,m}-1} \quad (71)$$

$$v_{ACV,c,m} = \sum_j^{n_{ACV,c,m}} \underline{v}_{ACV,c,m,j} \lambda_{ACV,c,m,j} \quad (72)$$

1654

C. Dullinger et al./Applied Thermal Engineering 128 (2018) 1646–1659

with $\underline{v}_{ACV,c,m,1} = 0$, $\underline{v}_{ACV,c,m,2} = v_{ACV,c,\min}$, and $\underline{v}_{ACV,c,m,n_{ACV,c,m}} = v_{ACV,c,\max}$. The numerical values $\underline{v}_{ACV,c,m,j}$ are sorted in ascending order.

$$P_{ACV,c,m} = \sum_j^{n_{ACV,c,m}} \underline{v}_{ACV,c,m,j} \cdot \lambda_{ACV,c,m,j} \quad (73)$$

$$\dot{Q}_{ACV,c,m} = \sum_j^{n_{ACV,c,m}} \underline{Q}_{ACV,c,m,j} \cdot \lambda_{ACV,c,m,j} \quad (74)$$

with $\underline{Q}_{ACV,c,m,j}(k+i) = \dot{Q}_{ACV,c,m,j}(\vartheta_{ODA}(k+i), \vartheta_{ACV,c}(k+i))$. For each m the quantities $\underline{v}_{ACV,c,m,j}$ and $\underline{Q}_{ACV,c,m,j}$ denote the supporting points of the piecewise linear approximation. Their numerical values are sorted in ascending order of $\underline{v}_{ACV,c,m,j}$.

The position of the (electronic/by-pass) valve, the cooling power, and the electrical power are obtained by

$$v_{ACV,c} = \sum_m^{n_{ACV,c}} v_{ACV,c,m} \quad (75)$$

$$\dot{Q}_{ACV,c} = \sum_m^{n_{ACV,c}} \dot{Q}_{ACV,c,m} \quad (76)$$

$$P_{ACV,c} = \sum_m^{n_{ACV,c}} P_{ACV,c,m} \quad (77)$$

5.5.3. Minimum consecutive ON/OFF constraints for compressors

If a compressor of a refrigeration machine (type “ACS”, “ACD”, or “ACV”) is switched on at some time instance $k+i$ it has to stay on for at least $T_{AC,ON,c}$ seconds respectively $n_{AC,ON,c} = T_{AC,ON,c}/T_s$ time samples. The latter assumes that $T_{AC,ON,c}$ is a whole-number ratio of the sampling time T_s . If at time instance $k+i$ the compressor is running the binary variable $\delta_{AC,ON,c}(k+i)$ takes a value of 1 otherwise 0. The minimum consecutive on constraints for the compressor read

$$\begin{aligned} \delta_{AC,ON,c}(k+r) &\geq \delta_{AC,ON,c}(k+i) - \delta_{AC,ON,c}(k+i-1) \\ \forall i &\in \{-n_{AC,ON,c}+1, \dots, 0, \dots, N_{c,MILP}-1\} \\ \forall r &\in \{i, \dots, \min(N_{c,MILP}-1, i+n_{AC,ON,c}-1)\} \wedge r \geq 0. \end{aligned} \quad (78)$$

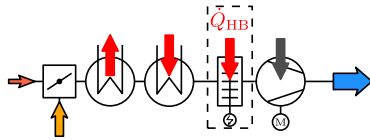
5.5.4. Refrigeration machines operable as heat pumps

If a refrigeration machine can be operated as heat pump it can not be in both modes at the same time. This is modeled by

$$\delta_{AC,ON,c} \leq 1 - \delta_{HP,ON,c} \quad (79)$$

$$\delta_{HP,ON,c} \leq 1 - \delta_{AC,ON,c} \quad (80)$$

5.6. Heater batteries (HB)



The electrical power consumption of a heater battery $P_{HB,c}$ is either modeled as a discrete, continuous, or semi-continuous

variable. Its heating power equals its electrical power consumption. I.e. $\dot{Q}_{HB,c} = P_{HB,c}$.

5.7. Total cooling and heating power

With the different refrigeration machines/heat pumps (Section 5.5) and the heater batteries (Section 5.6) the total cooling $\dot{Q}_C(k+i)$ and heating power $\dot{Q}_H(k+i)$ at time instance $k+i$ (for $i = 0, \dots, N_{p,MILP}-1$) read

$$\dot{Q}_C = \sum_c^{n_{ACS}} \dot{Q}_{ACS,c} + \sum_c^{n_{ACD}} \dot{Q}_{ACD,c} + \sum_c^{n_{ACV}} \dot{Q}_{ACV,c} \quad (81)$$

$$\dot{Q}_H = \sum_c^{n_{HPS}} \dot{Q}_{HPS,c} + \sum_c^{n_{HPD}} \dot{Q}_{HPD,c} + \sum_c^{n_{HPV}} \dot{Q}_{HPV,c} + \sum_c^{n_{HB}} \dot{Q}_{HB,c} \quad (82)$$

6. MILP optimization of the HVAC: objectives

In this section first the overall cost function of the MILP optimization is presented. Then its individual cost and penalty functions are derived.

6.1. Overall MILP cost function at time step k

The overall cost function of the MILP at k is given by

$$\begin{aligned} J(k) &= J_P(k) + J_{p,u_1}(k) + J_{p,u_2}(k) + J_{p,u_3}(k) \\ &\quad + J_{p,u_1,\vartheta_{\min}^v}(k) + J_{p,u_1,\vartheta_{\max}^v}(k) \\ &\quad + J_{p,ACS,\downarrow_{OFF,c}}(k) + J_{p,ACS,change,c}(k) \\ &\quad + \dots \\ &\quad + J_{p,HPV,\downarrow_{OFF,c}}(k) + J_{p,HPV,change,c}(k) \end{aligned} \quad (83)$$

It sums up a variety of individual cost and penalty functions. These individual contributions are outlined in the respective sections in the following.

6.2. Cost function term for power consumption

The MILP model computes the power consumption of the HVAC at time instance $k+i$ by

$$\begin{aligned} P(k+i) &= P_{SAF}(k+i) + \sum_c^{n_{HB}} P_{HB,c}(k+i) \\ &\quad + \sum_c^{n_{ACS}} P_{ACS,c}(k+i) + \sum_c^{n_{HPS}} P_{HPS,c}(k+i) \\ &\quad + \sum_c^{n_{ACD}} P_{ACD,c}(k+i) + \sum_c^{n_{HPD}} P_{HPD,c}(k+i) \\ &\quad + \sum_c^{n_{ACV}} P_{ACV,c}(k+i) + \sum_c^{n_{HPV}} P_{HPV,c}(k+i) \end{aligned} \quad (84)$$

$$\forall i \in \{0, \dots, N_c - 1\}$$

$$P(k+i) = P(k+i_f)$$

$$\text{with } i_f = N_{c,MILP} - 1$$

$$\forall i \in \{N_{c,MILP}, \dots, N_{p,MILP} - 1\} \quad (85)$$

With the weight $W_p(k+i)$ the cost function term with respect to power consumption added to the overall cost function (83) reads

$$J_p(k) = \sum_{i=0}^{N_{p,MILP}-1} \underline{W}_p(k+i) \cdot P(k+i) \quad (86)$$

6.3. Penalizing deviations from the desired net enthalpy flow

The MILP model computes (1) by

$$u_{1,MILP}(k+i) = \dot{m}_{ODA}(k+i)(\underline{h}_{ODA}(k+i) - \underline{h}_{IDA}(k+i)) - \dot{Q}_C(k+i) + \dot{Q}_H(k+i) + \dot{W}_{t,SAF}(k+i) - \dot{H}_{H_2O,COND}(k+i) \quad (87)$$

$$\forall i \in \{0, \dots, N_{c,MILP} - 1\}$$

$$u_{1,MILP}(k+i) = \dot{m}_{ODA}(k+i_f)(\underline{h}_{ODA}(k+i) - \underline{h}_{IDA}(k+i)) - \dot{Q}_C(k+i) + \dot{Q}_H(k+i) + \dot{W}_{t,SAF}(k+i_f) - \dot{H}_{H_2O,COND}(k+i) \quad (88)$$

$$\text{with } i_f = N_{c,MILP} - 1$$

$$\forall i \in \{N_{c,MILP}, \dots, N_{p,MILP} - 1\}$$

In (87) and (88) the quantity $\dot{H}_{H_2O,COND}$ is the enthalpy flow of the removed condensed water. The detailed MILP formulation for computing $\dot{H}_{H_2O,COND}$ and the mass flow of the removed condensed water $\dot{m}_{H_2O,COND}$ is not given here as it would exceed the scope of this paper.

With the auxiliary decision variable $\Delta_{u_1}(k+i) \geq 0$ the deviation between the first input of the plant MPC u_1 and the net enthalpy flow provided by the MILP HVAC $u_{1,MILP}$ is constrained by

$$-\Delta_{u_1}(k+i) \leq u_1(k+i) - u_{1,MILP}(k+i) \leq \Delta_{u_1}(k+i) \quad (89)$$

$$\forall i \in \{0, \dots, N_{p,MILP} - 1\}$$

Let $\underline{W}_{u_1}(k+i)$ be a penalty weight. The penalty term penalizing deviations from the desired net enthalpy flow $\underline{u}_1(k+i)$ introduced to the plant added to (83) reads

$$J_{p,u_1}(k) = \sum_{i=0}^{N_{p,MILP}-1} \underline{W}_{u_1}(k+i) \cdot \Delta_{u_1}(k+i) \quad (89)$$

6.4. Penalizing positive deviations from the desired net mass flow of CO₂

The MILP model computes (2) by

$$u_{2,MILP}(k+i) = \dot{m}_{ODA}(k+i)(\underline{c}_{ODA}(k+i) - \underline{c}_{IDA}(k+i)) \quad (90)$$

$$\forall i \in \{0, \dots, N_{c,MILP} - 1\}$$

$$u_{2,MILP}(k+i) = \dot{m}_{ODA}(k+i_f)(\underline{c}_{ODA}(k+i) - \underline{c}_{IDA}(k+i)) \quad (91)$$

$$\text{with } i_f = N_{c,MILP} - 1$$

$$\forall i \in \{N_{c,MILP}, \dots, N_{p,MILP} - 1\}$$

With $\Delta_{u_2}(k+i) \geq 0$ the following constraint has to hold

$$u_{2,MILP}(k+i) - \underline{u}_2(k+i) \leq \Delta_{u_2}(k+i) \quad \forall i \in \{0, \dots, N_{p,MILP} - 1\} \quad (92)$$

Let $\underline{W}_{u_2}(k+i)$ be a weight. The penalty term penalizing positive deviations between $u_{2,MILP}$ and \underline{u}_2 added to (83) reads

$$J_{p,u_2}(k) = \sum_{i=0}^{N_{p,MILP}-1} \underline{W}_{u_2}(k+i) \cdot \Delta_{u_2}(k+i) \quad (93)$$

Note that if the MILP HVAC provides a smaller net mass flow of CO₂ than the plant MPC requests the resulting deviation is not penalized.

6.5. Penalizing deviations from the desired net mass flow of H₂O

The MILP model computes (3) by

$$u_{3,MILP}(k+i) = \dot{m}_{ODA}(k+i) \cdot (\underline{x}_{H_2O,ODA}(k+i) - \underline{x}_{H_2O,IDA}(k+i)) - \dot{m}_{H_2O,COND}(k+i) \quad (94)$$

$$\forall i \in \{0, \dots, N_{c,MILP} - 1\}$$

$$u_{3,MILP}(k+i) = \dot{m}_{ODA}(k+i_f) \cdot (\underline{x}_{H_2O,ODA}(k+i) - \underline{x}_{H_2O,IDA}(k+i)) - \dot{m}_{H_2O,COND}(k+i) \quad (95)$$

$$\text{with } i_f = N_{c,MILP} - 1$$

$$\forall i \in \{N_{c,MILP}, \dots, N_{p,MILP} - 1\}$$

The approach outlined in Section 6.4 is utilized to penalize positive deviations between $u_{3,MILP}$ and \underline{u}_3 . However, also the approach outlined in Section 6.3 can be chosen to penalize positive and negative deviations between $u_{3,MILP}$ and \underline{u}_3 .

6.6. Penalizing supply air temperature ϑ_{SUP} violations

The MILP considers the supply air temperature constraints by approximation as outlined in the following.

Assuming that water content of the supply air $x_{H_2O,SUP}$ equals the vapor content, the enthalpy of the supply air is computed by

$$h_{SUP} = (\underline{c}_{p,a} + x_{H_2O,SUP} \cdot \underline{c}_{p,v}) \cdot \vartheta_{SUP} + x_{H_2O,SUP} \cdot \underline{I}_0 \quad (96)$$

Thus the enthalpy of the supply air is a function of the supply air temperature ϑ_{SUP} and the water content of the supply air $x_{H_2O,SUP}$.

Neglecting here possible condensate, the water content of the supply air can be computed from (3) by

$$x_{H_2O,SUP} = \alpha \cdot \underline{x}_{H_2O,ODA} + (1 - \alpha) \cdot \underline{x}_{H_2O,IDA} \quad (97)$$

The net enthalpy flow introduced to the plant due to the HVAC (i.e. the control variable u_1 of the linear MPC for the plant model, see Eq. (4)) is given by

$$\underline{u}_1 = \dot{m}_{SUP} \cdot (h_{SUP}(\vartheta_{SUP}, x_{H_2O,SUP}) - h_{IDA}) \quad (98)$$

Utilizing (98), (97) and (96) the supply air temperature ϑ_{SUP} as a function of the MILP decision variables is given by

$$\vartheta_{SUP} = \frac{\underline{u}_1 + \dot{m}_{SUP} \cdot h_{IDA} - (\alpha \underline{x}_{H_2O,ODA} + (1 - \alpha) \underline{x}_{H_2O,IDA}) \underline{I}_0}{(\underline{c}_{p,a} + (\alpha \underline{x}_{H_2O,ODA} + (1 - \alpha) \underline{x}_{H_2O,IDA}) \underline{c}_{p,v})} \quad (99)$$

For a given desired net enthalpy flow \underline{u}_1 , the given enthalpy of the indoor air h_{IDA} , water content of the indoor $\underline{x}_{H_2O,IDA}$ and outdoor air $\underline{x}_{H_2O,ODA}$, and assumed constant parameters \underline{I}_0 , $\underline{c}_{p,a}$, and $\underline{c}_{p,v}$, respectively, it is a nonlinear function in the decision variables \dot{m}_{SUP} and α .

To avoid adding nonlinear constraints to the MILP model (and consequently the MILP model becoming a computationally expensive MINLP model) the constraints on the supply air temperature are modeled indirectly. Furthermore, to prevent that the optimization problem gets infeasible these constraints where modeled as soft constraints as outlined in the following. Note that $\delta_{\alpha_j} = 1$ implies that the fresh air ratio $\alpha = \underline{\alpha}_j$. For time instance $k+i$ the constraints due to $\vartheta_{SUP,min}$ are

$$\underline{m}_{A_{u_1}, \vartheta_{SUP,min}^v} (1 - \delta_{\alpha_j}) \leq \Delta_{u_1, \vartheta_{SUP,min}^v} - (\dot{m}_{SUP}(\underline{h}_{SUP, \vartheta_{SUP,min}^j} - \underline{h}_{IDA}) - u_{1,MILP}) \quad (100)$$

with

$$\underline{h}_{SUP, \vartheta_{SUP,min}^j} = (\underline{c}_{p,a} + \underline{x}_{H_2O,SUP,j} \cdot \underline{c}_{p,v}) \cdot \vartheta_{SUP,min} + \underline{x}_{H_2O,SUP,j} \cdot \underline{I}_0 \quad (101)$$

and the constraints due to $\vartheta_{SUP,max}$ are

$$\underline{m}_{A_{u_1}, \vartheta_{SUP,max}^v} \cdot (1 - \delta_{\alpha_j}) \leq \Delta_{u_1, \vartheta_{SUP,max}^v} - (u_{1,MILP} - \dot{m}_{SUP}(\underline{h}_{SUP, \vartheta_{SUP,max}^j} - \underline{h}_{IDA})) \quad (102)$$

1656

C. Dullinger et al./Applied Thermal Engineering 128 (2018) 1646–1659

with

$$\dot{h}_{\text{SUP},\vartheta_{\text{SUP},\text{max}},j} = (\dot{c}_{p,a} + \dot{X}_{\text{H}_2\text{O},\text{SUP},j} \cdot \dot{c}_{p,v}) \cdot \dot{v}_{\text{SUP},\text{max}} + \dot{X}_{\text{H}_2\text{O},\text{SUP},j} \cdot \dot{I}_0 \quad (103)$$

In (100) and (102) the quantities $\underline{m}_{\Lambda_{\vartheta_{\text{SUP},\text{min}}^v}} \ll 0$ and $\underline{m}_{\Lambda_{\vartheta_{\text{SUP},\text{max}}^v}} \ll 0$ are appropriately chosen constants. Whereas the quantities $\Delta_{\vartheta_{\text{SUP},\text{min}}^v}(k+i) \geq 0$ and $\Delta_{\vartheta_{\text{SUP},\text{max}}^v}(k+i) \geq 0$ (for $i = 1, \dots, N_{p,\text{MILP}} - 1$) are auxiliary decision variables. In (101) and (103) $\dot{X}_{\text{H}_2\text{O},\text{SUP},j}$ is given by

$$\dot{X}_{\text{H}_2\text{O},\text{SUP},j} = \underline{\alpha}_j \cdot \dot{X}_{\text{H}_2\text{O},\text{ODA}} + (1 - \underline{\alpha}_j) \cdot \dot{X}_{\text{H}_2\text{O},\text{IDA}} \quad (104)$$

With the weight $\underline{W}_{\vartheta_{\text{SUP},\text{min}}^v}(k+i)$ the terms penalizing supply air temperature ϑ_{SUP} constraint violations by approximation added to (83) read:

$$J_{p,\vartheta_{\text{SUP},\text{min}}^v}(k) = \sum_{i=0}^{N_{p,\text{MILP}}-1} \underline{W}_{\vartheta_{\text{SUP},\text{min}}^v}(k+i) \Delta_{\vartheta_{\text{SUP},\text{min}}^v}(k+i) \quad (105)$$

$$J_{p,\vartheta_{\text{SUP},\text{max}}^v}(k) = \sum_{i=0}^{N_{p,\text{MILP}}-1} \underline{W}_{\vartheta_{\text{SUP},\text{max}}^v}(k+i) \Delta_{\vartheta_{\text{SUP},\text{max}}^v}(k+i) \quad (106)$$

6.7. Penalizing compressor on/off switching

In order to reduce switching, each time a refrigeration machine's compressor is switched from OFF to ON (or vice versa) a penalized term is added to the overall cost function (83). This is outlined in the following.

If at some time instance $k+i$ a compressor is switched from off to on the indicator

$$I_{AC,\text{ON},c}(k+i) = \delta_{AC,\text{ON},c}(k+i) - \delta_{AC,\text{ON},c}(k+i-1) \quad (107)$$

takes a value of 1, otherwise 0 or -1 . With (107) and the auxiliary binary decision variable $\delta_{AC,\text{ON},c}(k+i)$ the following constraints have to hold (at time instance $k+i$, $\forall i \in \{0, \dots, N_{c,\text{MILP}} - 1\}$):

$$I_{AC,\text{ON},c}(k+i) \leq \delta_{AC,\text{ON},c}(k+i) \quad (108)$$

$$-2 \cdot (1 - \delta_{AC,\text{ON},c}(k+i)) \leq I_{AC,\text{ON},c}(k+i) - 1 \quad (109)$$

$$I_{AC,\text{ON},c}(k+i) - 1 \leq -1 \cdot (1 - \delta_{AC,\text{ON},c}(k+i)) \quad (110)$$

With the user defined penalty weight $W_{AC,\text{ON},c}(k+i)$ the penalty term with respect to switching a compressor from OFF to ON reads

$$J_{p,AC,\text{ON},c}(k) = \sum_{i=0}^{N_{c,\text{MILP}}-1} W_{AC,\text{ON},c}(k+i) \cdot \delta_{AC,\text{ON},c}(k+i) \quad (111)$$

6.8. Penalizing changing electrical compressor power/rotational speed

Depending on the utilized MILP model for the refrigeration machine (Section 5.5.1 or 5.5.2, respectively) either a change of the electrical power consumption ("ACS" and "ACD" model) or a change of the rotational speed ("ACV" model) of the compressor can be penalized. This is outlined for the "ACS" model (see Section 5.5.1):

Let $W_{ACS,\text{change},c}(k+i)$ be a weight. The penalty term penalizing changes of the electrical power consumption between consecutive time steps added to (83) reads

$$J_{p,ACS,\text{change},c}(k) = \sum_{i=0}^{N_{c,\text{MILP}}-1} W_{ACS,\text{change},c}(k+i) \cdot (P_{ACS,c}(k+i) - P_{ACS,c}(k+i-1)) \quad (112)$$

7. Simulation results

7.1. Case study 1: Viennese Ultra Low Floor tram: presented hierarchical framework vs. state of the art state machine

In this case study the power consumption and the performance of the HVAC of the Viennese Ultra Low Floor (ULF) tram is investigated by simulation. The control concept of the currently implemented controller, a state of the art finite state machine (FSM), is compared to the presented hierarchical MPC + MILP-MPC framework. The thermal plant model and the HVAC model of the Viennese ULF tram operated by its FSM was validated based on a detailed measurement campaign, see [17]. Background on FSM can be found in [25–27].

7.1.1. HVAC components of the Viennese ULF tram

The HVAC of the Viennese ULF tram is rather simple and has only a few number of degrees of freedom (DOF) for control. However, even with this low number of DOF its rule based controller has 193 transitions (rules). These rules are the result of expert knowledge and time-consuming trial-and-error tests in a climatic chamber.

The mixing chamber of the HVAC can provide two different fresh air ratios α . The compressor of its refrigeration machine can be turned on or off. The cooling power can be reduced by opening a by-pass valve. The heater battery and the supply air fan both have three operating stages.

7.1.2. Simulation settings and results

A typical acceptance test conducted in a climatic chamber is simulated in the following. The outdoor temperature is increased and decreased between 0 °C and 30 °C (temperature gradient 3 °C/h). One vehicle side is exposed to radiation (600 W/m²; incidence angle 30° to the horizontal). Occupancy is 42 persons. Since the FSM is a non-predictive controller, for a fair comparison of the two control concepts $N_p = N_c = N_{p,\text{MILP}} = N_{c,\text{MILP}} = 1$ is chosen for the MPC + MILP-MPC framework. The respective results are denoted by "MPC + MILP" in this case. Note that this choice effectively eliminates the predictive nature but retains the other features of the presented framework. Fig. 4 compares the results in terms of the indoor air temperature. As evident from Fig. 4 with the rule based FSM larger deviations from the set point temperature occur. The HVAC control strategies are compared in Fig. 5. Both control concepts observe the minimum consecutive on/off constraints of the compressor. However, control action of the MPC + MILP is higher. Depending on the requirements compressor switching could be reduced by increasing the respective weights (see Section 6.7). The MPC + MILP utilizes "free cooling" by optimally varying the fresh air ratio α . With the FSM the overall energy

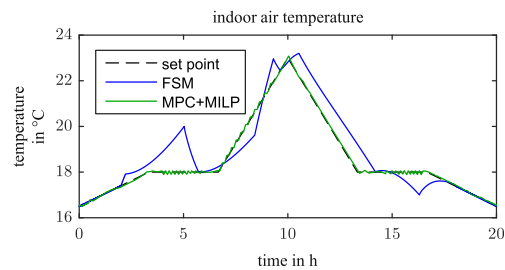


Fig. 4. Case study 1: indoor air temperature.

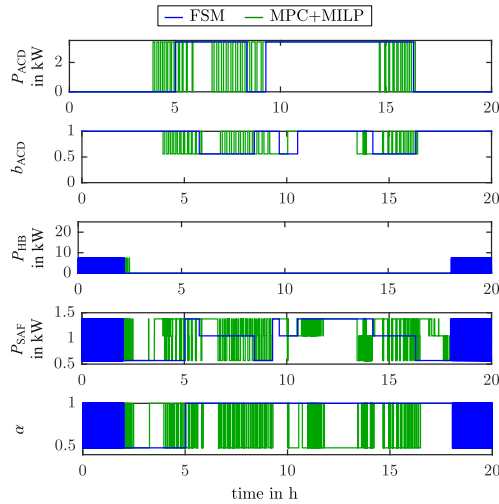


Fig. 5. Case study 1: HVAC control strategy.

consumption of the HVAC during the test is 66.44 kWh, whereas with the MPC + MILP it is only 61.66 kWh.

Fig. 6 shows a simulation where the dead band for the MPC + MILP is the area between the indoor air temperature achieved by the “FSM” and the set point. In this case the MPC + MILP’s energy consumption is only 60.34 kWh. This is a further reduction in energy consumption by 2.14%.

Setting $N_p \geq N_c \geq N_{p,MILP} \geq N_{c,MILP} > 1$ for the hierarchical MPC + MILP-MPC framework, performance, switching frequency, and energy consumption can be even more improved.

7.2. Case study 2: simultaneous control of temperature, CO₂ level, and humidity

This second case study demonstrates the ability of the MIMO MPC + MILP-MPC framework to control temperature, CO₂ level, and humidity simultaneously.

7.2.1. HVAC configuration

The HVAC of this second case study has a refrigeration machine (RM) with a variable speed compressor (see Section 5.5.1). Since frequency variable operation is only possible within a certain range its electrical power consumption P_{ACS} is a semi-continuous decision variable. The cooling power of this RM can be additionally

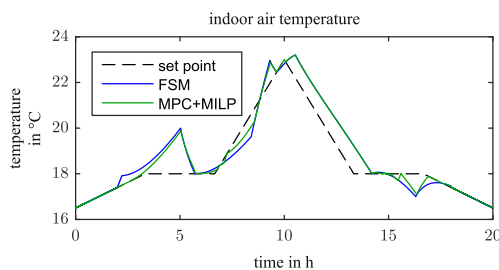


Fig. 6. Case study 1: indoor air temperature when dead band is the area between the indoor air temperature achieved by the “FSM” and the set point.

adjusted (reduced) by opening a by-pass valve. The minimum consecutive on/off time of the RM is $T_{ACS,ON} = 100 \text{ s}/T_{ACS,OFF} = 40 \text{ s}$. The supply air fan has 6 switching stages. The mixing chamber can provide 8 different fresh air ratios α and the heating power of the heater battery can be varied continuously.

7.2.2. Simulation settings and results

In the following a couple of step changes are performed. It is not claimed that these rapid changes are realistic. The aim is to show an illustrative simulation where each time step is clearly visible. The presented controller can handle even these extreme requirements. The outdoor air is cold (15 °C), has a high water content (10.24 g/kg), and a low CO₂ level (400 ppmv). Occupancy is 42 persons. CO₂ production rate per person is 0.7 g_{CO₂}/min. The mass of water due to one person’s perspiration depends on the indoor air temperature and varies around 0.48 g_{H₂O}/min.

Fig. 7 shows the indoor air temperature θ_{IDA} and step changes of its prescribed upper/lower limit. Fig. 8 shows the CO₂ level of the indoor air c_{IDA} and its upper limit step changes (no desired value is given). Fig. 9 shows the water content of the indoor air $x_{H_2O,IDA}$ and step changes of its prescribed upper/lower limit. Fig. 10 shows the HVAC control strategy.

From Figs. 7–9 it can be seen that the proposed concept effectively decouples the three control variables and achieves high tracking performance only limited by the actuators.

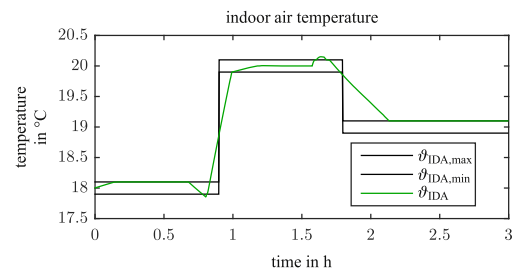


Fig. 7. Case study 2: indoor air temperature.

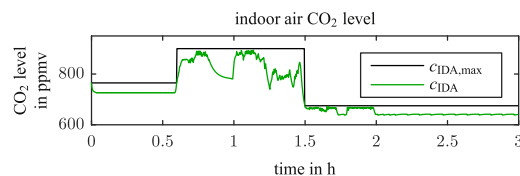


Fig. 8. Case study 2: indoor air CO₂ level.

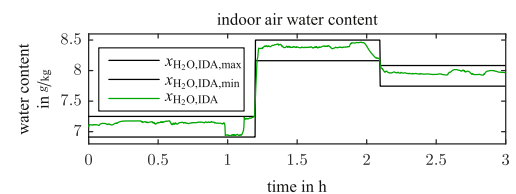


Fig. 9. Case study 2: indoor air water content.

1658

C. Dullinger et al./Applied Thermal Engineering 128 (2018) 1646–1659

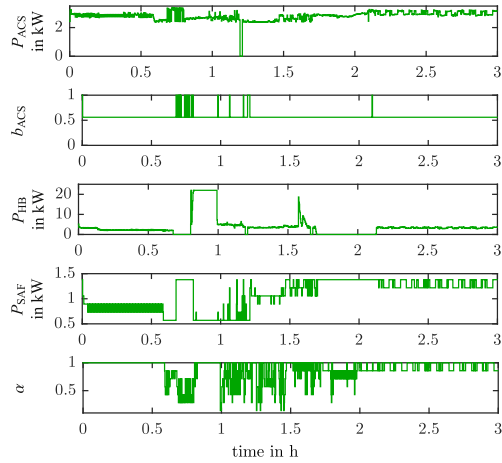


Fig. 10. Case study 2: HVAC control strategy.

7.3. Case study 3: non predictive MILP vs. predictive MILP-MPC

In this third case study it is shown that performance, switching moment, and energy consumption are improved by considering more than only the first sample of the future control trajectory $\mathbf{U}(k) = [\mathbf{u}^T(k), \dots, \mathbf{u}^T(k + N_c - 1)]^T$ of the plant MPC in the decision upon the optimal HVAC operation at the present moment k . In other words the third case study compares the case $N_p > N_c \geq N_{p,MILP} = N_{c,MILP} = 1$ with the case $N_p > N_c \geq N_{p,MILP} \geq N_{c,MILP} > 1$.

A situation is simulated where on a hot and sunny summer day the plant is first exposed to high ambient temperature and radiation (35 °C; 600 W/m²) followed by a step change to low ambient temperature and no radiation (10 °C; 0 W/m²). Such a situation could occur to a vehicle (e.g. a metro) entering a tunnel passage, or because of a sudden summer thunderstorm. It is assumed that predictions of ambient temperature and radiation are available from a look-ahead system utilizing position information, or the weather forecast, respectively. Instead of only one refrigeration machine (RM) the HVAC of this third case study has three RMs, see Fig. 11.

Two are equal and small (ACV, 1 and ACV, 2) with small compressors. These compressors have small minimum consecutive on/off times ($T_{ACV,1,ON} = T_{ACV,2,ON} = 100$ s, $T_{ACV,1,OFF} = T_{ACV,2,OFF} = 40$ s). Additionally, there is one large RM (ACV, 3) with a powerful compressor for which large minimum consecutive on/off times have to be observed ($T_{ACV,3,ON} = 800$ s, $T_{ACV,3,OFF} = 240$ s). The com-

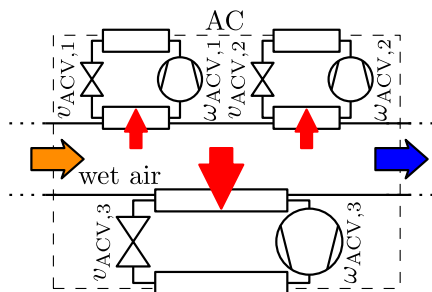


Fig. 11. Case study 3: conceptual refrigeration machines.

pressors of the small RMs can be operated with four rotational speeds. Whereas the compressor of the large RM can only be turned on and off. The small ones and the large ones have each a semi-continuous operable electronic expansion valve to adjust their cooling power. The motor of the supply air fan is frequency variable. The mixing chamber can provide two different fresh air ratios α and the heater battery has three switching stages. In all the HVAC has 1536 discrete states and 4 continuous states.

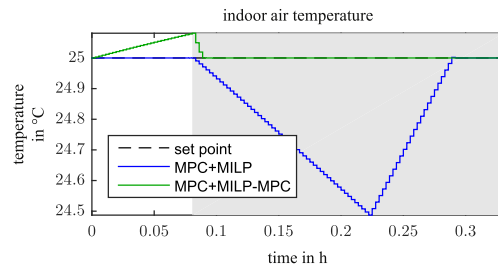


Fig. 12. Case study 3: indoor air temperature.

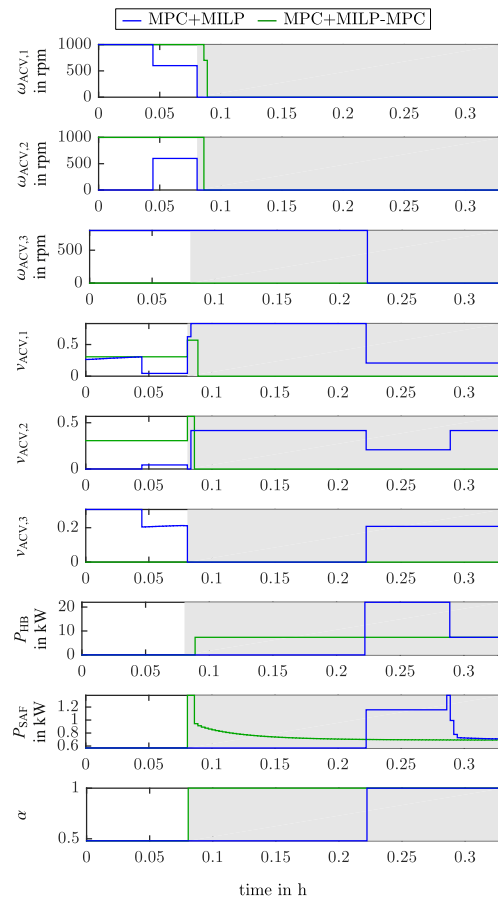


Fig. 13. Case study 3: HVAC control strategy.

Figs. 12 and Fig. 13 show the results of the third case study in terms of indoor air temperature and HVAC control strategy, respectively. The results denoted by “MPC + MILP” were obtained with $N_p = N_c = 82$ and $N_{p,MILP} = N_{c,MILP} = 1$. Whereas the results denoted by “MPC + MILP-MPC” were obtained with $N_p = N_c = N_{p,MILP} = N_{c,MILP} = 82$ (i.e. also the “MILP-MPC” oversees the minimum consecutive on/off times of the compressors). All other settings were the same. A sampling time of $T_s = 10$ s was used. In Figs. 12 and 13 the period with low ambient temperature and no radiation is shaded in gray. At the beginning in both cases the indoor air temperature equals its set point (see Fig. 12). As evident from Fig. 13 the non predictive MILP controller (case: “MPC + MILP”) optimizing the HVAC operation turns on all three compressors. Whereas the predictive MILP-MPC (case: “MPC + MILP-MPC”) does not turn on the large compressor with the large minimum consecutive on time $T_{ACV,3.ON} = 800$ s. After the step change the thermal load soon becomes negative, i.e. requiring heating. Since the large compressor once turned on can not be turned off for a long time, the temperature in the case “MPC + MILP” keeps falling under the set point temperature until the large compressor finally can be switched off. As evident from Fig. 12 the overall temperature performance in the case “MPC + MILP-MPC” is better. Furthermore the case “MPC + MILP-MPC” requires less compressor switching and because less cooling and counter-heating is applied it requires less energy consumption for the HVAC. Simultaneously heating and cooling was not allowed in both cases. As evident from this case study better results are obtained if also the HVAC operation optimization (i.e. the MILP) oversees the latency periods of the HVAC components.

8. Conclusion

A unified method for energy-, wear-, and comfort-optimized operation of HVACs, based on a flexible and modular MILP model of HVACs, is presented. A hierarchical MIMO MPC framework is proposed. On the upper-level a computationally inexpensive plant MPC with large control and prediction horizon takes care of the slow dynamics of the (thermal) plant. It takes all available disturbance predictions into account. On the lower-level a MILP-MPC based on a MILP model of an HVAC system optimizes the HVAC operation. As shown by a case study its prediction horizon should at least oversee the latency periods of the HVAC components with dwell times.

On the upper-level also a classical PID controller could be applied. However, the increasing availability of accurate disturbance forecasts (like ambient temperature, occupancy, driving speed, etc.) motivate the usage of an MPC in the upper-level which can attain extra performance by utilizing this information. Moreover, by this means, also the lower-level controller can be an MPC. As demonstrated in this work the lower-level MPC can utilize the first $N_{p,MILP}$ samples ($N_{p,MILP} \leq N_c$) of the future control trajectory $\mathbf{u}(k+i)$ (for $i = 0, \dots, N_c - 1$) of the upper-level MPC to consider future demand of net enthalpy and mass flows. In this way the optimal switching moment of HVAC components, for which minimum consecutive on/off constraints have to be fulfilled, can be achieved.

Acknowledgment

This work was supported by the project “EnerCom” (FFG, No. 846041) in cooperation with Siemens AG Österreich.

References

- [1] S.M. Attaran, R. Yusof, H. Selamat, A novel optimization algorithm based on epsilon constraint-rbf neural network for tuning {PID} controller in decoupled (HVAC) system, *Appl. Therm. Eng.* 99 (2016) 613–624, <https://doi.org/10.1016/j.applthermaleng.2016.01.025>.
- [2] Y. Liang, D. Wang, J. Chen, Y. Shen, J. Du, Temperature control for a vehicle climate chamber using chilled water system, *Appl. Therm. Eng.* 106 (2016) 117–124, <https://doi.org/10.1016/j.applthermaleng.2016.05.168>.
- [3] S.E. Shafiei, A. Alleyne, Model predictive control of hybrid thermal energy systems in transport refrigeration, *Appl. Therm. Eng.* 82 (2015) 264–280, <https://doi.org/10.1016/j.applthermaleng.2015.02.053>.
- [4] Y. Huang, A. Khajepour, F. Bagheri, M. Bahrani, Optimal energy-efficient predictive controllers in automotive air-conditioning/refrigeration systems, *Appl. Energy* 184 (2016) 605–618, <https://doi.org/10.1016/j.apenergy.2016.09.086>.
- [5] A. Bemporad, M. Morari, Control of systems integrating logic, dynamics, and constraints, *Automatica* 35 (3) (1999) 407–427, [https://doi.org/10.1016/S0005-1098\(98\)00178-2](https://doi.org/10.1016/S0005-1098(98)00178-2).
- [6] M. Morari, M. Barić, Recent developments in the control of constrained hybrid systems, *Comput. Chem. Eng.* 30 (10–12) (2006) 1619–1631, <https://doi.org/10.1016/j.compchemeng.2006.05.041>, Papers from Chemical Process Control (VVICPC) [VIISeventh] international conference in the Series.
- [7] Q. Wu, H. Ren, W. Gao, J. Ren, Modeling and optimization of distributed energy supply network with power and hot water interchanges, *Appl. Therm. Eng.* 94 (2016) 635–643, <https://doi.org/10.1016/j.applthermaleng.2015.10.157>.
- [8] L. Sun, C. Liu, Reliable and flexible steam and power system design, *Appl. Therm. Eng.* 79 (2015) 184–191, <https://doi.org/10.1016/j.applthermaleng.2014.11.076>.
- [9] M. Boix, L. Pibouleau, L. Montastruc, C. Azzaro-Pantel, S. Domenech, Minimizing water and energy consumptions in water and heat exchange networks, *Appl. Therm. Eng.* 36 (2012) 442–455, <https://doi.org/10.1016/j.applthermaleng.2011.10.062>.
- [10] M. Pan, I. Bulatov, R. Smith, J.-K. Kim, Optimisation for the retrofit of large scale heat exchanger networks with different intensified heat transfer techniques, *Appl. Therm. Eng.* 53 (2) (2013) 373–386, <https://doi.org/10.1016/j.applthermaleng.2012.04.038>, Includes Special Issue: PRO-TEM Special Issue.
- [11] A. Costa, A. Fichera, A mixed-integer linear programming (milp) model for the evaluation of {CHP} system in the context of hospital structures, *Appl. Therm. Eng.* 71 (2) (2014) 921–929, <https://doi.org/10.1016/j.applthermaleng.2014.02.051>, Special Issue: {MICROGEN} III: Promoting the transition to high efficiency distributed energy system.
- [12] J. Zábajník, M. Dvůrák, Power grid simulation model for long term operation planning, *Appl. Therm. Eng.* 70 (2) (2014) 1294–1305, <https://doi.org/10.1016/j.applthermaleng.2014.05.064>.
- [13] C. Miranda, C. Costa, J. Caballero, M. Ravagnani, Optimal synthesis of multiperiod heat exchanger networks: a sequential approach, *Appl. Therm. Eng.* 115 (2017) 1187–1202, <https://doi.org/10.1016/j.applthermaleng.2016.10.003>.
- [14] J.-Y. Lee, C.-L. Chen, T.-L. Wen, D.K.S. Ng, D.C.Y. Foo, T.-C. Wang, Synthesis and design of chilled water networks using mathematical optimization, *Appl. Therm. Eng.* 58 (1–2) (2013) 638–649, <https://doi.org/10.1016/j.applthermaleng.2013.04.024>.
- [15] J. Kallrath, *Gemischt-ganzzahlige Optimierung: Modellierung in der Praxis*, Springer Fachmedien Wiesbaden, 2013.
- [16] Y. Liang, C.-W. Hui, A shortcut model for energy efficient water network synthesis, *Appl. Therm. Eng.* 96 (2016) 88–91, <https://doi.org/10.1016/j.applthermaleng.2015.11.020>.
- [17] C. Dullinger, W. Struckl, M. Kozek, A modular thermal simulation tool for computing energy consumption of HVAC units in rail vehicles, *Appl. Therm. Eng.* 78 (2015) 616–629, <https://doi.org/10.1016/j.applthermaleng.2014.11.065>.
- [18] G. Bejarano, J.A. Alfaya, M.G. Ortega, M. Vargas, On the difficulty of globally optimally controlling refrigeration systems, *Appl. Therm. Eng.* 111 (2017) 1143–1157, <https://doi.org/10.1016/j.applthermaleng.2016.10.007>.
- [19] K. Ogata, *Discrete-Time Control Systems*, Prentice-Hall International Editions, Prentice-Hall, 1987.
- [20] A. Oppenheim, R. Schaffer, *Discrete-Time Signal Processing*, Always Learning, Pearson, 2013.
- [21] R.N. Hofstädter, T. Zero, C. Dullinger, G. Richter, M. Kozek, Heat capacity and heat transfer coefficient estimation for a dynamic thermal model of rail vehicles, *Math. Comput. Model. Dyn. Syst. 0(0)*, 1–14, doi:<https://doi.org/10.1080/13873954.2016.1263670>.
- [22] C. Dullinger, W. Struckl, M. Kozek, Simulation-based multi-objective system optimization of train traction systems, *Simul. Model. Pract. Theory* 72 (2017) 104–117, <https://doi.org/10.1016/j.simpat.2016.12.008>.
- [23] L. Wang, *Model Predictive Control System Design and Implementation Using MATLAB®*, Springer-Verlag, London, 2009, <https://doi.org/10.1007/978-1-84882-331-0>.
- [24] E. Beale, Branch and bound methods for mathematical programming systems, *Ann. Discrete Math.* 5 (1979) 201–219, [https://doi.org/10.1016/S0167-5060\(08\)70351-0](https://doi.org/10.1016/S0167-5060(08)70351-0).
- [25] F. Wagner, R. Schmuki, T. Wagner, P. Wolstenholme, *Modeling Software with Finite State Machines: A Practical Approach*, Taylor & Francis, Boca Raton, USA, 2006.
- [26] A. Kumar, *Fundamentals of Digital Circuits*, PHI Learning, New Delhi, India, 2009.
- [27] J. Davis, J. Davis, R. Reese, *Finite State Machine Datapath Design, Optimization, and Implementation, Synthesis Lectures on Digital Circuits and Systems*, Morgan & Claypool, California, USA, 2008.

List of scientific publications

International Journals:

1. C. Dullinger, W. Struckl, M. Kozek. A modular thermal simulation tool for computing energy consumption of HVAC units in rail vehicles. *Applied Thermal Engineering*, Volume 78, 2015, Pages 616-629.
DOI: 10.1016/j.applthermaleng.2014.11.065
2. C. Dullinger, W. Struckl, M. Kozek. Simulation-based multi-objective system optimization of train traction systems. *Simulation Modelling Practice and Theory*, Volume 72, 2017, Pages 104-117.
DOI: 10.1016/j.simpat.2016.12.008
3. C. Dullinger, W. Struckl, M. Kozek. A general approach for mixed-integer predictive control of HVAC systems using MILP. *Applied Thermal Engineering*, Volume 128, 2018, Pages 1646-1659.
DOI: 10.1016/j.applthermaleng.2017.09.104
4. R. N. Hofstädter, T. Zero, C. Dullinger, G. Richter, M. Kozek. Heat capacity and heat transfer coefficient estimation for a dynamic thermal model of rail vehicles. *Mathematical and Computer Modelling of Dynamical Systems*, Volume 23, 2017, Pages 1-14.
DOI: 10.1080/13873954.2016.1263670

Talks and Presentations on International Conferences:

1. C. Dullinger, A. Schirrer, M. Kozek, Advanced Control Education: Optimal & Robust MIMO Control of a Flexible Beam Setup, In Proc. of 19th IFAC World Congress (IFAC'14), August 24-29, 2014, Cape Town, South Africa. IFAC Proceedings Volumes, Volume 47, Issue 3, 2014, Pages 9019-9025, ISSN 1474-6670, ISBN 9783902823625,
DOI: 10.3182/20140824-6-ZA-1003.02201
2. C. Dullinger, A. Schirrer, M. Kozek, Data-based and analytic modelling for model-based control of a flexible beam, In Proc. of 8th Vienna Conference on Mathematical Modelling (MATHMOD 2015), February 18-20, 2015, Vienna, Austria. IFAC-PapersOnLine, Volume 48, Issue 1, 2015, Pages 73-74, ISSN 2405-8963,
DOI: 10.1016/j.ifacol.2015.05.112

Talks and Presentations:

1. W. Struckl, C. Dullinger. EcoTram II - Energieoptimierung der thermischen
Fahrzeugsysteme bei Schienenfahrzeugen
Vortrag: Science Brunch Energieeffiziente Fahrzeugtechnologien, Wien, Tech Gate,
09.04.2015

Curriculum Vitae

Personal Information

Name Dipl.-Ing. Christian Dullinger
Date of birth 14th of January, 1985
Birthplace Vöcklabruck
Citizenship Austria
Gender Male
Address Hörnesgasse 17/11, 1030 Vienna



Education

09/2014 - Vienna University of Technology
Doctoral studies in Mechanical Engineering
10/2004 - 07/2013 Vienna University of Technology
Diploma studies in Mechanical Engineering - Economics
Specialization in production and product management
Subject of the diploma thesis: feedback control
Final examination passed on July 25th, 2013
09/1999 - 07/2004 Higher technological collage (secondary school), Vöcklabruck
Final secondary-school examinations passed on June 29th, 2004
09/1995 - 07/1999 Federal High School, Vöcklabruck
09/1991 - 07/1995 Primary School, Vöcklabruck

Diploma Thesis

Title Comparison of optimal and robust MIMO control concepts for active vibration damping of a flexible beam laboratory setup
Supervisor Ao.Univ.Prof. Dipl.-Ing. Dr.techn. Martin Kozek

Professional Work Experience

11/2013 -	Project assistant at Vienna University of Technology Institute of Mechanics and Mechatronics Division of Control and Process Automation
8/2009 - 9/2009	Internship at BIS VAM Anlagentechnik GmbH, Wels Department of Engineering
7/2008 - 7/2008	Internship at BRP-Powertrain GmbH & Co KG, Gunskirchen Department of Operating Technology
7/2007 - 8/2007	Internship at SML Maschinengesellschaft mbH, Lenzing Department of Engineering
8/2006 - 9/2006	Internship at Lenzing AG, Lenzing Production Department
8/2004 - 8/2004	Internship at BIS VAM Anlagentechnik GmbH, Wels Department of Engineering
7/2003 - 8/2003	Internship at Vishay Semiconductor GesmbH, Vöcklabruck Diploma project for final secondary-school examination
7/2002 - 7/2002	Internship at SML Maschinengesellschaft mbH, Lenzing Department of Engineering
7/2001 - 7/2001	Internship at Maschinenbau Dullinger, Vöcklamarkt Mechanical workshop staff

IT Skills

Matlab, Simulink, ControlDesk, LabVIEW, LMS Imagine.Lab Amesim, Mathcad, Maple, ABACUS, Ansys Fluent, Catia, Solid Works, ME10, One Space Designer, AutoCAD, \LaTeX , HTML, MS Office, R, C, Java

Languages

German	native language
English	fluent in written and spoken

Leisure Interests

Traveling, Guitar, reading, cooking, running, volleyball, dancing